

Division of Biomedical  
and Life Sciences

Health &  
Medicine

Lancaster  
University



**MSc (*by research*) in Biomedical Science**

---

**Development of peptide inhibitor nanoparticles  
(PINPs) for treatment of Alzheimer's disease**

**Christos Michail**

**August 2015**

# Table of Contents

<b>Declaration</b> .....	<b>i</b>
<b>Acknowledgements</b> .....	<b>ii</b>
<b>Abbreviations</b> .....	<b>iii</b>
<b>ABSTRACT</b> .....	<b>vi</b>
<b>CHAPTER ONE - INTRODUCTION</b> .....	<b>1</b>
1.1 Diseases of the brain.....	1
1.2 Alzheimer’s disease - Overview of pathology .....	2
1.3 Clinical features of Alzheimer’s disease .....	4
1.4 The genetics of Alzheimer’s disease .....	6
1.5 Risk factors .....	8
1.6 Alzheimer’s disease and amyloidosis.....	9
1.7 Formation of A $\beta$ from the amyloid precursor protein (APP) .....	11
1.8 Amyloid cascade hypothesis .....	14
1.9 Current diagnosis of AD .....	16
1.10 Current symptomatic treatment of AD.....	17
1.11 The evolution of peptide inhibitors against the $\beta$ -amyloid oligomerization .....	22
1.12 Development of new therapies for AD .....	26
1.12.1 Biological aspects for drug delivery in the Central Nervous System (CNS).....	26
1.12.2 Blood Brain Barrier (BBB) .....	27
1.12.3 Blood–cerebrospinal fluid barrier (B-CSFB) .....	28
1.12.4 Strategies for overcoming the Blood Brain Barrier.....	29
1.13 Nanotechnology.....	29
1.13.1 Nanomedicine for drug delivery in the CNS.....	29
1.13.2 The generations of Nanoparticles (NPs) .....	31
1.14 Liposomes design and function .....	33
1.14.1 Liposomes general features.....	33
1.14.2 Classification of liposomes.....	35
1.14.3 Stealth liposomes and conventional liposomes.....	37
1.14.4 Attachment of targeting peptides on the surface of liposomes - Peptide Inhibitor Nanoparticles (PINPs) .....	38
1.15 Scope of the Thesis .....	41
<b>CHAPTER TWO – MATERIALS AND METHODS</b> .....	<b>42</b>
2.1 Buffers solutions .....	43

2.2 Thioflavin-T (Th-T) preparation.....	44
2.3 Amyloid- $\beta$ splitting.....	44
2.4 Development of nanoparticles attached with RI-OR2-TAT by <i>click chemistry</i> (PINPs)..	44
2.4.1 Preparation and hydration of lipid film.....	44
2.4.2 Freeze and thaw process .....	45
2.4.3 Bath sonication .....	45
2.4.4 Vesicle extrusion .....	46
2.4.5 The attachment of peptide inhibitor on the surface of the liposome .....	47
2.5 Dynamic Light Scattering (DLS) analysis.....	49
2.6 Bicinchoninic acid (BCA) Assay.....	49
2.7 Colorimetric determination of phospholipids with ammonium ferrothiocyanate (Stewart's Method) .....	50
2.8 Phospholipid Assay – Choline oxidase · DAOS method (Wako assay) .....	51
2.9 Concentrate the liposomes.....	53
2.10 Preparation of three types of liposomes for Transmission Electron Microscopy (TEM) .....	53
2.10.1 Staining of plain, MAL-PEG-PE liposomes and PINPs for TEM .....	53
2.10.2 TEM photographic image processing.....	54
2.11 Toxicity assays.....	55
2.11.1 MTS cell proliferation colorimetric assay Kit .....	55
2.11.2 Thioflavin-T (ThT) assay.....	56
2.12 Cell penetration assay.....	58
<b>CHAPTER THREE - DLS RESULTS.....</b>	<b>59</b>
3.1 Conjugation of RI-OR2-TAT-Cys peptide to PEGylated liposomes to create PINPs .....	59
3.2 Characterization of liposomes by size.....	60
3.2.1 Characterization of standard gold nanoparticles using DLS .....	60
3.2.2 Characterization of simple liposomes using (DLS) .....	67
3.2.3 Characterization of MAL-PEG liposomes by size using DLS .....	78
3.2.4 Characterization of Peptide Inhibitor Nanoparticles (PINPs) using DLS .....	83
<b>CHAPTER FOUR - TEM RESULTS.....</b>	<b>91</b>
4.1 Ultrastructural characterization of liposomes by size and shape using Transmission Electron Microscope (TEM).....	91
4.1.1 Morphology and ultrastructure of simple liposomes .....	91
4.1.2 Morphology and ultrastructure of PEGylated liposomes using TEM.....	95
4.1.3 Morphology and ultrastructure of PINPs using TEM .....	98

<b>CHAPTER FIVE – CELL TOXICITY AND CELL PENETRATION RESULTS .....</b>	<b>105</b>
5.1. Cell toxicity using the three different types of liposomes .....	105
5.1.1 Simple liposomes .....	105
5.1.2 PEGylated liposomes and PINPs.....	107
5.2 Statistical analysis of cell viability results using T-test.....	109
5.3 Ability of liposomes to rescue SHSY-5Y cells in the presence of A $\beta$ .....	111
5.3.1 Simple and PEGylated liposomes .....	111
5.3.2 PINPs .....	113
5.4 Statistical analysis of the ability of liposomes to rescue SHSY-5Y cells in the presence of A $\beta$ using T-test .....	114
5.5 Conclusion applying cell toxicity assay (MTS).....	115
5.6 Cell penetration assay – Fluorescent microscopy using 200 nm of PEGylated liposomes and PINPs .....	116
5.6.1 Conclusion cell penetration assay.....	125
5.7 PINPs are potent aggregation inhibitors (Th-T assay).....	127
<b>CHAPTER SIX - DISCUSSION .....</b>	<b>130</b>
6.1 Background .....	130
6.2 Findings of the study.....	132
6.2.1 Creation of liposomes in three distinct sizes .....	133
6.2.2 DLS investigation.....	134
6.2.3 TEM investigation.....	136
6.2.4 MTS and Th-T assays investigation .....	138
6.2.5 Cell penetration investigation.....	139
6.3 Study’s limitations.....	140
6.4 Future prospective .....	142
6.5 Conclusion.....	146
<b>References.....</b>	<b>148</b>

## **Declaration**

This thesis is submitted to the University of Lancaster in accordance with the requirements of the degree of Master of Science in the department of Biomedical and Life Sciences. I confirm that this thesis has not been submitted for any other degree of any examining body.

## **Acknowledgements**

There are many people I would like to thank who have helped me in different ways. First of all I would like to thank my supervisor Professor David Allsop for giving me the opportunity to work in his team and on this interesting project in the field of neuroscience and specifically in the field of nanomedicine but also I would like to thank him for his important guidance during this year in order to write this thesis. Furthermore, I am grateful to Dr. Mark Taylor for his valuable help in the laboratory, encouragement and enduring support, Dr. Nigel Fullwood for his willingness to help me to take some Transmission Electron micrographs for my project and also Dr. Jane Andre who helped me with using the confocal microscope. I am also very grateful to Dr. Paul McKean for his willingness to give me some helpful advice on writing of my thesis. I would also like to thank the Physics and Chemistry Departments at the University of Lancaster for allowing me to use some of their equipment in order to complete my experiments.

I would also like to acknowledge PhD students Maria Michael and Claire Tinker for the valuable help and important advice they offered for my thesis. Last, I would like to thank my parents and my brothers for their encouragement during my postgraduate studies.

## Abbreviations

Abbreviation	Meaning
AChE	Acetylcholinesterase
AD	Alzheimer's disease
AFM	Atomic Force Microscopy
A $\beta$	Amyloid- $\beta$
A $\beta$ -Derived Diffusible Ligands	ADDLs
APLP1,2	Amyloid Precursor – Like Protein 1,2
APP	Amyloid Precursor Protein
APOE	Apolipoprotein E
BBB	Blood Brain Barrier
BCA	Bicinchoninic Acid
B-CSFB	Blood-Cerebrospinal Fluid Barrier
CJD	Creutzfeldt-Jacob disease
CLSM	Confocal Laser Scanning Microscopy
CNS	Central Nervous System
CSF	Cerebrospinal Fluid
CT	Computerized Tomography
DAOS	N-ethyl-N-(2-hydroxy-3-sulfopropyl)-3,5-dimethoxyaniline

<b>DAPI</b>	<b>4', 6-diamino-2-phenylindole dihydrochloride</b>
<b>DLB</b>	<b>Dementia with Lewy Bodies</b>
<b>DLS</b>	<b>Dynamic Light Scattering</b>
<b>DM2</b>	<b>Diabetes Mellitus 2</b>
<b>EPR</b>	<b>Enhanced Permeation and Retention</b>
<b>ESEM</b>	<b>Environmental Scanning Electron Microscopy</b>
<b>FTD</b>	<b>Frontotemporal Dementia</b>
<b>HD</b>	<b>Huntington's Disease</b>
<b>HIV</b>	<b>Human Immunodeficiency Virus</b>
<b>LDH</b>	<b>Lactate Dehydrogenase</b>
<b>LDPF</b>	<b>Liposomal Dry Powder Formulation</b>
<b>LOAD</b>	<b>Late-onset Alzheimer's disease</b>
<b>LTP</b>	<b>Long Term Potentiation</b>
<b>MCI</b>	<b>Mild Cognitive Impairment</b>
<b>MLV</b>	<b>Multilamellar Large Vesicles</b>
<b>MPS</b>	<b>Mononuclear Phagocyte System</b>
<b>MRI</b>	<b>Magnetic Resonance Imaging</b>
<b>PD</b>	<b>Parkinson's disease</b>
<b>NMDA</b>	<b>N-methyl-D-aspartate</b>
<b>NPs</b>	<b>Nanoparticles</b>
<b>NTA</b>	<b>Nanoparticle Tracking Analysis</b>



<b>PEG</b>	<b>Polymer-poly - (ethylene glycol)</b>
<b>PET</b>	<b>Positron Emission Tomography</b>
<b>PiB</b>	<b>Pittsburgh compound B</b>
<b>PINPs</b>	<b>Peptide Inhibitor Nanoparticles</b>
<b>PS1, PS2</b>	<b>Presenilin 1,2</b>
<b>PrPc</b>	<b>Prior protein cellular form</b>
<b>PrPSc</b>	<b>Prior protein scrapie form</b>
<b>REV</b>	<b>Reverse-Phase Evaporation</b>
<b>SUV</b>	<b>Small Unilamellar Vesicles</b>
<b>TAT</b>	<b>Trans-activating transcriptional activator</b>
<b>TEM</b>	<b>Transmission Electron Microscope</b>
<b>TREM2</b>	<b>Triggering Receptor Expressed on Myeloid cells 2</b>
<b>Th-T</b>	<b>Thioflavin-T</b>

**Title:** Development of peptide inhibitor nanoparticles (PINPs) for treatment of Alzheimer's disease.

**Author:** Christos Michail, August 2015.

### **ABSTRACT**

**Purpose:** To investigate the best carrier technology for our  $\beta$ -amyloid ( $A\beta$ ) aggregation inhibitors by developing three types of liposomes (a) plain liposomes, (b) MAL-PEG liposomes, and finally the combination of retro-inverted peptide RI-OR2-TAT (Ac-rGffvlkGrrrrqrrkkGyc-NH<sub>2</sub>) attached onto the surface of MAL-PEG liposomes, creating Peptide Inhibitor Nanoparticles (PINPs) of three different sizes (50, 100 and 200 nm). In addition, these nanoliposomes (NLPs) (with particular focus on PINPs) were examined for their ability to affect  $A\beta$  aggregation, and to protect against  $A\beta$  cytotoxicity.

**Methods:** The creation of NLPs was carried out by the use of a mini extruder, while the elution of PINPs from a size exclusion column was assessed by Dynamic Light Scattering (DLS). The quantification of peptide bound to liposomes was determined by bicinchoninic acid (BCA) assay, while phospholipid content was quantified by Wako phospholipid assay. The effects of the different types of liposomes on  $A\beta$  toxicity and viability of SHSY-5Y neuronal cells were examined by MTS assay, whereas effects on  $A\beta$  aggregation were determined by Thioflavin-T (Th-T) assay. In addition, a cell penetration assay was carried out in order to examine the ability of liposomes to penetrate into neuroblastoma SHSY-5Y cells.

**Results:** Low concentrations of PINPs 0.1  $\mu$ M inhibited A $\beta$  aggregation and toxicity *in vitro*. MAL-PEG liposomes and PINPs were able to penetrate into neuroblastoma SHSY-5Y cells and were also more stable than simple liposomes. Stability means the ability of liposomes to keep their size and their shape stable for long time. In addition, the three types of liposomes were not toxic towards SHSY-5Y neuroblastoma cells. Cytotoxicity is the quality of being toxic to cells. So, none of the three types of our liposomes showed any negative effect on the viability towards SHSY-5Y neuroblastoma cells.

**Conclusion:** NLPs are an ideal carrier for our aggregation inhibitors because they affect A $\beta$  aggregation and toxicity at low doses, and according to other data generated by our group, can cross the Blood Brain Barrier (BBB).

# CHAPTER ONE - INTRODUCTION

## 1.1 Diseases of the brain

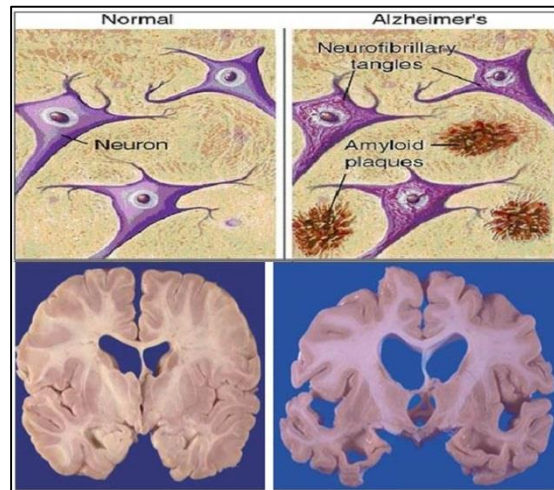
Each living organism in order to function properly needs healthy cells to correctly perform all of their required functions. Cells are the smallest units of life and their function is based on thousands of different proteins (Dobson, 1999). If a particular protein is disrupted, the three dimensional structure can become misfolded, and this can lead to the aggregation of that protein. Many previous studies and observations support the idea that the aggregation of misfolded proteins in various organs and tissues is directly associated with numerous human systemic and neurodegenerative diseases, the latter being driven by the accumulation of misfolded protein fibrils in the brain. This group of brain diseases includes: Alzheimer's disease (AD), Parkinson's disease (PD), dementia with Lewy bodies (DLB), Creutzfeldt-Jacob disease (CJD), motor neuron disease (MND), Huntington's disease (HD) and frontotemporal dementia (FTD) (Soto, 2003). All are due to the degeneration of a specific population of nerve cells in the brain and spinal cord leading to corresponding clinical features of the disease.

The majority of the neurodegenerative diseases noted above are age related and are often caused by a combination of both environmental and genetic factors. Furthermore, all are incurable diseases (Martin, 1999; Soto, 2003). This is a particular problem in the case of AD which is recognized as the most common neurodegenerative disease caused by the uncontrolled accumulation of misfolded proteins in the brain. Consequently, scientists are trying to understand the causes of this disease and how to diagnose and treat it more efficiently, including development

of drugs which limit the accumulation of misfolded proteins in the brain. In the next sections of the introduction I will consider more about AD (risks factors, diagnostic methods, current treatments) and generally how PINPs might function as an efficient drug for this disease.

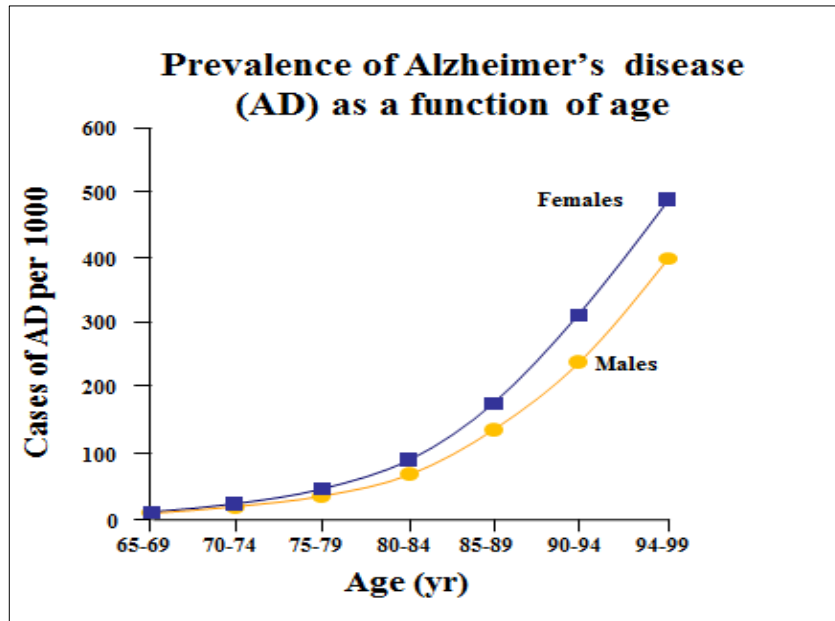
## **1.2 Alzheimer's disease - Overview of pathology**

At the beginning of 19<sup>th</sup> century (1906), the German psychiatrist Alois Alzheimer described the first recognized case of AD, in a fifty one year old female patient called Auguste Deter, reviewed by (Moller and Graeber, 1998). She suffered from unstable behavior (usually aggressive behavior), disorientation and language problems. After the death of this patient, Alois Alzheimer brought to light the presence of two lesions in her brain: (a) senile plaques, now known to contain paired helical filaments amyloid  $\beta$ -protein ( $A\beta$ ) and (b) neurofibrillary tangles, now known to be composed of hyperphosphorylated, aggregated Tau protein (figure 1.1) (Haass and Selkoe, 2007). In the early stages of AD the most common symptom is difficulty in remembering recent events, known as short term memory loss (memory impairment) (Selkoe, 2001).



**Figure 1.1: Comparison of normal, healthy neuronal cells/brain and those in AD.** *This illustration shows a normal brain with healthy neuronal cells (healthy neurons and absence of amyloid plaques) and an AD brain with senile amyloid plaques (brown) and neurofibrillary tangles (purple unhealthy cells). The photograph of the brain with AD shows shrinkage and loss of cerebrocortical grey matter together with the enlargement of the fluid-filled ventricles (Bird, 2008).*

Since this first recognised case of AD described by Alois Alzheimer, many scientists have tried to understand the cause of this neurodegenerative disorder and how to develop a method to cure it. AD is the most common neurodegenerative disease and affects people of both genders mainly over the age of 65 years (Blennow et al., 2006). It is important to note that, due to the development and improvement of the sector of medicine and technology over the years, the average of human life span is increasing continuously and as a result more people will have a higher risk of developing this disease (figure 1.2). According to Ferri et al. (2005) in the year 2000 around 24 million people worldwide were affected by AD and this number is expected to approximately double every 20 years, to 48 million in 2020 and 96 million in 2040.



**Figure 1.2:** The graph shows the number of cases of AD in males and females as a function of age. *It is observed that as age increases, the risk of developing AD increases exponentially (Nussbaum and Ellis 2003).*

### 1.3 Clinical features of Alzheimer's disease

The clinical features which characterize the disease are memory problems, aphasia (difficulty with speech and loss of ability to understand speech), apraxia (inability to make voluntary movements) and agnosia (difficulty with recognition of objects). Additionally, people with AD often present with aggressive behavior, sleep disturbances, mental uneasiness, impaired judgment and delusions (Blennow et al., 2006). Underlying these clinical features of AD, there are various neuropathological changes such as: decrease in brain volume, gliosis, enlargement of ventricles within the brain, extreme shrinkage of the hippocampus and parts of the cerebral cortex, loss of the synapses which are necessary for communication between nerves cells, an inflammatory response, and extensive and early oxidative damage, as well as

changes in the acetylcholine transmitter system in the brain due to loss of cholinergic neurons. It is now realized that some of these changes start to occur 2-3 decades before any overt clinical features are manifested (Davies et al., 1988). The first symptoms of AD probably emerge when the amyloid plaque and the neurofibrillary tangle burden accumulate above a certain critical threshold, which may vary between individuals. An early stage of the disease is called Mild Cognitive Impairment (MCI), where there are mild but noticeable changes in cognitive function (Peterson, 2004). Some people with MCI will progress to develop full-blown AD. AD itself is divided into three distinct stages: (a) early diagnosis, where some cognitive symptoms appear along with mood swings and personality changes, (b) mild-moderate, which is defined by the appearance of some behavioral problems, in conjunction with memory impairment such that patients are unable to learn and recall new information. The third stage (c) is the severe-late stage, which is defined by advanced symptoms of the disease such as complete loss of memory, inability to eat or swallow, and partial loss of motor skills, which finally leads to death (Blennow et al., 2006). The cause of sporadic disease is presumably due to a mix of genetic and environmental factors, while a small percentage (5%) of cases are caused by gene mutations resulting in familial AD (Westermarck, 2005).



#### 1.4 The genetics of Alzheimer's disease

It is important to note that AD is divided into two forms, the inherited early-onset form and the sporadic late-onset form (Allsop and Mayer, 2014). The inherited form of the disease generally affects individuals younger than 60 years (32-59 years) and usually progresses more rapidly than late-onset AD. The mutations responsible for familial AD are found in genes encoding the amyloid precursor protein (APP), presenilin 1 (PS1) and presenilin 2 (PS2) (Mattson 2010; Sherrington et al., 1995). The first familial cases of AD discovered were caused by mutations in the APP gene on chromosome 21, which result in an increase in the levels of A $\beta$  in general or A $\beta$ 42 in particular (more information about A $\beta$  below). Currently 25 pathogenic APP mutations are associated with FAD. In Down's syndrome, trisomy of chromosome 21 leads to overexpression of the APP gene product which leads to overproduction of amyloid- $\beta$  (Selkoe, 2001). Later it was discovered that the most common reason for familial AD is due to mutations in the highly homologous presenilin 1 (PSEN1) and presenilin 2 (PSEN2) genes, which are actually components of the  $\gamma$ -secretase enzyme complex and also lead to an increase in the levels of A $\beta$ 42 peptide.

Furthermore, in 1993 two groups of scientists pointed out an association between of Apolipoprotein E (APOE)  $\epsilon$ 4 and AD and it was revealed that the presence of APOE  $\epsilon$ 4 increases the risk of developing the disease by three times in heterozygotes and by 15 times in homozygotes. APOE is a glycoprotein which is a constituent of lipoproteins and is composed of  $\sim$  300 amino acids. Its role is related to the transport of cholesterol to the cells (Pfrieger, 2003; Wernette-Hammond et al., 1989). APOE  $\epsilon$ 4 constitutes one of the alleles of APOE. There are three alleles ( $\epsilon$ 2,  $\epsilon$ 3,

ε4) resulting in 3 (E2, E3, E4) different APOE isoforms which differ only by one or two amino acid substitutions at residues 112 or 158 (Mahley et al., 2006). The ε4 allele of the APOE gene was found to be an important genetic risk factor for late-onset AD (Namba et al., 1991; Wisniewski and Frangione, 1992), with risk increasing for people with one and two ε4 alleles (Corder et al., 1993).

<u>Chromosome</u>	<u>Gene product</u>	<u>Inheritance</u>	<u>Phenotype</u>
14	Presenilin-1	Autosomal dominant	Early onset AD - PS mutation increases the levels of Aβ <sub>42</sub> peptide.
1	Presenilin-2	Autosomal dominant	Early onset AD - PS mutation increases the levels of Aβ <sub>42</sub> peptide.
21	APP	Autosomal dominant	Early onset AD - APP mutations increases the levels of Aβ in total or Aβ <sub>42</sub> in particular.
21	APP	Trisomy 21	Down's syndrome.
19	ApoE4 polymorphism	Risk factor for LOAD	Increased Aβ plaque load.

**Table 1.1: The genes involved in familial AD.** *The table indicates the different chromosomes and genes which cause an increase in the levels of Aβ<sub>42</sub> peptide and are consequently linked to AD.*

In addition, triggering receptor expressed on myeloid cells 2 (TREM2) has been identified as a gene which is associated with late-onset sporadic AD and increases the risk of developing the disease to a similar extent as APOE ε4. TREM2 is a transmembrane glycoprotein and is primarily expressed by microglia of the central nervous system (CNS) (Bouchon et al., 2000; Guerreiro et al., 2013; Sessa et al., 2004). The expression of TREM2 occurs simultaneously with the formation of senile

plaques. In addition the expression of TREM2 affects the function of microglia by stimulating them to induce proliferation CD4+ T cells and promote the secretion of tumor necrosis factor and CCL2 into the extracellular milieu (Melchior et al., 2010).

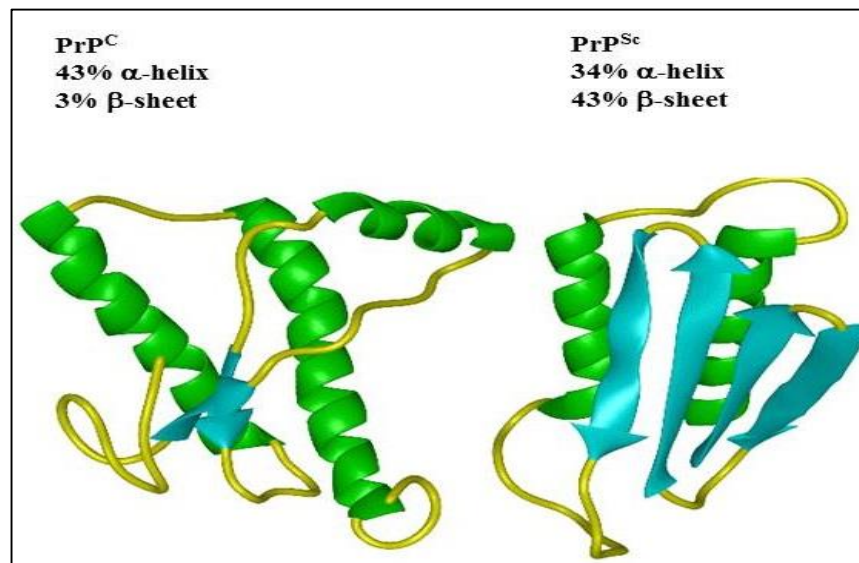
### **1.5 Risk factors**

The most obvious and unquestionable risk factor for AD is ageing, most likely related to ageing of the brain. Apart from ageing, various epidemiological studies, support the fact that a decreased brain reserve (small size brain, poor educational achievement) along with reduced mental and physical activity in later life constitute important risk factors for developing AD (Mayeux, 2003; Mortimer et al., 2003). In addition, brain injury (head trauma) can also apparently cause AD by precipitating formation of amyloid plaques and neurofibrillary tangles or by reducing the brain reserve (Jellinger, 2004). Additionally, some other risks factors include high levels of cholesterol, high blood pressure, atherosclerosis, smoking and diabetes, which can arise due to an unhealthy lifestyle. Diabetes mellitus type 2 (DM2) also constitutes a major risk factor for the development of early-onset AD. All of these risks factors are directly associated with vascular disease which can also cause AD by accelerating plaque and the tangle formation (Mayeux, 2003; Biessels et al., 2006; Haan, 2006). Consequently, many of the environmental risk factors can be limited and can be controlled by engaging in a healthy lifestyle.

## 1.6 Alzheimer's disease and amyloidosis

Amyloidosis is a general term used to describe diseases which are caused by the deposition of insoluble amyloid fibrils in various tissues and organs of the body (Allsop and Mayes, 2014). It is important to note that all amyloid deposits share common physical, histological and structural features such as: reactivity to thioflavin and Congo red stains, high levels of insolubility, and presence of 7-10 nm diameter fibrils with a rope-like structure (Allsop and Mayes, 2014). The formation of amyloid fibrils constitutes a big challenge in dealing with AD since they have the ability to resist proteolytic degradation and can sometimes accumulate in vast quantities which can cause physical damage and precipitate apoptosis of cells, leading to organ failure, and this can ultimately prove fatal. It is noteworthy that amyloid is also often found in healthy individuals in controlled quantities in most major tissues and organs without causing any overt pathological damage. Contrariwise, the accumulation and the high concentration of amyloid fibrils in disease states are pathogenic and damaging to cells and tissues. Many of the brain diseases can be characterized as amyloidoses and the most common type of amyloidosis is AD (Wisniewski et al., 1997). There are more than 30 different types of proteins which are responsible for the formation of amyloid but regardless of the type of the protein from which amyloid is formed they all share the common physical, histological and ultrastructural properties mentioned above (Ghisso and Frangione, 2002).

The formation of amyloid fibrils follows a specific pathway whereby its native form of the protein becomes misfolded and starts to aggregate. This can be illustrated by the prion protein (PrP) where the native form is predominantly  $\alpha$ -helix/random coil but can become misfolded into the “scrapie” form (PrP<sup>Sc</sup>) which is infectious and rich in  $\beta$ -sheet structure (figure 1.3) (Gosal et al., 2006; Soto, 2003; Pan et al., 1993).



**Figure 1.3: The structure of protein when misfolded into  $\beta$ -sheets.** Illustration shows the three dimensional shape and structure of the two types of prion protein, PrP<sup>C</sup> = cellular form (non-infectious) and PrP<sup>Sc</sup> = ‘scrapie’ form (infectious). The PrP<sup>Sc</sup> form has a large increase in  $\beta$ -sheet content.

The conversion of the native protein into the misfolded form is due to various changes in structure of the protein, creating an unstable intermediate misfolded protein which due to hydrophobic interactions with other similar protein molecules leads to the formation of more stable  $\beta$ -sheet oligomers. Next, the  $\beta$ -sheet oligomers grow further to form protofibrils, which finally twist around each other to form amyloid fibrils (Soto, 2003). The amyloidoses are divided in two broad categories: systemic (widespread throughout the body) or local where the amyloid is restricted only to a specific organ (such as heart, pancreas, brain, etc.). AD is classified as a local

amyloidosis due to accumulation of  $\beta$ -amyloid protein selectively in the brain, following its release by proteolytic cleavage from the amyloid precursor protein (APP).

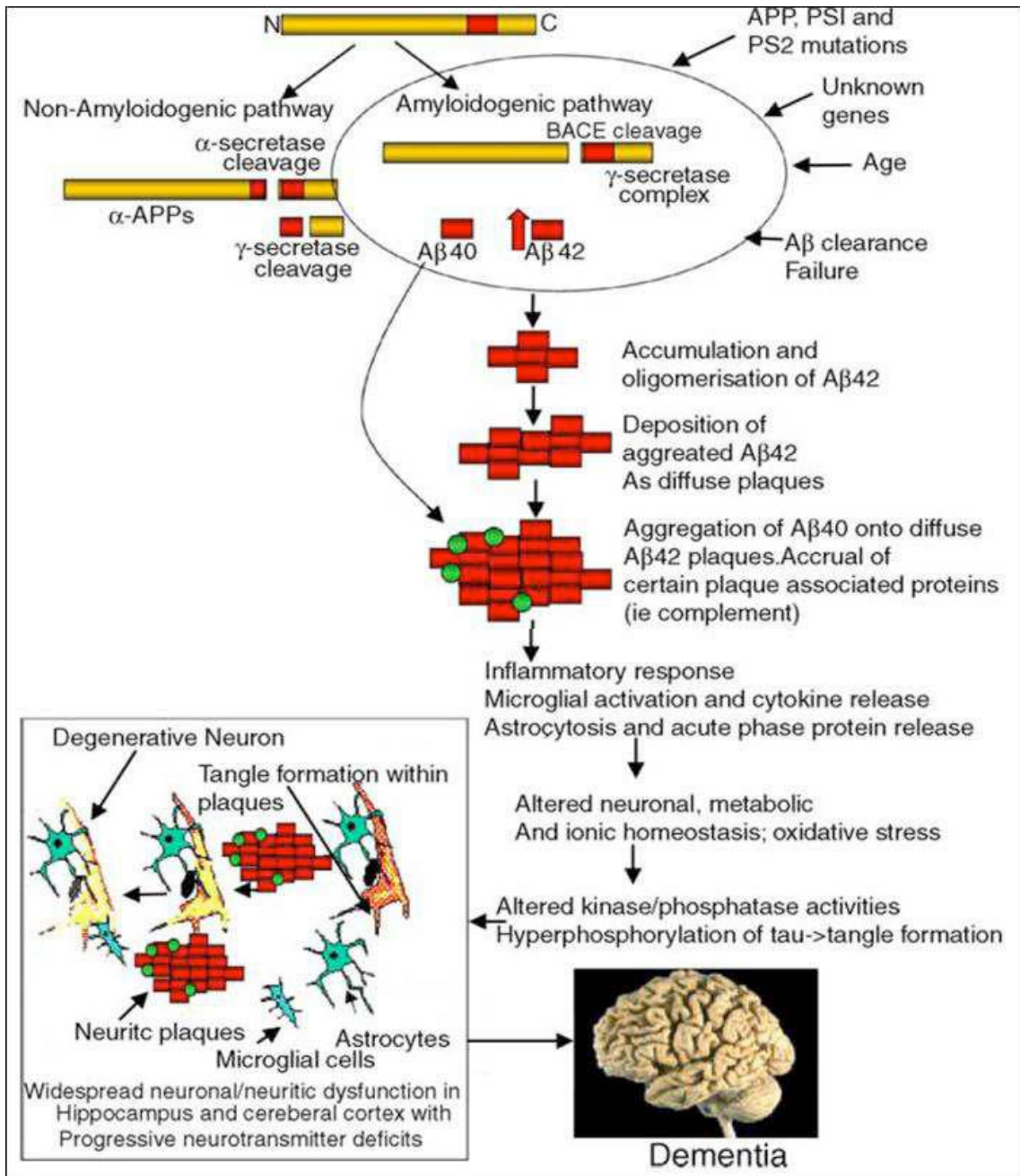
### **1.7 Formation of A $\beta$ from the amyloid precursor protein (APP)**

The amyloid precursor protein (APP) is an integral transmembrane glycoprotein and is expressed in many tissues and organs, including neuronal cells. APP belongs to a family of proteins which comprises APP along with the amyloid precursor-like proteins (APLP1 and APLP2) in animals (O'Brien and Wong, 2011). APP is processed by proteolysis to generate A $\beta$ . Alternate splicing of APP can occur and result in the generation of eight different length isoforms of the protein, but three of these are the most common. The first isoform is composed of 770 amino acids, the second is composed of 751, and both are expressed in multiple tissues and organs, while the smallest common isoform is composed of 695 amino acids and is mainly concentrated in the CNS, specifically in the brain (Allsop and Mayes, 2014; Bayer et al., 1999).

The amyloid- $\beta$  peptide is composed of 39-43 amino acids and is found even in healthy people, but in the case of AD it becomes misfolded and aggregates to form amyloid fibrils which may be toxic for nerve cells (Austen et al., 2008). A $\beta$  exists in two major forms: A $\beta$ 42 and A $\beta$ 40. Both spontaneously aggregate *in vitro* into amyloid fibrils but A $\beta$ 42 does this more rapidly than A $\beta$ 40, and so is more pathogenic. APP is partially embedded in the plasma membrane of the cell, while a large part of the protein protrudes from the surface. The A $\beta$  section of APP is also

partially embedded in the plasma membrane with the larger part (28 amino acids) of the domain outside of the transmembrane region and a smaller part (12-14 residues) embedded in the interior of the membrane (Blennow et al., 2006).

According to the action of specific proteases called secretases, APP is cleaved at three distinct sites, producing two alternative pathways, one of which is non-pathogenic, while the other releases A $\beta$ , so potentially leading to AD (see figure 1.4). The three secretases which can cleave APP are:  $\alpha$ -secretase,  $\beta$ -secretase and  $\gamma$ -secretase (Thornton et al., 2006). The pathogenic pathway resulting in production of amyloid- $\beta$  is also called the “amyloidogenic” pathway while the normal cleavage of APP does not produce A $\beta$  and is called non-amyloidogenic pathway. In the case of the non-amyloidogenic pathway, the cleavage of APP is initiated by  $\alpha$ -secretase cleavage between residues 16-17 of the A $\beta$  domain, and then  $\gamma$ -secretase follows to generate a nonpathogenic peptide called p3.



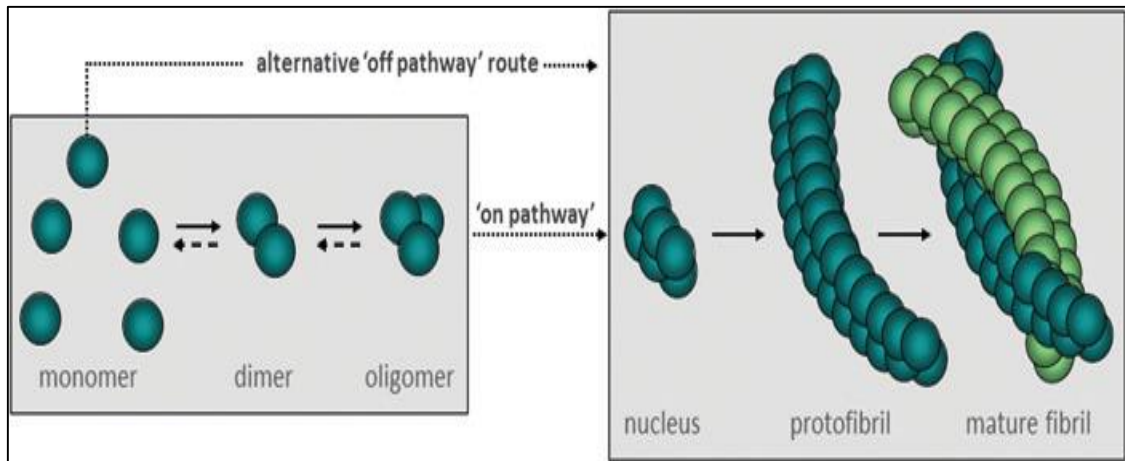
**Figure 1.4: The Amyloid cascade hypothesis.** This illustration shows how the cleavage of APP by the different secretases can lead to the non-amyloidogenic and amyloidogenic pathways (Verdile et al., 2004).



## 1.8 Amyloid cascade hypothesis

Despite many years of research the underlying cause of AD remains unclear and is still under debate (Dong et al., 2012). Among the various hypotheses for the cause of AD, the one which prevails today and is the most accepted globally is the “amyloid cascade” hypothesis (Bachman et al., 2013).

According to this hypothesis, the main event for the pathogenesis of this neurodegenerative disorder is disruption of the control mechanisms related to production of A $\beta$  and the ability to clear this toxic peptide from the brain. An imbalance in this system in favour of brain accumulation results in formation of amyloid fibrils which are potentially toxic to nerve cells (Verdile et al., 2004; Glenner and Wong 1984) and precipitate a cascade of events, including tangle formation, which culminates in neural cell damage/death. In the case of inherited diseases mutations in APP, PS1, PS2 genes result in overproduction of A $\beta$ , while in the case of sporadic disease, there is likely to be a problem with A $\beta$  clearance (Blennow et al., 2006). In a more recent “variant” of this hypothesis, toxic oligomers of A $\beta$  inhibit long-term potentiation (LTP) and disable synaptic capacity, resulting in the loss of communication between nerve cells and ultimately in their death (Blennow et al., 2006; Hardy and Selkoe 2002).



**Figure 1.5:** The diagram shows the formation of amyloid fibrils from monomeric A $\beta$ . For the formation of mature fibrils as it shown in the diagram above the monomers follow two pathways. The “ON” pathway which the monomers gradually assemble to oligomer, and then to nucleus and finally to mature fibrils while in the case of the “OFF” pathway the monomers assemble directly to nucleus and then to mature fibril. In both pathways, it is believed that the A $\beta$  oligomers are more toxic than mature fibrils (Allsop and Mayes, 2014).

According to the latter hypothesis the oligomers (dimers, trimers) are considered as a potential drug target and are believed to be more toxic than A $\beta$  fibrils. The amyloid oligomers or A $\beta$ -Derived Diffusible Ligands (ADDLs) are small, soluble and diffusible toxic entities which can block LTP and affect memory process (Tabner et al., 2005).

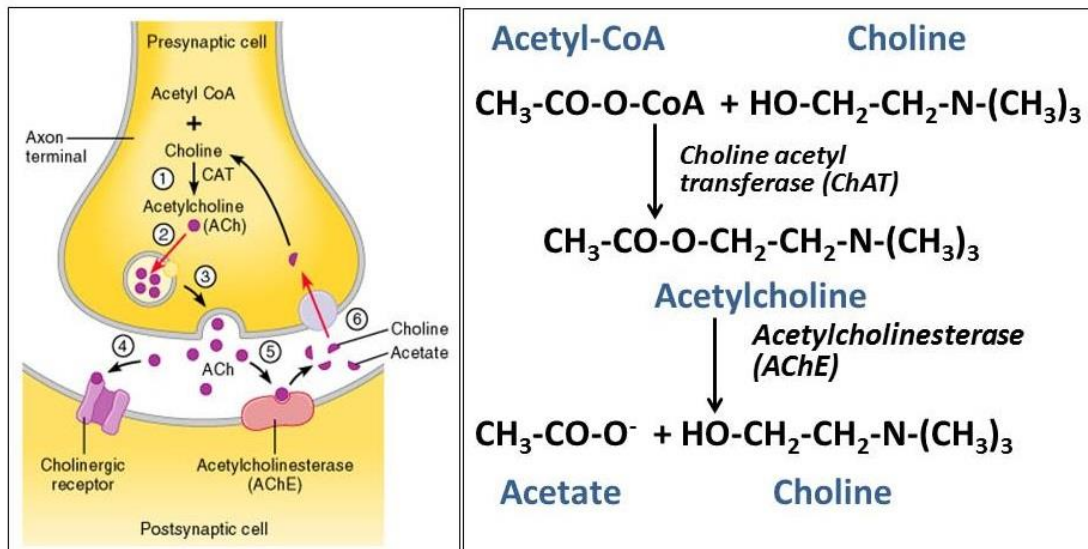
## 1.9 Current diagnosis of AD

The early diagnosis of AD could lead to early intervention and so play an important role in the treatment of the disease. Nowadays, there are a variety of methods which are used for diagnosis, but a definitive diagnosis of AD can still only be made after death when the presence of large numbers of senile plaques and neurofibrillary tangles can be verified (Van der Zee et al., 2008). A correct diagnostic work up is usually based on the medical history of the patient, memory tests and rating scales (e.g. MMSE) which confirm genuine cognitive impairment, and a neuropsychiatric examination. These above medical examinations identify any symptoms at the early stage of the disease, and, importantly can exclude other possible causes of dementia. In addition, two more useful diagnostic methods which are used to exclude other causes of dementia (e.g. brain tumor, stroke, etc.) and also reveal cerebral atrophy (an indicator of neurodegeneration) and simultaneously detect AD are Magnetic Resonance Imaging (MRI) which detects hippocampal and cerebral atrophy and Computerized Tomography (CT) (Blennow et al., 2006). Other clinical diagnostic methods which can aid in the diagnosis of AD are: cerebrospinal fluid (CSF) levels of amyloid- $\beta$  (especially A $\beta$ 42) and *Tau* protein, fluorodeoxyglucose positron emission tomography (FDG-PET) to detect a decrease in the metabolic rate of glucose utilization and Positron Emission Tomography (PET) which can be used to quantify A $\beta$  deposition in the living brain (Apostolova et al., 2010). Pittsburgh compound B (PiB) is a labelled compound which is used in PET imaging to bind to amyloid fibrils in the living brain (Forsberg et al., 2008). One of the most important aims in diagnosis of AD is early detection of the disease, because the destruction of nerves cells probably begins many years before the appearance of AD symptoms.

This can be avoided if the patient is diagnosed early. Irreversible damage to the brain and generally early diagnosis should lead to a more effective treatment, especially if there is an appropriate, disease-modifying therapy available (Nazem and Mansoori 2008; Mortimer et al., 2005).

### **1.10 Current symptomatic treatment of AD**

Even today, the effective treatment of AD remains a goal that has not been accomplished. The current treatments for AD are still only used for temporary mitigation of symptoms. The cholinergic hypothesis of AD comes from some of the first studies showing that the cholinergic neurons which protrude from the low areas of the brain up to the higher areas, and are involved in memory, are selectively lost early in the course of AD. In other words, the loss of cholinergic function is directly associated with the loss of short term memory. This finding led scientists to look for alternative ways to increase acetylcholine, or protect these neurons, and initially resulted in the development of Aricept as an effective acetylcholinesterase (Ache) inhibitor (Terry and Buccafusco, 2003).



**Figure 1.6: "Cholinergic hypothesis" of AD.** The illustration on the left shows the mechanism of how AChE inhibitors block the breakdown of ACh while the picture on the right shows the chemical reaction (the reactants and products) for the formation and the breakdown of ACh.

Acetylcholinesterase (AChE) inhibitors have the ability to block the breakdown of ACh at the synapse, in order to boost cholinergic transmission. These types of drugs, however, are only symptomatic treatments which delay cognitive decline (for 6-12 months) in some (approximately 50%) patients with AD (Blennow et al., 2006). Galantamine (Reminyl®), Donepezil-HCl (Aricept®) and Rivastigmine (Exelon®) are the 3 acetylcholinesterase inhibitor drugs currently approved by NICE for mild-moderate AD.

These drugs have little effect in severe, advanced cases of AD and are almost certainly not targeted at the underlying cause of disease and so their effects are expected to be purely symptomatic. In addition, the AChE inhibitors also have some side-effects such as nausea, vomiting, diarrhea, and some of them can cause liver toxicity. However, gastrointestinal symptoms can easily be controlled by starting the treatment with a low dose, and the drugs must be consumed with food to delay the absorption of the drug (Blennow et al., 2006).

Memantine is a differently acting drug which is used to modulate a healthy balance in the levels of glutamate neurotransmission in the brain. In normal conditions, glutamate and its interaction with the N-methyl-D-aspartate (NMDA) receptor are involved with learning and memory. On the other hand, in abnormal conditions such as AD, an increase of glutamate concentration can cause decreased function of NMDA receptors and be fatal for nerve cells. Memantine is a non-competitive antagonist of the NMDA receptor (Areosa et al., 2005) and is the only drug currently approved by NICE for more advanced AD, but again has only a modest effect on the disease. In addition to the AChE inhibitors there are also some alternative therapeutic approaches which have been under development for AD.

#### *Inhibition of $\beta$ -secretase or $\gamma$ -secretase and stimulation of $\alpha$ -secretase*

The secretases play important role in the proteolysis of APP and generation of A $\beta$  which then aggregates into toxic oligomers. More specifically,  *$\beta$ -secretase* and  *$\gamma$ -secretase* are the two secretases which are responsible for the production of A $\beta$ , and so inhibition of either of these two secretases could provide a viable therapy for AD.  *$\beta$ -secretase* activity is due to an integral membrane aspartyl protease called BACE1, but development of BACE1 inhibitors has proved to be difficult because of inherent medicinal chemistry problems (the enzyme has a large binding pocket). Regarding  *$\gamma$ -secretase*, this enzyme also cleaves notch and so inhibitors of this enzyme will also interfere with notch processing. Notch receptor is single-pass transmembrane receptor protein. Notch signaling has the ability to proliferate signaling during neurogenesis (Xiao, et al., 2009). On the other hand, the action of  *$\alpha$ -secretase* prevents the formation of A $\beta$ , although it also cleaves several important growth

factor precursors at the membrane. This enzyme has been identified as a metalloprotease, but it is easier to develop drugs which inhibit rather than stimulate enzyme activity. Moreover, stimulation of  $\alpha$ -secretase could have negative consequences due to a decrease in the levels of cholesterol, and effects on activation of G-protein-coupled receptors (Grandy, 2005; Petit et al., 2001).

### A $\beta$ immunotherapy

In the field of immunotherapy, scientists have developed an AD vaccine (AN1792) in the form of aggregated A $\beta$ 42 or anti-A $\beta$  antibodies which can clear the amyloid plaques from the brain (Fu et al., 2010). Unfortunately, trials of this type of vaccine were initially stopped during phase III because some patients developed severe aseptic encephalitis and brain inflammation (Fu et al., 2010; Blennow et al., 2006). There are two types of immunotherapy: (a) active and (b) passive immunotherapy. In the case of active immunotherapy attenuated A $\beta$  or synthetic A $\beta$  was administered to patients in order to stimulate cellular and humoral immune responses in the host and to generate anti-A $\beta$  antibodies, while in passive immunotherapy, A $\beta$ -specific antibodies are directly injected into the patient (Fu et al., 2010). AN1792 vaccine was an example of active immunotherapy. Treatment of AD has also involved use of passive immunotherapies such as: Lilly's solanezumab, Pfizer's bapineuzumab and Roche's Gantenerumab, which substantially reduced A $\beta$ . Solanezumab is a humanized monoclonal antibody against A $\beta$  which failed against its target, although it did show 30% efficacy in patients with mild disease. NIH taking this further with a 1,000-patient study that is expected to yield results in 2018. Bapineuzumab was stopped in clinical phase III trials in 2014 because it did not have

any improvement in the clinical outcomes of AD, while Gantenerumab was stopped in phase III in 2014 in the people with mild cognitive impairment (MCI).

### *Inhibition of TAU protein*

Another possible therapy is to inhibit formation of the neurofibrillary tangles which are created from the aggregation of Tau protein. Neurofibrillary tangles are dense rays of filaments that form inside the nerve cells. They are likely to be damaging to nerve cells, for example by inhibiting axonal transport (Mangialasche et al., 2010). However, inhibitors of Tau aggregation have produced disappointed results, with some drugs such as valproate and lithium giving side-effects, although others such as methylioninium chloride have produced better results (Mangialasche et al., 2010; Brodaty et al., 2011). Methylioninium chloride is also called methylene blue or “Rember” and is one of the most promising drugs for inhibition of Tau protein aggregation. According to a recent study, Wischik and coworkers have postulated that the aggregation of Tau protein inside the nerve cells leads more directly to the development of dementia (Wischik et al., 2008). In 2008, Wischik and coworkers reported that methylioninium chloride phase 2 clinical trials in AD gave promising results, with positive expectations for the future (Wischik et al., 2008). However, methylioninium chloride is likely to have multiple effects, for example it also has an effect on mitochondrial function by enhancing key mitochondrial biochemical pathways. Here, methylioninium chloride is able to limit the inhibition and increase the complex IV activity, which is directly associated with AD (Atamna et al., 2008).



### A $\beta$ fibrillization inhibitors

The aim of these inhibitors is to prevent the conformational change of A $\beta$  to  $\beta$ -sheet structures, and finally to fibrilization of A $\beta$ , by intervening in interactions between A $\beta$  - A $\beta$  or A $\beta$  - ApoE. One of the drugs which has been shown to reduce the formation of A $\beta$  fibrils is NC-531 which interferes with the association between glycosaminoglycans and A $\beta$ . This drug is still in phase III clinical trials. Another drug which was used for the inhibition of A $\beta$  fibrils is the metal chelator clioquinol (PBT-1), which initially showed positive results, but after phase II clinical trials was stopped due to toxic impurities (a di-iodo form of clioquinol). A previous version of drug which called PBT-2 and does not contain any toxic compounds, such as iodine, is currently undergoing clinical trials (Geerts, 2004; Cherny et al., 2000; Ritchie et al., 2003).

### Inhibition of A $\beta$ oligomer formation

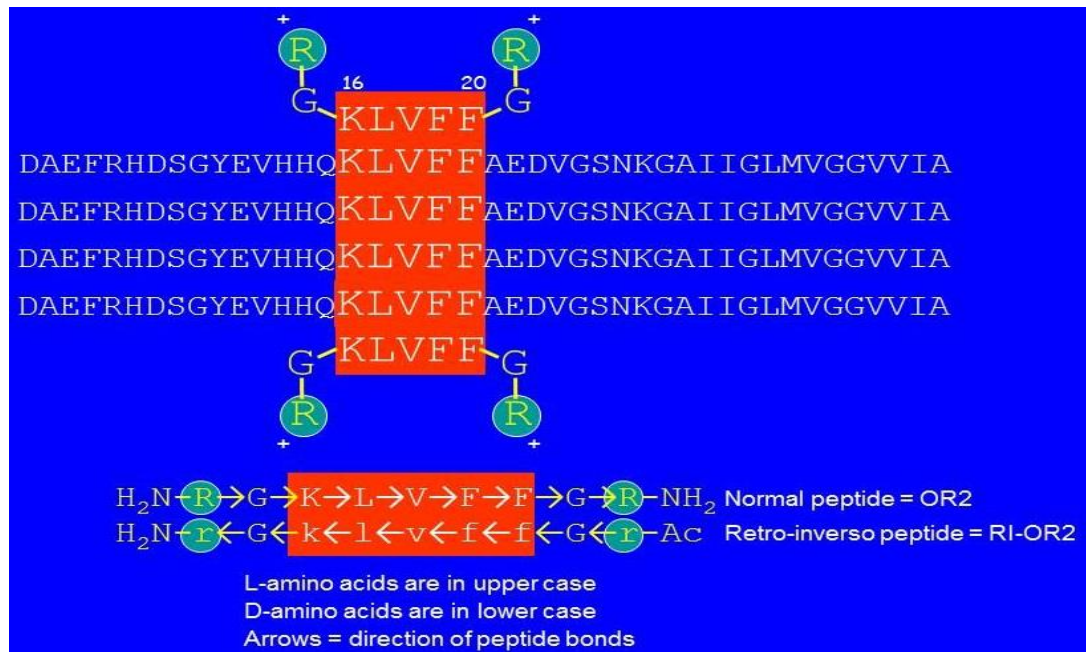
The development of small molecules or peptide inhibitors which have the potential to bind to A $\beta$  and prevent the formation of toxic A $\beta$  oligomers is a promising strategy (Parthsarathy et al., 2013) which could delay or even halt the progression of AD, if given at an early stage during the course of the disease.

#### **1.11 The evolution of peptide inhibitors against the $\beta$ -amyloid oligomerization**

We and others have been working on development of peptides which have the potential to bind to A $\beta$  and inhibit the formation of early amyloid- $\beta$  oligomers. A variety of different types of A $\beta$  aggregation inhibitors have been described in the

literature but most of them are unsuitable for clinical development, and so few of them have progressed to animal testing and even fewer to human clinical trials (Taylor et al., 2010; Howlett, 2011; Karran et al., 2011; Parthasarathy et al., 2013; Ma et al., 2009). Many of the peptide-based inhibitors are based on the finding that the internal sequence KLVFF (amino acids 16-20) is involved in binding interactions between A $\beta$  molecules (Tjernberg et al., 1996; Tjernberg et al., 1999).

Initially, many of the attempts to develop aggregation inhibitors were based on inhibition of the late fibrillary form of A $\beta$  rather than the early oligomeric assemblies. Soto and colleagues (Soto et al., 1996, Soto et al., 1998) developed “ $\beta$ -sheet breaker peptides” by adding proline residues into the binding region of the amyloid peptide, for destabilization of the  $\beta$ -sheet-rich structure which initiates aggregation (Adessi and Soto, 2002). The use of N-methylated peptides (or meptides) is an alternative approach, where the inhibitors has the ability to bind to the aggregating A $\beta$  peptide via one face of the inhibitor but is unable to bind via the other (Kokkoni et al., 2006). Another different strategy was based on ten residues of the A $\beta$  peptide sequence (specifically from residues 15-25 of the peptide) linked to an oligolysine disrupting element. Unfortunately, these types of peptide inhibitors proved to be unsuitable for further clinical development as they don't completely inhibit the aggregation but cause a change in aggregation kinetics (Ghanta et al., 1996).



**Figure 1.7: Peptide inhibitors of A $\beta$  aggregation.** This illustration indicates the structure and the sequence of amino acids of the two inhibitor generations: the normal peptide (OR2) and retro-inverso peptide (RI-OR2). In the case of RI-OR2 version all of the L-amino acids are replaced with D-amino acids and the sequence is reversed resulting in the generation of a peptide which has a similar 3D orientation but the backbone of the peptide is backwards. The red highlighted region on the amino acid sequence (16-20) indicates the binding site of the peptide inhibitor. The Arginine – Glycine termini were added to prevent self-aggregation of the peptide.

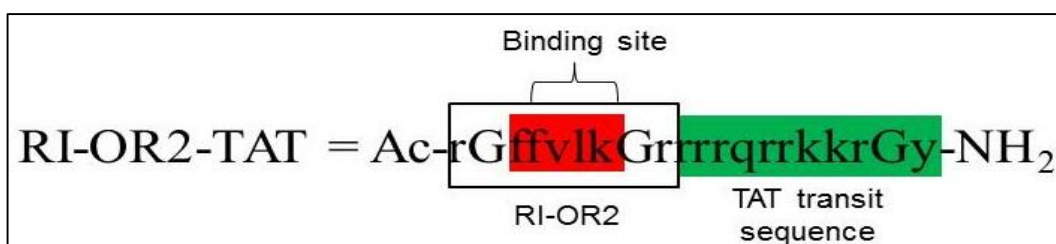
In a more, recent study Austen et al. (2008) designed two peptide aggregation inhibitors having as their main sequence the central amino acid region of A $\beta$  (residues 15-25 KLVFF) which is responsible for the binding association between A $\beta$  peptides. The two peptide inhibitors were OR1 and OR2, and contained additional arginine (R) and glycine (G) residues on both ends of the molecule, in order to enhance solubility. The cationic arginine (R) was added to the peptide sequence through a simple Glycine (G) spacer, which prevents them from self-aggregating, while still allowing the interaction between the inhibitor peptides and amyloid- $\beta$  molecules. The only difference between the two peptide inhibitors is that OR1 has an

amine group at the N-terminal end and a carboxyl group at the C-terminal end, while the OR2 inhibitor has an acetyl group on N terminal and amide on C.

Both OR1 (H<sub>2</sub>N-RGKLVFFGR-COOH) and OR2 (H<sub>2</sub>N-RGKLVFFGR- NH<sub>2</sub>) had the ability to inhibit the formation of A $\beta$  fibrils, but according to results obtained with different techniques such as Th-T assay, Transmission Electron Microscopy (TEM), ELISA assays and Congo red binding, OR2 was proven to be more effective than OR1 because it had the greater potential to inhibit the formation of early A $\beta$  oligomers (Taylor et al., 2010). On the other hand OR1 appeared to block formation of fibrils but not early A $\beta$  oligomers. Consequently, further efforts were then focused on the OR2 inhibitor peptide. Despite the effective anti-aggregational properties of the OR2 peptide inhibitor, there are many proteolytic sites on the inhibitor which would render it unsuitable as a drug candidate (Taylor et al., 2010; Austen et al., 2008). In order to overcome this limitation, a new “retro-inverso” version of the OR2 inhibitor peptide called RI-OR2 was developed (Chorev and Goodman 1995; Taylor et al., 2010). Taylor and co-workers developed this new version of the peptide inhibitor by replacing the L-amino acids with D-amino acids and by reversing the bonds of the peptide.

Even though RI-OR2 was still effective as an aggregation inhibitor it was not designed for penetration through the Blood Brain Barrier (BBB). Consequently, Parthasarathy and co-workers attached a retro-inverted version of the HIV (Human Immunodeficiency Virus) protein “TAT” (trans-activating transcriptional activator) onto RI-OR2 in order to increase its delivery into nerves cells, and also facilitate its

passage across the BBB. The newly formed version of the peptide was called RI-OR2-TAT (Ac-rGffvlkGrrrrqrrkkrGy-NH<sub>2</sub>) (Parthsarathy et al., 2013).



**Figure 1.8: The modification of peptide to enable brain penetration.** *This illustration shows the different functional regions of the peptide inhibitor RI-OR2-TAT and specifically the TAT transit sequence which was also retroinverted.*

## 1.12 Development of new therapies for AD

### 1.12.1 Biological aspects for drug delivery in the Central Nervous System (CNS)

The brain is one of the most sensitive systems of the human body and the presence of the BBB is necessary for the maintenance of its homeostasis (Masserini, 2013). The anatomy in the capillaries of brain has evolved in such way as to prevent the passage of any toxic or unwanted molecules or chemicals which can harm the brain (Gabathuler, 2010). The BBB and the blood-cerebrospinal fluid barrier (B-CSFB) are the two types of barriers which coexist in the human organism and function simultaneously in order to separate the peripheral circulation from the CNS. Furthermore, in order to function properly, all of the biochemical processes of the nervous system, such as neurotransmission, the generation of new neurons, the development of new blood vessels, and other functions, require both barriers to be intact to keep in balance the chemical composition of the neuronal “milieu” (Spuch

and Navarro, 2011). The BBB has as a functional unit the cerebrovascular endothelial cells, the B-CSFB has as a functional unit the choroid plexus epithelium, and eventually the third barrier is the arachnoid epithelium (Neuwelt et al., 2008).

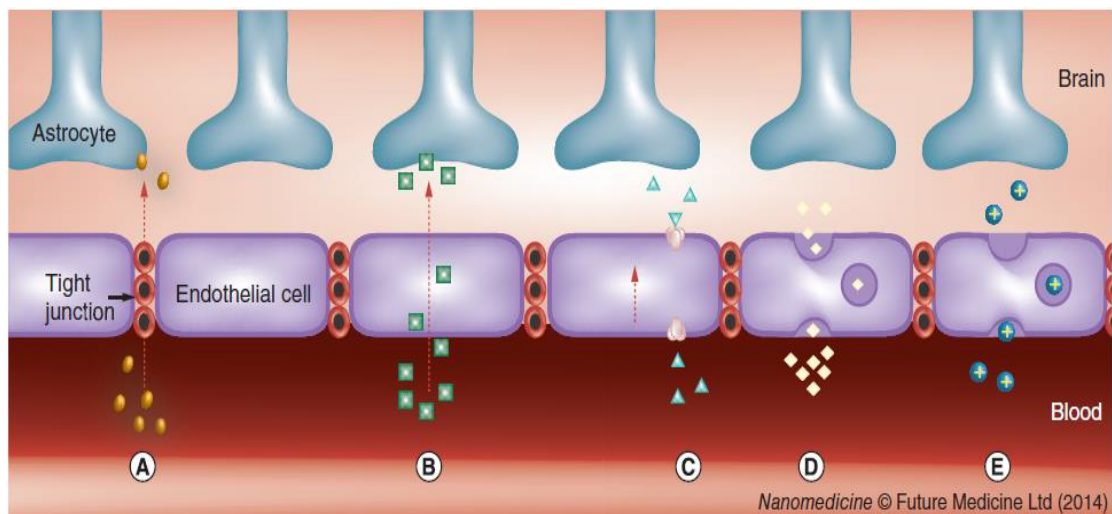
### **1.12.2 Blood Brain Barrier (BBB)**

The BBB is composed of a complex of capillary endothelium, astrocytes, pericytes, and extracellular matrix and forms an effective security system for the brain. The presence of tight junctions among the endothelial cells makes the barrier impermeable for many substances found in the blood (Sandoval and Witt, 2008). The BBB is only permeable to certain molecules, ions and specific macromolecules such as nutrients which must enter the brain or exit from it as waste products. Based on a recent study, only the 2% of the small molecules with molecular weight smaller than 500 Da in the blood are able to cross the barrier while all of the larger molecules in the blood, with molecular weight greater than 1 kD do not cross the BBB (Pardridge, 2007). Figure 1.9 shows the possible ways by which a molecule or ion can pass through the BBB. However, the BBB also restricts the delivery of numerous drugs designed to prevent the treatment of many neurological diseases. Only a small number of drugs are able to cross the BBB and finally reach their target in the brain. To be able to do so these molecules require some special properties such as lipophilicity, a size smaller than ~50 Da, and evasion of the mechanism of active extrusion (Gabathuler, 2010). Consequently, due to the strict limitations to the permeability of different molecules and drugs from the blood circulation through the

BBB, some diseases which are related with the brain or the CNS are difficult or even impossible to diagnose and cure effectively.

### 1.12.3 Blood–cerebrospinal fluid barrier (B-CSFB)

The cerebral ventricles in the brain coexist with the choroid plexus which is a branched vascular tissue. The epithelial cells of the choroid plexus constitute the B-CSFB which are joined together by tight junctions and control the permeability of different molecules and nutrients. In addition, on the surface of the epithelial cells are numerous villi which project from the cells and facilitate the secretion of cerebrospinal fluid (Spector and Johanson, 1989).



**Figure 1.9: Forms of passage of substances into the brain across the blood-brain barrier.** *This illustration shows five possible ways of passage of substances through the BBB accord to the nature of the substance. (A) Paracellular aqueous pathway, (B) transcellular pathway, (C) Through membrane proteins, (D) receptor-mediated transcytosis of macromolecules and (E) Adsorptive transcytosis (Loureiro et al., 2014).*

#### **1.12.4 Strategies for overcoming the Blood Brain Barrier**

CNS disorders constitute one of the main challenges for pharmaceutical companies and academic research teams due to their complexity, but also due to the presence of the BBB which prevents use of a wide spectrum of drugs. This especially applies to drugs directed at CNS diseases such as AD, PD and brain tumors. So the challenge for scientists is to discover strategies and construct drugs which have the potential to penetrate from the blood circulation system through the BBB. This has already started and they have managed to overcome this obstacle with the help of nanotechnology.

### **1.13 Nanotechnology**

#### **1.13.1 Nanomedicine for drug delivery in the CNS**

Nanotechnology can be defined as the science and engineering required for construction and manipulation of small particles on the nanometer scale (Burda et al., 2005). Nanotechnology and nanoparticles have started to be applied in a wide spectrum of scientific sectors in the last decade, such as the environmental sector, industrial and food agriculture sector, and of course in the field of biomedicine (Zaman et al., 2014). Interactions of artificial nanoparticles with biological systems with the aim of providing improved diagnosis and treatment of various diseases, is referred as “nanomedicine” which is a sub category of nanotechnology. In other words, nanomedicine is the medical application of nanotechnology (Gondin et al., 2011).



Nowadays, the development of nanoparticles (NPs) plays very important role in the diagnosis and the treatment of many CNS diseases. A variety of different types of nanoparticles are used in medicine, such as: lipoplex, dendrimers, polymeric nanoparticles, polymeric micelles, nanotubes, silica nanoparticle, quantum dots, gold nanoparticles, magnetic nanoparticles, solid lipid nanoparticles, non-polymeric micelles and liposomes but the majority of them are composed of polymers and lipids, or a combination of both of these two (Wong et al., 2011). Consequently, the chemical composition of the nanoparticles constitutes an important element for their correct function. In addition, to their chemical composition, the size, shape and surface charge are also important parameters which can influence the ability of nanoparticles to pass through the BBB as well as determine their stability in the blood circulation system (Conti et al., 2006; Euliss et al., 2006). The rationale of using nanoparticles specifically for brain drug delivery is due to their unique features and advantages as biological carriers (Tassa et al., 2010). NPs can be defined as small, spherical and colloidal particles which have the ability to transfer a drug or therapeutic agent either inside of the nanoparticle, or by covalent attachment onto the surface of the nanoparticle. Some of the properties of these particles which make them ideal for the use in the field of medicine are:

1. These particles can carry many diagnostic and therapeutic agents either by attaching them by covalent bonds on their surface or encapsulated them.
2. The materials from which these nanoparticles are made can be biocompatible and biodegradable, such as lipids (nanoliposomes).
3. Additionally, due to some unique features of nanoparticles such as chemical and biological stability, maintenance of NPs in the circulation system for a


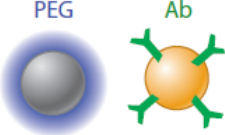
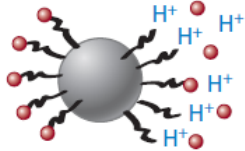
long time after administration is feasible as well multiple ways of administration (oral, inhalational and paracentral), and so nanoparticles can be considered as ideal drug carriers for medical use (Pektar et al., 2011).

4. Modification of the liposome surface with targeting agents such as polyethylene glycol (MAL-PEG) can lead to the creation of liposomes with high stability in the blood circulation and increase their lifespan.
5. These PEGylated liposomes have “stealth properties” and as a result can hide from the immune system – protecting them for immune system clearance and helping to prevent adverse immune reactions.

### **1.13.2 The generations of Nanoparticles (NPs)**

Based on many previous studies, scientists have managed to improve the nanoparticles to a great degree by modifying them, and learning more about their key characteristics such as size, structure, chemical composition and surface charge. Figure 1.10 summarizes the three generations of nanoparticles which have been applied in a variety of biological systems and experiments. Nanoparticles which belong to the first generation are made of innovative nanomaterials which were tested for their toxicity, cell uptake and biocompatibility (Kirchner, et al. 2005; Chithrani, et al., 2006). These experiments confirmed that nanoparticles of the first generation were unstable, and rapidly cleared from biological systems, which led scientists to design a new generation of nanoparticles (De Jong et al., 2008; Cherukuri et al., 2006). This second generation involved upgrading the chemical surface to improve stability, and their evolution was focused on two interconnected

concepts: (a) stealth, where liposomes are more stable and have a longer lifespan in the circulating system and (b) active targeting. An important molecule which was applied to the surface of the second generation of nanoparticles was the synthetic polymer poly-(ethylene glycol) (PEG). The incorporation of PEG molecule into liposomes led to the development of an innovative generation of more stable nanoparticles and more specifically nanoliposomes with great potential in the sector of medicine (Perrault et al., 2009; Zhang et al., 2009; Gref et al., 2000; Needham et al., 1992). However, the evolution of nanoparticles has continued with the development of a third generation with emphasis on how to design a much more sophisticated and responsive nano device which can deliver a therapeutic compound and act as an effective drug carrier in biological systems (Albanese et al., 2012).

	1 <sup>st</sup> generation	2 <sup>nd</sup> generation	3 <sup>rd</sup> generation
			
<b>Nano-materials</b>	<ul style="list-style-type: none"> <li>• Material design</li> <li>• Water solubility</li> <li>• Biocompatibility</li> </ul>	<ul style="list-style-type: none"> <li>• Maximize delivery</li> <li>• Stealth (passive)</li> <li>• Active targeting</li> </ul>	<ul style="list-style-type: none"> <li>• Environment-responsive</li> <li>• Dynamic properties</li> <li>• Biological or external cues</li> <li>• Theranostic abilities</li> </ul>
<b>Biological challenges</b>	<ul style="list-style-type: none"> <li>• Unstable</li> <li>• Removal by MPS</li> <li>• Poor tumor targeting</li> </ul>	<ul style="list-style-type: none"> <li>• Overreliance on EPR effect</li> <li>• No “universal” antigen</li> <li>• Active targeting is disappointing</li> <li>• &lt;10% dose in tumor</li> </ul>	<ul style="list-style-type: none"> <li>• To be determined</li> </ul>

**Figure 1.10: The three generations of nanoparticles.** The following diagram shows and compares the three generations of nanoparticles and their characteristics as well as and the fundamental bio-nano studies (MPS: mononuclear phagocyte system, EPR: enhanced permeation and retention) (Albanese, et al., 2012).

Despite all of the options which scientists had, to develop the ideal drug carrier, relatively simple nanoparticles made of liposomes (nanoliposomes) consisting of a single lipid bilayer (unilamellar) or many bilayers (multilamellar vesicles) have proved to be the most common and the most suitable type of nanoparticle for medical use.

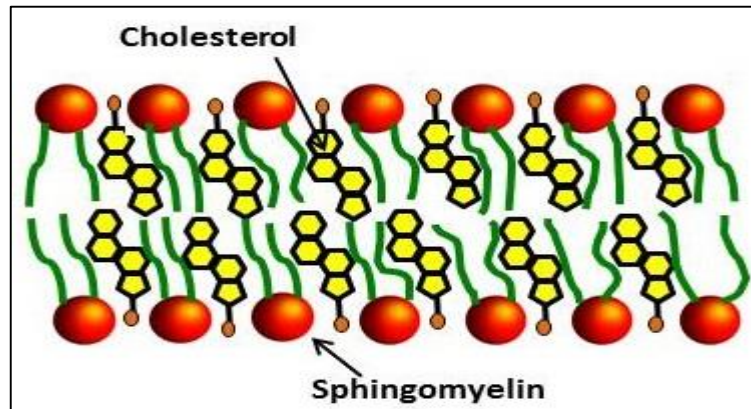
## **1.14 Liposomes design and function**

### **1.14.1 Liposomes general features**

Liposomes are small auto-assembly spherical vesicles which are mainly made from non-toxic lipids, and phospholipids, and were first described by haematologist Dr. Alec Bangham in the early 1960s (Dua et al., 2012). Liposomes have been widely used as delivery systems. Their size usually varies from a few nanometers (~20 nm) to several micrometers (~5  $\mu\text{m}$ ) but the ideal size for medical use is in the range 50 – 450 nm (Etheridge et al., 2013). The most common materials which are used for the creation of liposomes are biocompatible and biodegradable lipids such as sphingomyelin, phosphoglycerides and phosphatidylcholine, and two or more lipids can be combined together in a mixture. Phospholipids are amphipathic molecules which have hydrophobic and hydrophilic properties (two hydrophobic tail made of hydrocarbon chains and a hydrophilic head which consisted by a phosphate group). For the creation of a liposome mixture, the lipids usually are dissolved in an organic solvent (e.g. chloroform) and then, the evaporation of lipid mixture follows to obtain a lipid film. Then, when the dry lipid film comes in contact with water, it spontaneously forms spherical vesicles, separating the inner space from the outer

(Vemuri and Rhodes, 1995; Vuilleumard, 1991; Gabizon et al., 1998; Akbarzadeh et al., 2013). The hydrophobic and hydrophilic properties of the lipids determine the spherical shape of liposomes, in which an aqueous volume is encapsulated in the central core of each liposome. The chemical composition of liposomes is obviously an important factor for their correct function, and in addition to standard phospholipids, the insertion of cholesterol can improve the structural characteristics of the membrane.

The presence of cholesterol in the membrane of liposomes is very important because it maintains the stability of the membranes *in vivo* and *in vitro*, and also decreases their permeability (Masserini, 2013; Lee et al., 2005). This is mainly due to the hydrophobic properties of cholesterol, based on its molecular structure with the four hydrocarbon rings, and as a result it has a tendency to interact with the central region of the membrane. Specifically when cholesterol reacts with unsaturated lipids which form kink in the chain, it is able to cover the space and so create a more stable, and rigid membrane by decreasing the flexibility of surrounding lipid chains. Cholesterol molecule in membranes is located parallel with phospholipids and the hydroxyl group interacts with the nearby phospholipid head groups (see figure 1.11) (Bozzuto and Molinari 2015). Consequently, cholesterol is considered an important lipid for the creation of liposomes because it can affect their properties.



**Figure 1.11:** Cholesterol disrupts the tight packing of the fatty acids. *The illustration shows the orientation of cholesterol with sphingomyelin in membranes to the fatty acid chains and also the hydroxyl group of cholesterol (orange) interacts with the head group (red) of sphingomyelin.*

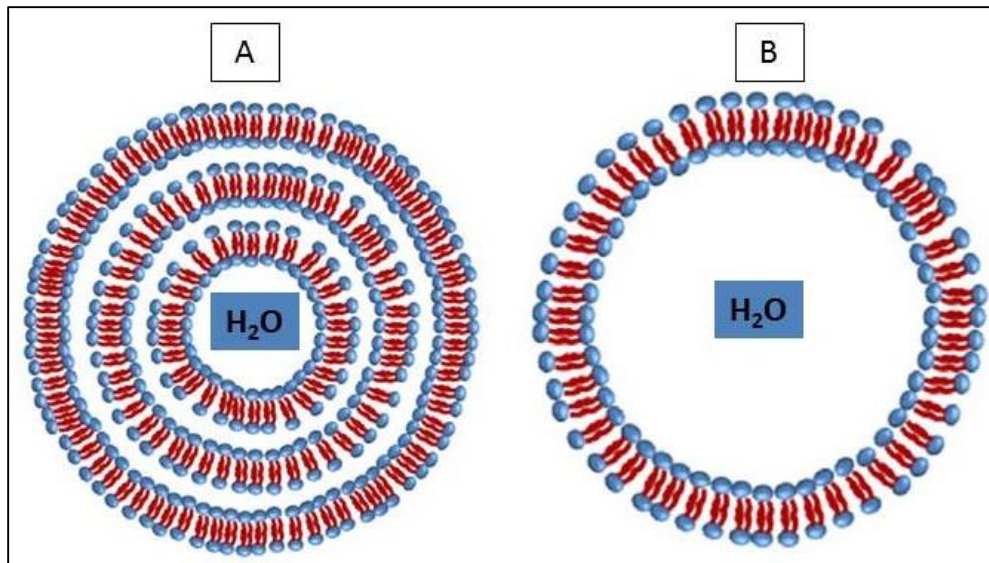
There are four classical methods which are used for the production of liposomes: Bangham method (hydration of lipid film), Reverse-Phase Evaporation (REV) technique, solvent (ether or ethanol) injection technique and detergent dialysis. Selection of the preparation method depends on several factors such as: the physicochemical characteristics of lipids, the toxicity of the loaded component, the cost of the whole method, and the size of liposome. Nevertheless, the most common technique is the Bangham method. The production of the liposomes is followed by a freeze and thaw process, sonication, and finally the extrusion of the liposomes through a membrane in order to generate liposomes with controlled sizes (Dua et al., 2012; Wagner and Vorauer-Uhl 2011; Bangham et al., 1965).

#### **1.14.2 Classification of liposomes**

In addition to their composition, liposomes are also classified based on their size and the number of bilayers (lamellarity) which are formed during their preparation. The size of liposomes plays a crucial role in determining whether they can pass through the blood vessel walls to target the lesions in cancer for example or pass through the BBB (in the case of brain diseases such as AD). Consequently, the

size of liposomes constitutes an important factor which can affect the success of the nanocarrier. Based on previous studies, scientists have found that liposomes of around 100-140 nm present some advantages, such as avoiding the interaction with plasma proteins, and evading the reticuloendothelial system (RES), which contribute to a longer half-life in the blood circulation (Fanciullino and Ciccolini 2009). On the other hand, PEGylated liposomes larger than 100 nm in diameter have a shorter half-life because they are less able to evade the reticuloendothelial system. In a previous study which was carried out in order to test the time for the clearance of PEGylated liposomes of the same composition, it was found that those with 250 nm size were removed from the circulation more than twice as fast as liposomes 100 nm size (Woodle et al., 1992). However, smaller liposomes in the region of ~100 nm have a limited drug-storage capacity compared with larger sized liposomes (Allen, 1995).

With regard to the number of bilayers, liposomes belong in two main categories: (a) multilamellar vesicles (MLV) and (b) unilamellar vesicles. Multilamellar vesicles range from 100 nm upwards and can reach a diameter of a few  $\mu m$  with many bilayers formed by the incorporation of many unilamellar liposomes inside one another to form an onion-like structure, while in unilamellar vesicles, the liposome has only one bilayer with a diameter of 0.25  $\mu m$  – 400 nm and they can encapsulate hydrophilic drugs. In addition, unilamellar vesicles can also be divided into two subcategories as follows: (i) Large Unilamellar Vesicles (LUV) with a diameter larger than 100 nm and (ii) Small Unilamellar Vesicles (SUV) with diameter about 20 nm up to 100 nm (Amarnath and Sharma 1997; Shaheen et al., 2006; Masserini, 2013).



**Figure 1.12: Modified illustration indicates the structure of two types of simple liposomes based on the number of layers.** The (A) illustration represents a multilamellar vesicle which has three layers while the illustration (B) represents a unilamellar vesicle with a single layer. With both types of liposomes, during their formation, an aqueous volume is encapsulated in the central core. The hydrophilic heads of lipids interact with water while the hydrophobic tails avoid the interactions with water (Patil and Jadhav, 2014).

### 1.14.3 Stealth liposomes and conventional liposomes

It is important to note that the majority of artificial liposomes are composed of the same lipids as those found in the cell membrane, and so they constitute a familiar and friendly environment for transfer of any agent into the cell (Huang et al., 2014). Liposomes are therefore a harmless “invader” for the human body. Nevertheless, liposomes can be detected by the mononuclear phagocytic system (MPS) and cleared during blood circulation, creating some issues with their stability (Akbarzadeh et al., 2013; Maruyama et al., 1992).



As referred to above, the evolution of nanoparticles has solved some of these problems, one of these being their limited stability *in vivo*. Combining several methods, scientists have managed to overcome some of the limitations of liposomes by using coated liposomes (e.g. with chitin derivatives) and mainly by PEGylation of liposomes (attachment of polyethylene glycol molecules on the surface of the liposomes) (Shaheen et al., 2006). These are defined as “stealth liposomes” because, with PEGylation, liposomes are able to evade the immune system by decreasing their clearance from MPS so increasing their half-life *in vivo* (Bedu-Addo et al., 1996; Korgel et al., 1998; Drummond et al., 1999).

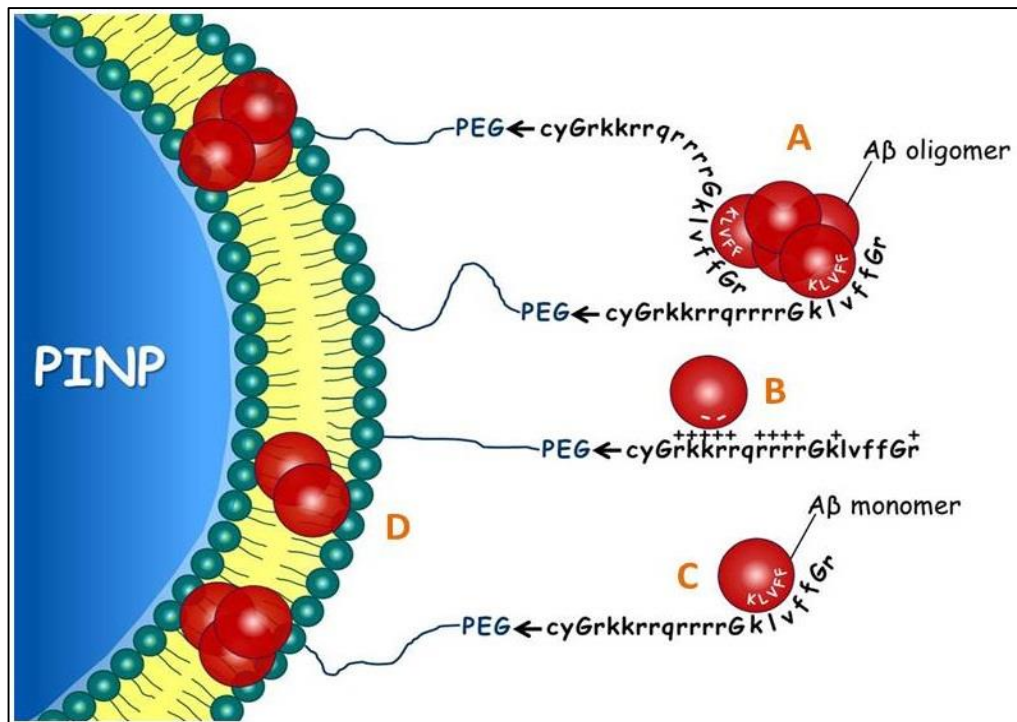
#### **1.14.4 Attachment of targeting peptides on the surface of liposomes - Peptide Inhibitor Nanoparticles (PINPs)**

The development of “stealth liposomes” has provided many prospects for the treatment of various diseases in the future, and they act as targeted bioactive molecules. There are several methods for the conjugation of targeting peptides, antibodies, proteins or drugs on the surface of liposomes, but for the design of targeted vesicles there are two main approaches (a) the attachment of the targeted ligand onto the surface of the liposome can be done during the preparation of the liposomes, or (b) the ligand can be conjugated onto the surface of the liposomes after their preparation, by covalent bonding. The most common type of ligand conjugation on the surface of liposomes is carried out by ligands which contain molecules with a thiol group to react with maleimide or bromoacetyl anchors, forming two types of bonds (thioether or disulfide bonds) (Schuber et al., 2007;

Barbet et al., 1981). In addition, another common type of conjugation of a ligand on the surface of vesicles is where the ligand is coupled at the end of a polyethylene glycol (PEG) chain molecule which is already attached on the liposome's surface (Zalipsky et al., 1997; Sudimack and Lee, 2000).

In the current study, I have attached the peptide inhibitor (RI-OR2-TAT) onto the surface of nanoliposomes to improve its potency as a drug for inhibiting aggregation of amyloid- $\beta$  in the brain. PINPs due to the presence of MAL-PEG molecules attached on their surface have the properties of stealth NPs and which can hide from the immune system – improving circulation time and bioavailability. Based on previous studies, RI-OR2-TAT has shown promising prospects such as BBB permeability and good stability in the blood circulation that would make it a suitable drug for the treatment of AD. A group of collaborating scientists in Italy have used an artificial cell BBB model with a monolayer of hCMEC/D3 cells in order to check the ability of PINPs to pass through the monolayer. The results of that experiment suggested that PINPs should cross into the brain without any difficulty. In addition, PINPs themselves are not toxic to cells as they are composed of simple lipids and the peptide. Previous to this project, the nanoliposomes were prepared in Italy, and specifically in Milano at the University of Milano-Bicocca, by Professor Massimo Masserini and Dr. Maria Gregori using cholesterol and sphingomyelin phospholipids (1:1/molar ratio) with 2.5% maleimide, and sent to us for analysis. One of the main aims of this project was to be able to manufacture and develop our own PINPs at Lancaster University, by producing the nanoliposomes, with their attached peptide, in a similar way to the Italian group, in three different sizes (50 nm, 100 nm and 200 nm). Each PINP with approximately 100 nm diameter has ~1690 peptides molecules

attached, and could capture many A $\beta$  monomers, oligomers or fibrils with the possible mechanisms shown in figure 1.13.

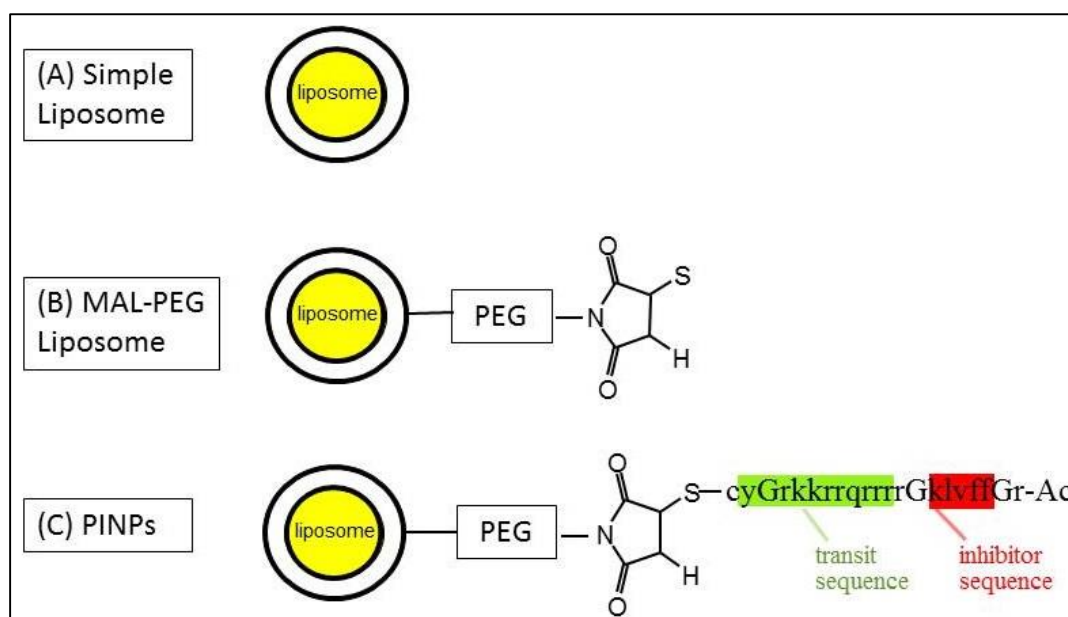


**Figure 1.13: Possible mechanism of action of PINPs on A $\beta$  monomers or oligomers.** *This illustration indicates the possible mechanisms by which PINPs could act on A $\beta$ . Each red sphere represents a monomer of A $\beta$ . The PEGylated liposome has the RI-OR2-TAT peptide attached on its surface and potentially captures monomers or oligomers, the latter involving multivalent interactions (A and C). Probably interactions with the charged region of the transit sequence as well as insertion of oligomers into the membrane of the liposome are feasible (B and D) (Gregori et al., 2015 manuscript submitted).*

## 1.15 Scope of the Thesis

The aims of the project are to investigate the best carrier technology for RI-peptide inhibitors.

1. To produce and characterize (by size and shape-ultrastructure) simple, PEGylated liposomes and PINPs in three different sizes (50 nm, 100 nm and 200 nm).
2. To evaluate their ability to penetrate into neuroblastoma cells (SH-SY5Y).
3. Finally to test whether the three types of liposomes were toxic to neuroblastoma cells (SH-SY5Y) and to examine their ability to inhibit the aggregation and toxicity of A $\beta$ .



**Figure 1.14:** The following illustration indicates the structure of the three types of liposomes. (A) Shows the illustration of a simple liposome (B) shows the illustration of a PEGylated liposome and (C) shows the illustration of a PINP (the peptide inhibitor is attached on a PEG molecule).

## CHAPTER TWO – MATERIALS AND METHODS

**Table 2.1: Chemicals**

Chemicals	Producer
<ul style="list-style-type: none"> <li>Ammonium hydroxide 0.1 %</li> <li>BBI solutions (gold nanoparticles)</li> <li>Sepharose 4B-CL</li> </ul>	Agar Scientific (Cardiff, UK)
DMEM-Dulbecco's Modified Eagle Medium	Lonza (Verviers, Belgium)
<ul style="list-style-type: none"> <li>Chloroform</li> <li>Sodium sulphate anhydrous</li> </ul>	AnalaR® (Poole, UK)
Ethanol 70%	Fisher Scientific (Loughborough, UK)
PBS tablets	Oxoid, IVD (Hampshire, UK)
CellTiter 96 <sup>®</sup> AQueous One Solution Reagent	Promega (Madison, USA)
<ul style="list-style-type: none"> <li>Bovine Serum Albumin (BSA)</li> <li>Phosphotungstic acid</li> <li>Ammonium Thiocynate</li> <li>Iron (III) Chloride</li> <li>Thioflavin -T</li> <li>Fluoroshield™ with DAPI</li> </ul>	Sigma – Aldrich (Poole, UK)
Kit Contents for BCA assay <ul style="list-style-type: none"> <li>Micro BCA Reagent A (MA)</li> <li>Micro BCA Reagent B (MB)</li> <li>Micro BCA Reagent C (MC)</li> </ul>	Thermo Scientific (Loughborough, UK)
LabAssay™ Phospholipid	Wako chemicals (Richmond, USA)
Opti-MeM	Invitrogen - Gibco® (Carlsbad, CA, USA)

**Table 2.2: Peptide inhibitor, Aβ42**

Peptide inhibitor (Ac-rGffvlkGrrrrqrrkkrGyc-NH <sub>2</sub> )	Cambridge peptides (Birmingham, UK)
Aβ <sub>1-42</sub>	rPeptide (Bogart, Georgia, USA)

**Table 2.3: Lipids**

Name	Abbreviation	Net Charge at pH 7	Producer
Bovine brain sphingomyelin	SM	No charge	Avanti Polar Lipids Inc., U.S.A.
Cholesterol (plant derived)	CH	No charge	Avanti Polar Lipids Inc., U.S.A.
1,2-distearoyl-sn-glycero-3-phosphoethanolamine-N-[maleimide(polyethylene glycol)-2000] (mal-PEG-PE)	PEG	No charge	Avanti Polar Lipids Inc., U.S.A.
23-(dipyrrometheneboron difluoride)-24-norcholesterol	N/A	No charge	Avanti Polar Lipids Inc., U.S.A.
Cholesterol 95% stabilized	CH	No charge	Acros Organics
L- $\alpha$ -Phosphatidylcholine	N/A	No charge	Sigma - Aldrich

## 2.1 Buffers solutions

- **Phosphate Buffer Saline (PBS):** 8g of NaCl (137 mM), 0.2g of KCl, 1.44g of  $\text{Na}_2\text{HPO}_4$  and 0.24g of  $\text{K}_2\text{HPO}_4$  were dissolved in 1L distilled deionized water to make a solution of 10 mM buffer pH 7.4.
- **PB:** In addition, phosphate buffer was created by dissolving 8.4g of  $\text{NaH}_2\text{PO}_4$  with 15.62g of  $\text{Na}_2\text{HPO}_4$  in 1L distilled deionized water to make a solution of 10 mM buffer pH 7.4.
- **PB2S:** Furthermore, PB2S was also created by dissolving 16g of NaCl (274 mM), 0.2g of KCl, 1.44g of  $\text{Na}_2\text{HPO}_4$  and 0.24g of  $\text{K}_2\text{HPO}_4$  in 1L distilled deionized water to make a solution of 10 mM buffer pH 7.4.

## 2.2 Thioflavin-T (Th-T) preparation

A stock solution was prepared by dissolving thioflavin-T in PB to make a 15 mM solution. This was stored in the dark at 4°C for up to four weeks prior to use.

## 2.3 Amyloid- $\beta$ splitting

A volume of 2 mL of 0.1%  $\text{NH}_4\text{OH}$  was added in hexafluoroisopropanol (HFIP) treated  $\text{A}\beta_{1-42}$  for 10 mins and then the sample was vortexed for 1 min. After that, the solution was divided into 10 Eppendorf tubes (0.2 mL in each tube). Then, the samples were then placed in a Speedvac (Savant, Thermo Scientific) with the lids open for 4 h until no sign of liquid remains in the tubes and a small pellet of  $\text{A}\beta$  remained (100 $\mu\text{g}$   $\text{A}\beta$ ). This stored at -30°C.

## 2.4 Development of nanoparticles attached with RI-OR2-TAT by *click chemistry* (PINPs)

### 2.4.1 Preparation and hydration of lipid film

Two lipids (cholesterol and sphingomyelin) were dissolved in chloroform at 2.5 mM of each one mixed with 5 molar % of MAL-PEG-PE. The lipid mixture with MAL-PEG-PE was dissolved in chloroform. The liposome mixture was composed of a matrix of Sphingomyelin/Cholesterol (1:1 molar ratio) and containing 5% molar of MAL-PEG-PE of total lipids (5 mM). Then, using the rotary evaporator (Rotavapor RII BÜCHI, Switzerland) the round bottom flask was attached to the distillation tube of the

evaporator and the flask was rotated for about 1 h at ~207 bar nitrogen pressure until the chloroform was evaporated from the flask and a thin lipid film was formed. After the evaporation of chloroform a thin lipid film was created, which was resuspended in filtered PBS, pH 7.3 at 5 mM lipid. Then, the hydrated lipid film was vortexed to detach the lipid film from the flask and the solution was stored overnight at 4°C.

#### **2.4.2 Freeze and thaw process**

Repeated freeze and thawing is the next experimental process required for the preparation of liposomes. This is necessary to produce liposomes smaller than 200 nm and also creates unilamellar vesicles from multilamellar vesicles (Akbarzadeh et al., 2013; Traïkia et al., 2000; Sriwongsitanont and Ueno, 2011). The solution of 10 mL of filtered PBS containing the lipid film was shaken well and vortexed until the thin lipid film was detached from the glass flask and was invisible by eye. Then, the liposome suspension was split by adding 1 mL into of each ten Eppendorf tubes. After that, each tube containing the lipid suspension was frozen for 15 secs in liquid nitrogen and immediately thawed using a heating block at 42°C. The freeze and thaw steps were repeated for 5 cycles for each tube.

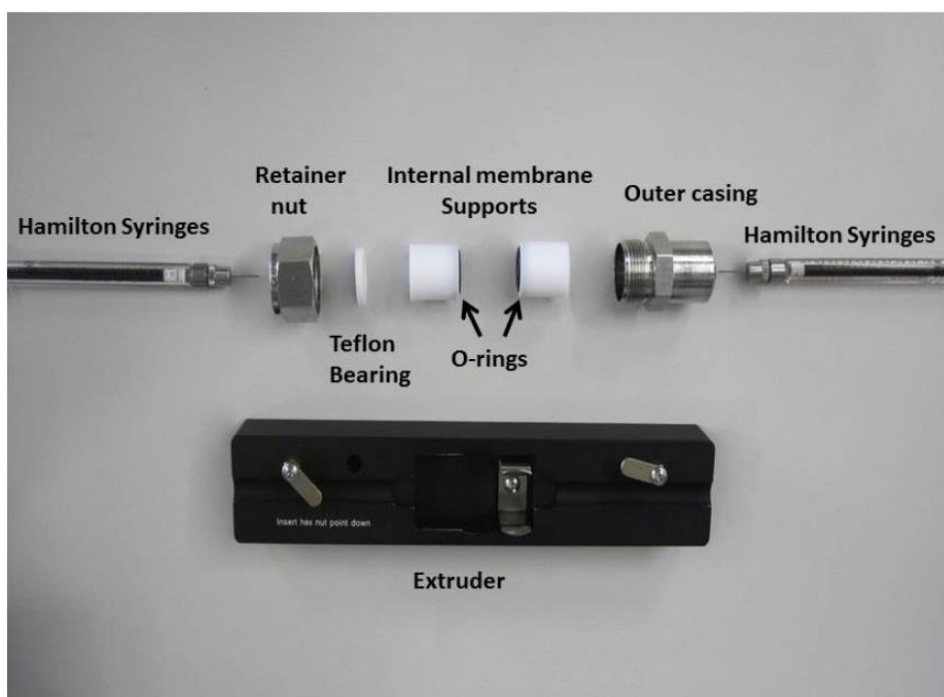
#### **2.4.3 Bath sonication**

The nanoliposome suspensions were then sonicated for 5-10 mins in a bath sonicator (ULTRAWAVE).



#### 2.4.4 Vesicle extrusion

The extrusion of unilamellar PEGylated liposomes was achieved by the use of AVANTI's mini extruder. After the assembly of the mini extruder, the whole system was checked for any leaks by pumping filtered PBS through the two O-rings. The two Hamilton syringes were rinsed and filled with distilled water and then with filtered PBS. After checking the system from any leaks, the liposome suspension was added into one syringe with final volume 1 mL, and this was attached to the extruder and the vesicle solution was slowly passed through the membrane. This represents one passage. Eleven passages were performed for each sample. The same procedure was carried out to make liposomes of different sizes by using 50 nm, 100 nm and 200 nm pore polycarbonate membranes.



**Figure 2.1: AVANTI's mini extruder.** This picture shows all the parts (labelled) of the Avanti's mini extruder and its assembly.

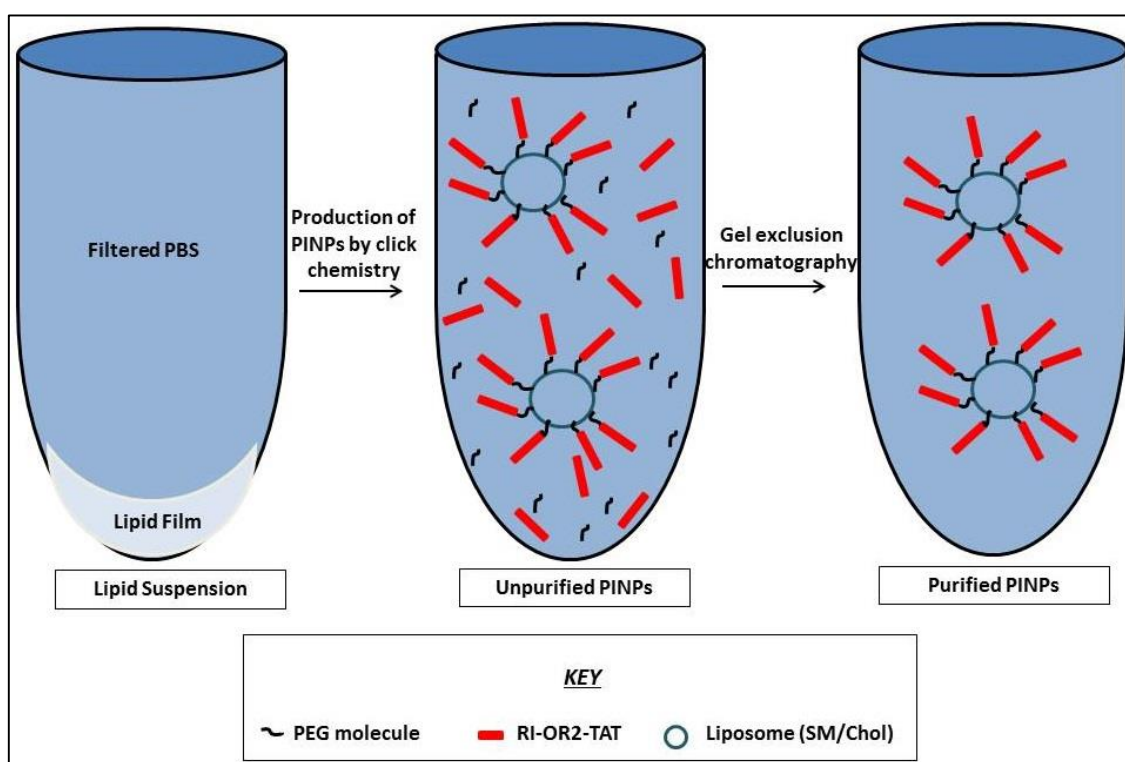
#### **2.4.5 The attachment of peptide inhibitor on the surface of the liposome**

The covalent attachment of the peptide onto the surface of the liposomes using 'click chemistry' required an additional cysteine amino acid residue which was added at the N terminal end of the peptide inhibitor, resulting in Cys-RI-OR2-TAT (Ac-rGffvlkGrrrrqrrkkrGyc-NH<sub>2</sub>). Once the extrusion of the PEGylated liposomes was completed, the peptide inhibitor was added at 2.5% of the total molarity of the liposome suspension (5 mM) and incubated for 2 h at 37°C (with vortexing once every hour) and then overnight at 4°C, to obtain the PINPs (in theory from the 5% of mal-PEG-PE the 2.5% was entrapped inside of the liposomes, while the rest 2.5% was attached on the surface of liposomes). In order to remove any unbound peptide inhibitor, the liposome suspension was purified by gel exclusion chromatography using a Sepharose 4B-CL column (18 cm x 1.6 cm) (see figure 2.2). The elution of PINPs after gel exclusion chromatography was assessed by DLS in order to determine the size of liposomes while the amount of bound peptide onto the surface of liposome was quantified using BCA assay and the amount of phospholipid present by LabAssay Phospholipid (WAKO).

The above procedure describes the production of PINPs. In the case of MAL-PEG liposomes, exactly the same procedure was followed with the only difference being that the attachment of the peptide inhibitor onto the MAL-PEG liposomes was not carried out. For the production of simple liposomes, no MAL-PEG-PE was added to the lipid suspension. In addition, the same procedure was carried out using different lipids and in some cases different molar ratios such as: (L- $\alpha$ -Phosphatidylcholine/ cholesterol (1:1 molar ratio) and Sm/Chol/Fluor Cholesterol

(23-(dipyrometheneboron difluoride)-24-norcholesterol-bodipy), (1:0.9:0.1 molar ratios).

For the creation of fluorescent liposomes exactly the same procedure was used but instead of normal cholesterol some quantity of bodipy cholesterol was included at the above molar ratio. It is important to note that during the preparation of fluorescent liposomes the whole procedure was carried out in a dark room because fluorescent cholesterol is sensitive to light.



**Figure 2.2: Production of NL decorated with RI-OR2-TAT-Cys (purified) by click chemistry (PINPs).** The illustration shows the production of liposomes from lipid film to PINPs. Free peptide inhibitor (RI-OR2-TAT-Cys) and PEG molecule is removed by gel exclusion chromatography.

## **2.5 Dynamic Light Scattering (DLS) analysis**

Nanoliposome size and polydispersity index (Pdl) were obtained by dynamic light scattering (DLS) at 25°C using a Zetasizer Nano ZS instrument, (Malvern Instruments Ltd., U.K.). For each liposome sample, 50 µL was added into a disposable solvent resistant micro cuvette. Particle size and polydispersity index were obtained from photon correlation spectroscopy, collecting backscattering at an angle of 173°. The data presented in the current thesis arise from the mean of three different measurements.

## **2.6 Bicinchoninic acid (BCA) Assay**

Six diluted BSA standards were prepared from 0.02 mg/mL with the maximum BSA concentration at 200 µg/mL and the minimum at 0 µg/mL. After that, the Working Reagent (WR) was prepared by mixing in a clean glass bottle 25 parts of Micro BCA reagent A (MA), 24 parts of reagent B (MB) and 1 part of reagent C (MC) (25:24:1, Reagent MA:MB:MC) (Thermo SCIENTIFIC). Then, in a clear 96 well microplate (NUNC™), 25 µL of the standard sample or the unknown sample plus 200 µL of working reagent was added to each well. The 96 well microplate was covered by sealing tape and incubated for 2 h at 37°C and then the absorbance of each well was measured at 562 nm on a plate reader (Wallac VICTOR<sup>2</sup> 1420 Multilabel Counter) using the Pekin Elmer 2030 Manager program. Each sample was assayed in triplicate and the mean and standard deviation calculated.

## **2.7 Colourimetric determination of phospholipids with ammonium ferrothiocyanate (Stewart's Method)**

### *Ammonium Ferrothiocyanate*

A 1L glass bottle was cleaned by distilled deionized water, and 0.4 mol ammonium thiocyanate  $\text{NH}_4\text{SCN}$  (SIGMA – ALDRICH) and 0.06 mol iron (III) chloride ( $\text{FeCl}_3 \cdot 6\text{H}_2\text{O}$ ), (SIGMA – ALDRICH) were added. The solution was mixed well and stored at room temperature.

### *Lecithin (L- $\alpha$ -phosphatidylcholine) preparation (Standard phospholipid solution)*

0.64 mM of L- $\alpha$ -phosphatidylcholine (SIGMA-ALDRICH) in 5 mL of chloroform (AnalaR®) was added to a round bottom flask. The solution was well shaken and vortexed for 2 mins and stored in the fridge at 4°C.

### *Sphingomyelin standard solution Preparation (Standard phospholipid solution)*

0.5 g of sphingomyelin (Avanti Polar Lipids Inc., U.S.A) was dissolved in 5 mL of chloroform (AnalaR®) in a 5 mL round bottom flask. From this 5 mL sphingomyelin solution in chloroform at a concentration 0.1 mg/mL was prepared. The solution was mixed well and vortexed for 2 mins and stored in the fridge at 4°C.

### *Generation of a calibration curve of sphingomyelin*

For the calibration curve to estimate liposome concentration, six dilutions of sphingomyelin were prepared. The six concentrations were: 0.1 mg/mL, 0.08 mg/mL, 0.06 mg/mL, 0.04 mg/mL, 0.02 mg/mL and 0 mg/mL. Each dilution had final volume 1 mL. For the preparation of the six standards sphingomyelin solution and chloroform

was used. Into each dilution, 1 mL of ammonium ferrothiocyanate was added, and the mixture was mixed well and then centrifuged (MIKRO 120Zentrifugen 2RPMx1000 for 5 mins. After centrifugation, two layers were formed. The lower layer (chloroform) was removed with a glass Pasteur pipet. The chloroform phase then was added in a glass cuvette (Hellma Quartz Cuvette) and the optical density read at  $\lambda$  490 nm.

#### Colourimetric determination of phospholipids in liposomes

The same procedure as above was carried out using the liposomes mixtures, and the absorbance compared to a standard curve was obtained to determine the concentration of phospholipid in each suspension. These liposomes mixtures were plain liposomes, MAL-PEG liposomes or PINPs.

#### **2.8 Phospholipid Assay – Choline oxidase · DAOS method (Wako assay)**

This assay was used as an alternative of Stewart's assay because we had some technical issues and did not work properly. The quantification of sphingomyelin in liposomes was performed by using an enzyme assay, Wako LabAssay Phospholipid B test kit. This assay is based on phospholipids such as lecithin, lysolecithin and sphingomyelin. In this case the assay is based on sphingomyelin in a sample which hydrolyzed to choline by phospholipase D enzyme. This phospholipid assay is based on an enzymatic reaction using N-ethyl-N-(2-hydroxy-3-sulfopropyl)-3,5-dimethoxyaniline (DAOS) as a blue pigment.

*Preparation of reagents:*

- Colour Reagent: 50 mL of chromogen substrate were dissolved into 50 mL of buffer (1:1). The mixture was mixed well and stored at 4°C.

*Preparation of standard solution (microplate method):*

This phospholipid assay used three standards with following concentrations (see table 2.4). In the current experiment the standards were diluted in 1:20 by giving the follow concentrations: (a) 7 mg/dL, (b) 15 mg/dL and (c) 29.8 mg/dL.

No.	Phospholipid Standard	Deionized water	Sample volume	Phospholipid concentration
1	100 $\mu$ L	100 $\mu$ L	2 $\mu$ L	150 mg/dL
2	Undiluted	-	2 $\mu$ L	300 mg/dL
3	Undiluted	-	4 $\mu$ L	596.1 mg/dL

**Table 2.4:** This table shows how to prepare the three phospholipid standards for the Wako assay

*Perform the assay in a clear 96 well plate:*

The three standards were added in a final volume of 300  $\mu$ L into each well. As regards for the liposome sample solutions, 25  $\mu$ L of each liposome suspension were added to each well plus 275  $\mu$ L of colour reagent to the same wells in order to make a final volume of 300  $\mu$ L. The plate was shaken well and incubated at 37°C for 5 mins. After the incubation of the plate, the absorbance at 600 nm using the plate reader was measured. All samples and standards were measured in triplicate.

## **2.9 Concentrate the liposomes**

After the determination of PINPs using the BCA and phospholipid assay, the fractions were collected in two centrifugal concentrator tubes (Vivaspin 6) in equal volumes and spun at 4000 rpm (3000 $\times$ g), at 4°C for approximately 15 mins. After spinning, the liposomes were collected.

## **2.10 Preparation of three types of liposomes for Transmission Electron Microscopy (TEM)**

### **2.10.1 Staining of plain, MAL-PEG-PE liposomes and PINPs for TEM**

For the staining of liposome samples, the heavy metal 2 % phosphotungstic acid (PTA) (SIGMA-ALDRICH) was used. For its preparation 6.94  $\times$   $\mu$ mol of PTA was dissolved in 1 mL of distilled water. Then, the solution was vortexed for 1 min and centrifuged (MIKRO 120Zentrifugen 14000 rpm) for 5 mins.

The liposome suspension was pipetted onto copper grids (G2004, 400Thin, copper 3.05 mm - ATHENE). On the shiny side of the grid one drop (1  $\mu$ M) of liposome suspension was added for 2 mins until the liposomes particles were adsorbed and the surplus was removed carefully with clean filter paper. After that, a drop of 2% (w/v) of PTA (5  $\mu$ L) was added and left for 2 mins. The surplus PTA was also removed with filter paper and the sample was dried at room temperature. Finally, the grids were stored in a glass petri dish with the shiny side facing upwards until the sample was ready for examination under TEM (JEOL JEM 1010). EM pictures were taken by Dr. Nigel Fullwood.



### **2.10.2 TEM photographic image processing**

After the examination of samples under the TEM, the film plates which were located in the TEM were collected for further processing. The dehydration of film plates using vacuum dessicator was a necessary step before the development of pictures. Next, the exposed film plates (Kodak Electron Microscopy Film 4489, Agar scientific, UK) were placed in a black developing rack. The rack was immersed in a black container which contained developer (Ilford phenisol developer) for 4 mins (1 part developer to 4 parts distilled water). The temperature of the developer was approximately 20°C. Next, the developing rack was transferred into another container which contained water and immersed for 1 min. Afterwards, the rack was placed into the fixation solution (Ilford hypam fixer) for 5 mins. At each stage, the developing rack was agitated in order to promote the even development of films. Then, the rack was placed into a running bath water for 2 h with 5 drops of wetting agent (Kodak foto – flo). The whole process was carried out in a dark room. After that, the racks were store in a drying cabinet to air-dry (Baird and Tatlock Ltd, UK) overnight. Finally, the developed images were scanned using an EPSON Scanner and processed in Microsoft Office Picture Manager 2007.

## 2.11 Toxicity assays

### 2.11.1 MTS cell proliferation colorimetric assay Kit

For this assay, SHSY-5Y human neuroblastoma cells were used. The culture and the splitting of cells were done by maintaining the cells in Dulbecco's Modified Eagle Medium (DMEM, Gibco) containing 10% Fetal Calf Serum, 100 U/mL penicillin, 50 µg/mL streptomycin, at 37°C and 5% CO<sub>2</sub> in a humidified incubator. The cultured SHSY-5Y human neuroblastoma cells were transferred into a sterile 96 clear well growth plate (100 µL at ~20,000 cells) per well and were incubated for 24 h at 37°C in order to adhere into the base of each well. After 24 h incubation of cells, the media was removed and the different dilutions of the three types and sizes of liposomes were added, in order to check the toxicity of liposomes. In order to test the toxicity of the three sizes (200, 100 and 50 nm) and the three types of liposomes (simple, PEGylated and PINPs), dilutions of liposomes with DMEM were prepared at four different concentrations: 50 µm, 10 µm, 1 µm and 0.1 µm. In addition, 100 µL of each size and each concentration of liposomes was added in each well in growth medium (four wells per condition) and the plate was incubated again for 24 h. Then, the viability of SHSY-5Y cells or the toxicity of liposomes was assessed using the CellTiter 96AqueousOne Solution Cell Proliferation (MTS) Assay (Promega) kit. The sterile 96-well plate (COSTAR®) was incubated for 2 – 4 h at 37°C in a humidified, 5% CO<sub>2</sub> atmosphere and then the plate was read at 490 nm on a plate reader (Wallac VICTOR<sup>2</sup> 1420 Multilabel Counter). Furthermore, for the experiments which examined the ability of PINPs and MAL-PEG liposomes to affect the amyloid beta aggregation and protect against Aβ cytotoxicity the cell growth medium from DMEM

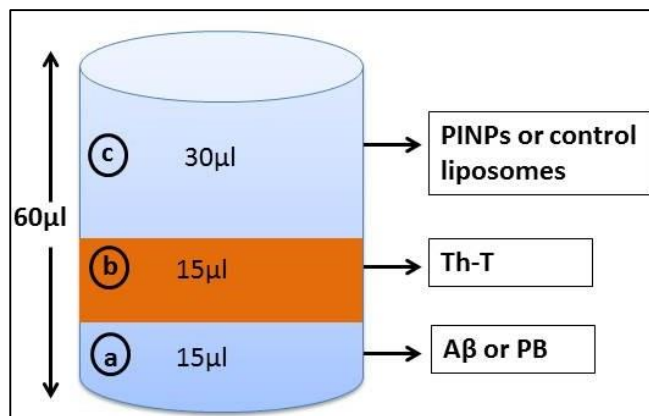
was changed to Opti-MeM (Invitrogen) while the A $\beta$ <sub>1-42</sub> had been pre-aggregated (for 24 h at 25°C in filtered PBS) was added to a concentration of 5  $\mu$ M. The plates were incubated again for 24 h and the viability of cells was examined as above.

As referred above, the MTS assay examines the viability of cells. The compound which added into the cells (MTS tetrazolium) reacts with the cells and has the property to self-reduce into another compound called formazan. This coloured formazan product is soluble in culture medium. The chemical reaction occurs due to the production of NADPH or NADH by dehydrogenase enzymes in metabolically active cells (WWW, Promega).

### **2.11.2 Thioflavin-T (ThT) assay**

Th-T assay was performed using HFIP-treated synthetic A $\beta$ <sub>1-42</sub> peptides. Th-T binds to fibrils as they form. Th-T is used for the identification and quantification of A $\beta$  fibrils. When Th-T is added in a sample which contains  $\beta$ -sheet-rich structures such as A $\beta$ , it reacts because Th-T creates micelles which bind to amyloid fibrils and produce a strong fluorescent signal (Hudson et al., 2009). The A $\beta$  was dissolved in PB to give a final concentration of 100  $\mu$ M. Two types of liposomes (PEGylated liposomes and PINPs) were tested in this assay in order to examine if they are capable of inhibiting the aggregation of A $\beta$ . Th-T assay was conducted in 384 well black (Corning) microtitre plate with clear bottom, with 25  $\mu$ M A $\beta$ -42, 15  $\mu$ M Th-T, and a range of concentrations of PINPs and PEGylated liposomes, in 10 mM PBS, pH 7.4, with a total reaction volume of 60  $\mu$ L and Th-T fluorescence was monitored every 10 mins. Apart from the first wells which contained A $\beta$ +Th-T+PBS in order to

define the maximum aggregation of A $\beta$ , the rest of the wells of the plate contained the samples shown in the figure below.



**Figure 2.2:** This illustration shows the amount and the sequence which each reactant into the wells for the Th-T assay.

After the filling of the plate with the corresponding samples and concentrations of liposomes the 384 well (Corning) microtitre plate was sealed with a transparent film to prevent any evaporation of the samples and the accumulation of fibrillar A $\beta$  was monitored using a BioTek Synergy plate reader ( $\lambda_{ex} = 442 \text{ nm}$ ,  $\lambda_{em} = 483 \text{ nm}$ ) over 48 h at 25°C. Each condition was assayed three times and the final result for each condition was calculated by the average of the three individual measurements.

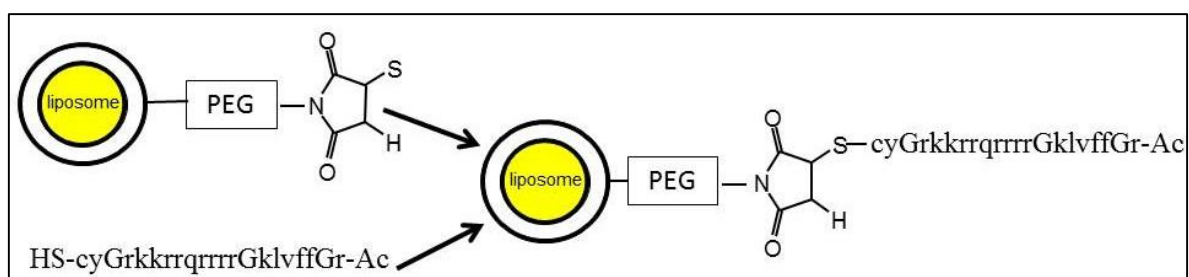
## 2.12 Cell penetration assay

In order to test whether the liposomes were able to penetrate into the neuroblastoma cells (SHSY-5Y), they were incubated together with the cells in complete medium (DMEM) as standard mammalian cell culture conditions for 24 h. It is important to note that, in this assay, fluorescent (bodipy) cholesterol had replaced some of the normal cholesterol in the liposomes (see above). In this assay the neuroblastoma cells were grown in a 6 well plate using DMEM as growth medium. Cover slips were presented in each well allowing the growth of cells on the surface of the coverslips. The cells were incubated for 24 h at 37°C in order to adhere on the surface of coverslips. Then, different concentrations of 200 nm of PEGylated liposomes and PINPs (0.1 µM, 1 µM and 10 µM) were added in each well and the plate was incubated for 1 h at 37°C. After that, using a needle, the cover slips from the wells of the plate were transferred onto the slides and specifically the side of cover slip with the cultured cells was put upside down in order for the side with cells to touch the drop of Fluoroshield™ with DAPI (4', 6-diamino-2-phenylindole dihydrochloride) (Sigma – Aldrich) which was already added onto the slide. Then, the samples were examined under a confocal microscope (LSM 510 – Laser Module – ZEISS) and pictures were taken.

## CHAPTER THREE - DLS RESULTS

### 3.1 Conjugation of RI-OR2-TAT-Cys peptide to PEGylated liposomes to create PINPs

According to a previous study (Parthasarathy et al., 2013), a TAT sequence was added onto the RI-OR2 peptide creating a more efficient peptide to inhibit A $\beta$  aggregation, but which also allowed it to penetrate into cells and cross the BBB successfully. Further studies showed that the peptide could be made more potent by combining it with nanomedicine. In the current study, I have covalently attached the RI-OR2-TAT peptide to liposomes by 'click chemistry'. A cysteine residue added to C-terminus of the RI-OR2-TAT peptide provides a thiol group which reacts with a maleimide-functionalized phospholipid (mal-PEG-PE) present on the surface of the nanoliposomes, creating a complex between the peptide inhibitor and the liposomes (see figure 3.1).



**Figure 3.1:** This illustration shows the creation of PINP through 'click chemistry' using the peptide inhibitor and PEGylated liposome.

### **3.2 Characterization of liposomes by size**

After the preparation of liposomes, the diameter, the polydispersity and the stability of each distinct size (50 nm, 100 nm and 200 nm) and type (plain, mal-PEG-PE, PINPs) of nanoliposomes were assessed using Dynamic Light Scattering (DLS) (Zetasizer Nano ZS, Malvern Instruments Ltd., U.K.). The different sizes of the three types of liposomes were examined (by DLS) in several conditions such as:

- Liposome suspensions at different dilutions (different concentrations).
- By heating the extruder to 75°C.
- Preparation of liposomes by applying the freeze and thaw process using liquid nitrogen and bath sonication.
- Preparation of liposomes without these methods.

Before testing any of the nanoliposomes, standard gold nanoparticles of four distinct sizes (2 nm, 10 nm, 20 nm and 100 nm) were examined in order to calibrate the system and determine how consistent DLS is for measurement of these standard nanoparticles.

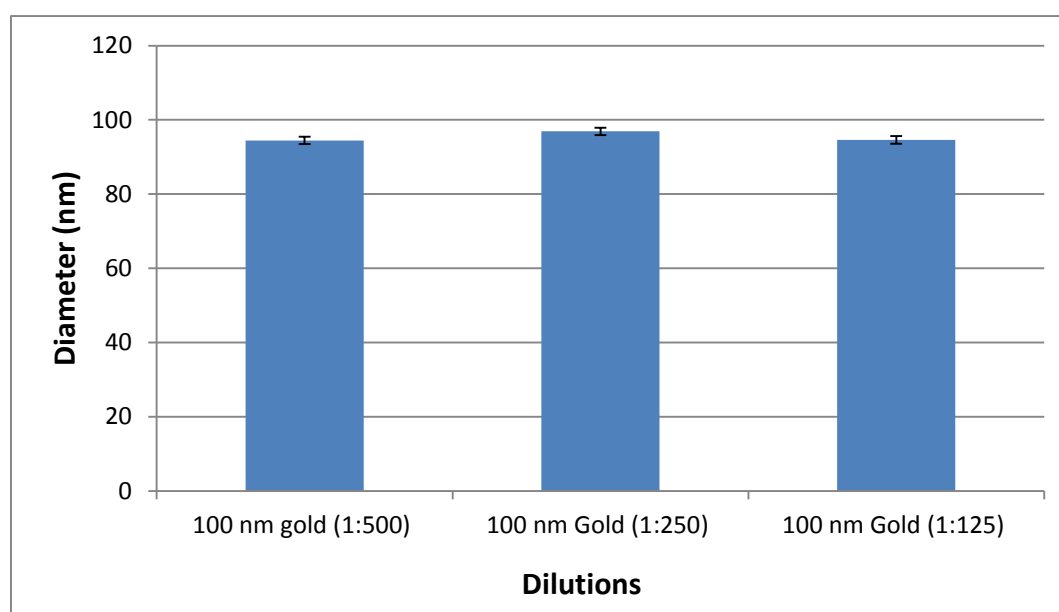
#### **3.2.1 Characterization of standard gold nanoparticles using DLS**

The consistency of DLS was examined using four different distinct sizes (2 nm, 10 nm, 20 nm and 100 nm) of gold colloids (BBI, Agar Scientific) in order to cover a wide spectrum of sizes. Each size of gold nanoparticle was examined at three different dilutions (1:500, 1:250, and 1:125) in order to determine and compare which dilution is the most suitable for each size, and if the different dilutions would

affect the measurements using DLS. The different dilutions were prepared using filtered Phosphate Buffered Saline (PBS). Before the preparation of MAL-PEG liposomes and PINPs, we experimented on simple liposomes using them in different experiments as shown below.

100 nm gold nanoparticles:

Starting with the largest nanoparticles of 100 nm, the gold nanoparticles dilution of 1:500 gave a mean size  $\pm$  standard deviation ( $\pm$ SD) of  $94.46 \pm 3.4$  nm, the dilution of 1:250 gave a mean size of  $96.91 \pm 3$  nm and the dilution of 1:125 gave a mean size of  $94.60 \pm 3.1$  nm (see figure 3.2).

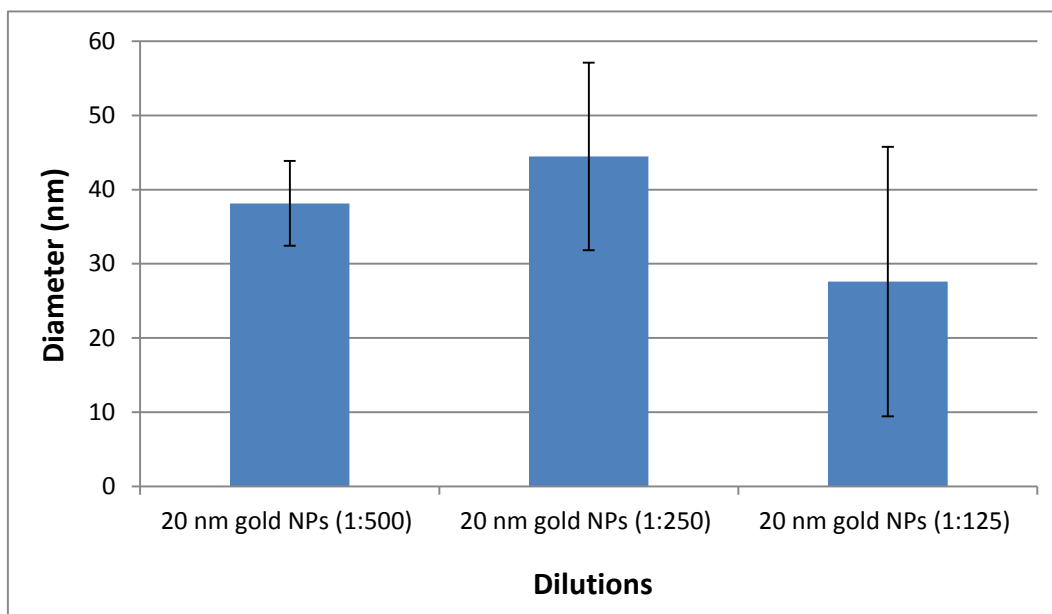


**Figure 3.2:** The graph shows the average diameter of 100 nm gold nanoparticles at different dilutions. Bars show the mean  $\pm$  SD of 100 nm gold nanoparticles after three measurements ( $n=3$ ). The values were accurate and close to 100 nm with very small  $\pm$  SD.



### 20 nm gold nanoparticles:

For the 20 nm standard gold nanoparticles the dilution of 1:500 gave a mean size of  $38.14 \pm 5.72$  nm while the dilution of 1:250 gave a mean size of  $44.47 \pm 12.6$  nm and, finally, the dilution of 1:125 gave a mean size of  $27.6 \pm 18.14$  nm (see figure 3.3).

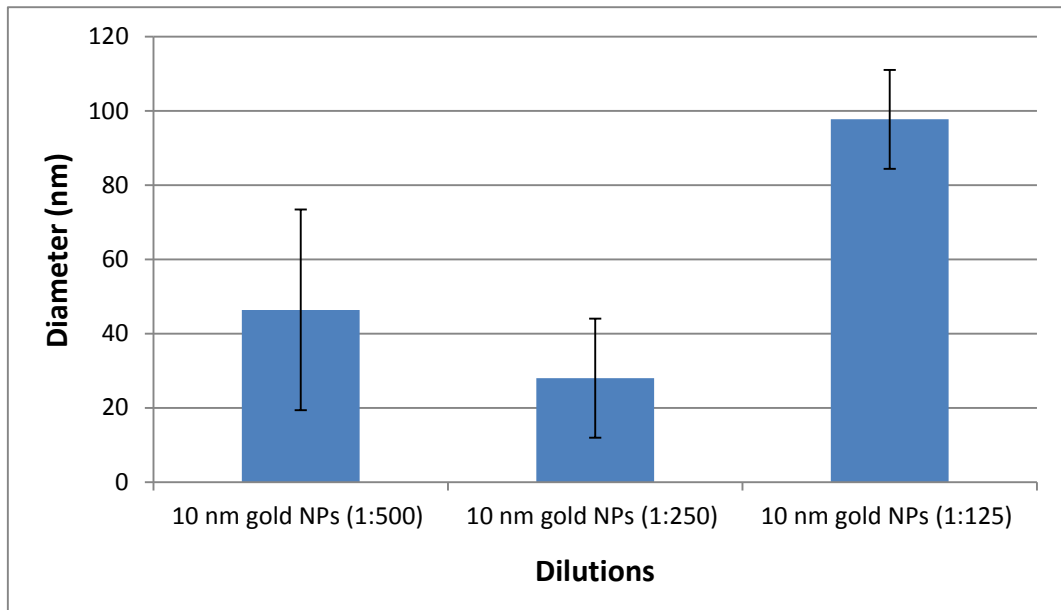


**Figure 3.3:** The graph shows the average diameter of 20 nm gold nanoparticles at different dilutions.

*Bars show the average diameters for each dilution after three measurements. The x-axis describes the different dilutions, while the y-axis describes the diameter recorded by DLS. All values were slightly higher than expected, with relatively large  $\pm$  SD.*

### 10 nm gold nanoparticles:

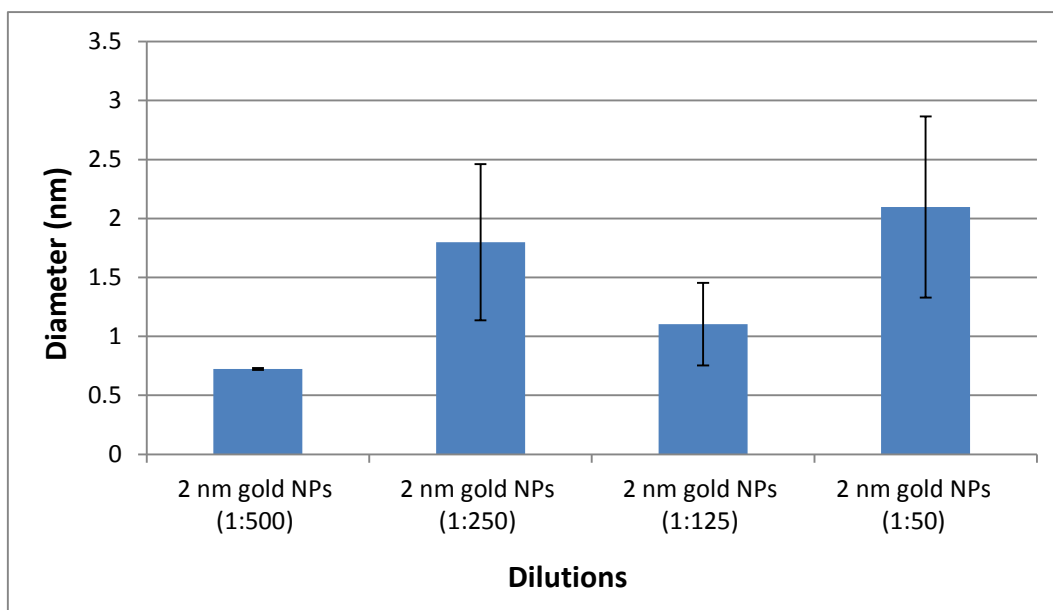
For the 10 nm gold nanoparticles the dilutions of 1:500, 1:250 and 1:125 gave mean sizes of  $46.4 \pm 27$  nm,  $28.0 \pm 16$  nm and  $97.7 \pm 13.3$  nm, respectively (see figure 3.4).



**Figure 3.4:** The graph shows the average diameter of 10 nm gold nanoparticles at different dilutions. Bars show the average diameters  $\pm$ SD for each dilution, after three measurements. The x-axis describes the different dilutions, while the y-axis describes the diameter recorded by DLS. The values were higher than expected.

### 2 nm gold nanoparticles:

The measurements of 2 nm standard gold nanoparticles were of little relevance to the work with liposomes, but it was a challenge to determine the ability of DLS to measure nanoparticles with a very small diameter. For the dilutions of 1:500, 1:250, 1:125 and 1:50, DLS gave mean sizes of  $0.72 \pm 0.0085$  nm,  $1.79 \pm 0.66$ ,  $1.1 \pm 0.34$  nm and, finally,  $2.098 \pm 0.77$  nm, respectively (see figure 3.5).

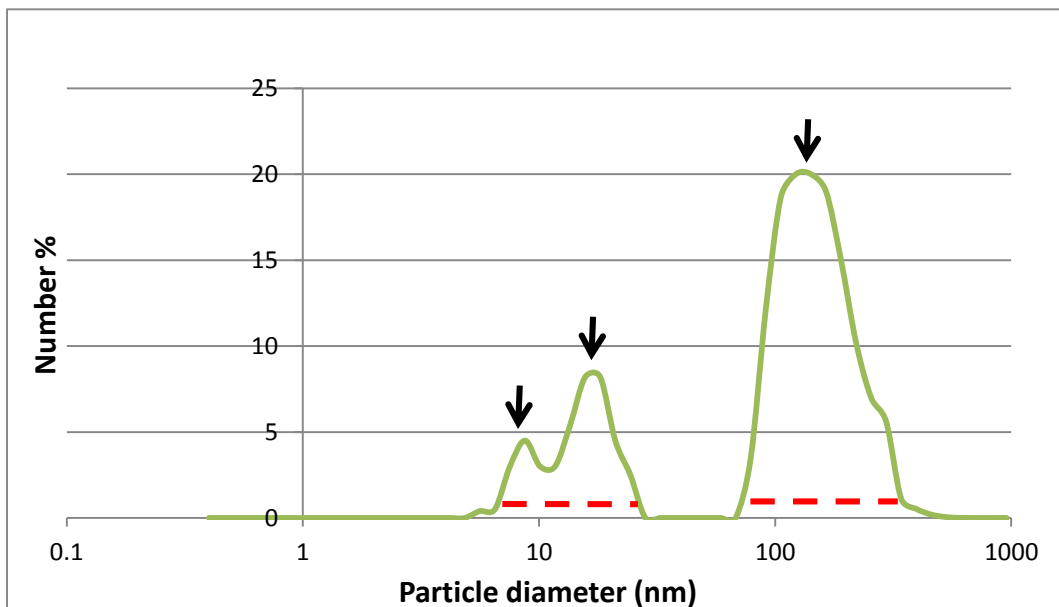


**Figure 3.5: The graph shows the average diameter of 2 nm gold nanoparticles at different dilutions.**

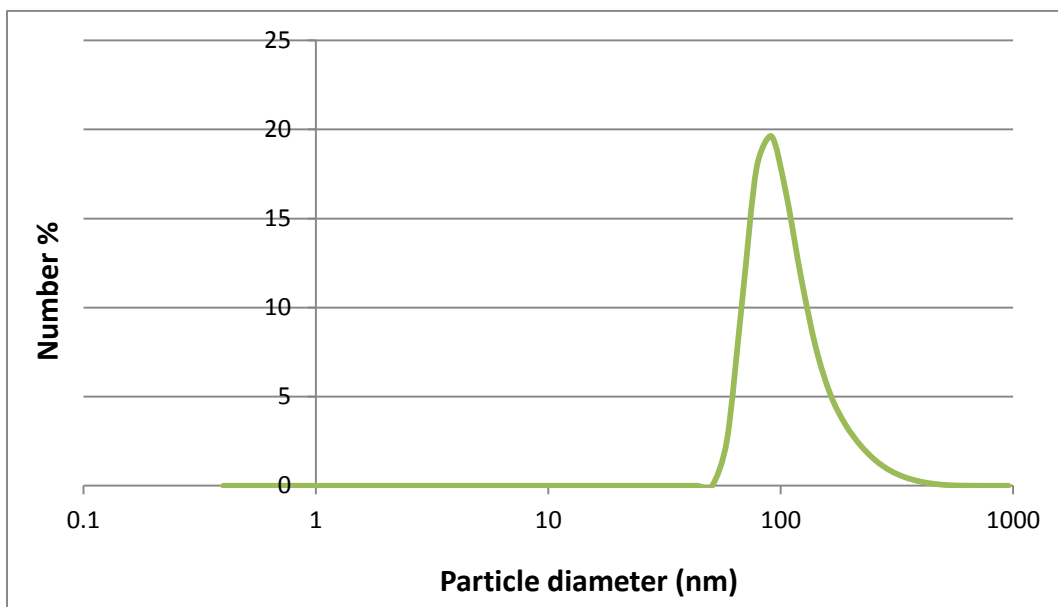
*Bars show the average diameters  $\pm$  SD for each dilution after three measurements. The x-axis describes the different dilutions, while the y-axis describes the diameter recorded by DLS. The different dilutions gave a variety of values but with dilutions of 1:50 and 1:250 the results were quite accurate and close to 2 nm.*

### **Size distribution of 100 nm gold nanoparticles**

In order to examine how DLS tests perform with nanoparticles of different concentrations, the size distribution of 100 nm gold standard nanoparticles was determined at two different concentrations (at high and low concentration). As can be seen from figure 3.6, which shows the measurement of 100 nm particles at high concentration, multiple peaks were present indicating that DLS detected more than one population, with a high polydispersity index. On the other hand, the examination of a more diluted sample (low concentration) gave more accurate and more reliable results with a single peak which indicates one population with low polydispersity, as shown in figure 3.7.

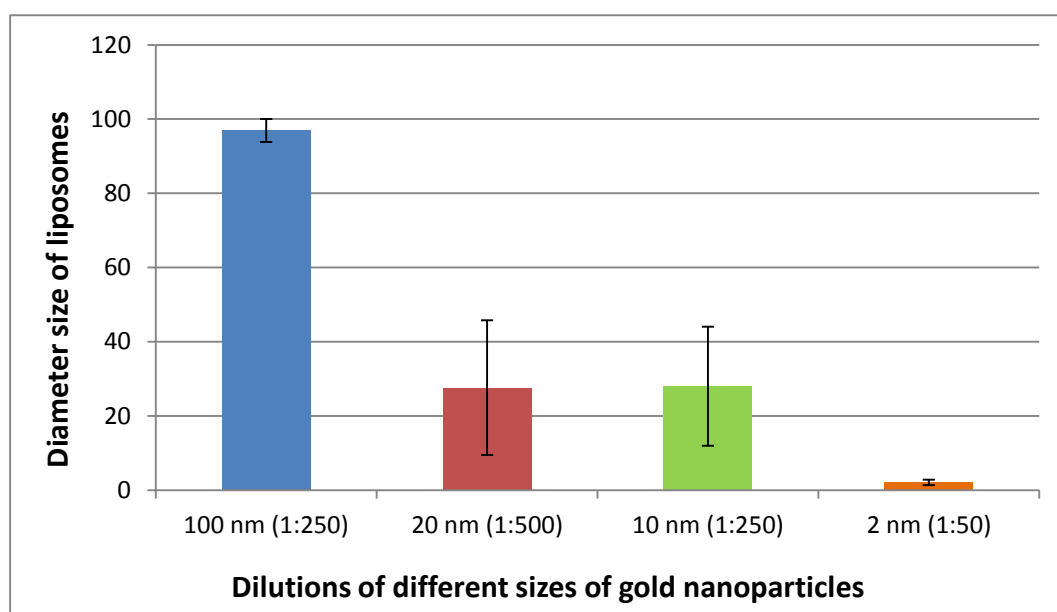


**Figure 3.6:** The graph represents the size distribution of 100 nm liposomes at 2.5 mM concentration. The graph shows a concentrated sample of 100 nm liposomes which reveals multiple peaks with high polydispersity index. The red dashed line indicates the spectrum of size of the nanoparticle population while the black arrows indicate the highest percentage of nanoparticle population in the specific spectrum.



**Figure 3.7:** The graph shows the size distribution of 100 nm liposomes at 10  $\mu$ M concentration. The graph shows a sample of 100 nm liposomes at an appropriate (low) dilution which reveals a single peak with low polydispersity index.

Consequently, based on these different concentrations of standard gold nanoparticles, I concluded that the correct dilution is needed to give the most reliable and most accurate results. For the 100 nm gold particles the dilution 1:250 gave a mean value of 96.91 nm, for the 20 nm particles the most reliable dilution was 1:500 which gave a mean value of 27.6 nm, for the 10 nm particles the dilution 1:250 gave a mean value of 28.01 nm and, finally, for the 2 nm particles the most accurate dilution was 1:50 which gave a mean value of 2.1 nm (see figure 3.8). Once the measurements of standard gold nanoparticles were completed and the consistency of DLS was assessed, the three sizes of NL prepared at Lancaster were examined, starting from simple liposomes.



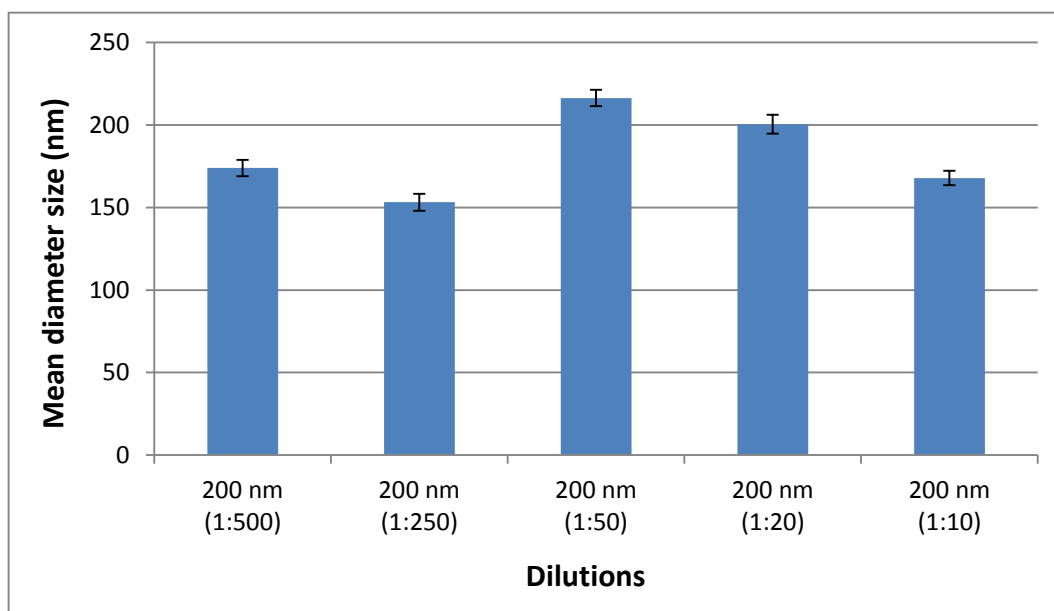
**Figure 3.8:** The graph shows the average diameter of gold nanoparticles using DLS at the most accurate dilutions. Bars show the most accurate average ( $\pm$  SD) at different dilutions for 100 nm, 20 nm, 10 nm and 2 nm gold nanoparticles ( $n=3$ ). The x-axis describes the sizes of the gold nanoparticles, while the y-axis describes the diameter recorded by DLS.

### 3.2.2 Characterization of simple liposomes using (DLS)

Simple liposomes were composed of sphingomyelin and cholesterol (1:1 molar ratio), the first stage of making PINPs. The size of simple liposomes was examined by DLS using liposome suspensions at different dilutions (based on the standard gold nanoparticle results) in filtered PBS for the three different sizes (200 nm, 100 nm and 50 nm).

#### 200 nm Simple liposomes

For the 200 nm simple liposomes the dilutions 1:500, 1:250, 1:50, 1:20, and 1:10 gave mean sizes of  $173.9 \pm 4.95$  nm,  $153.1 \pm 5$  nm,  $216 \pm 5$  nm,  $200.4 \pm 5.6$  nm and  $167.9 \pm 4.3$  nm respectively (see figure 3.9).

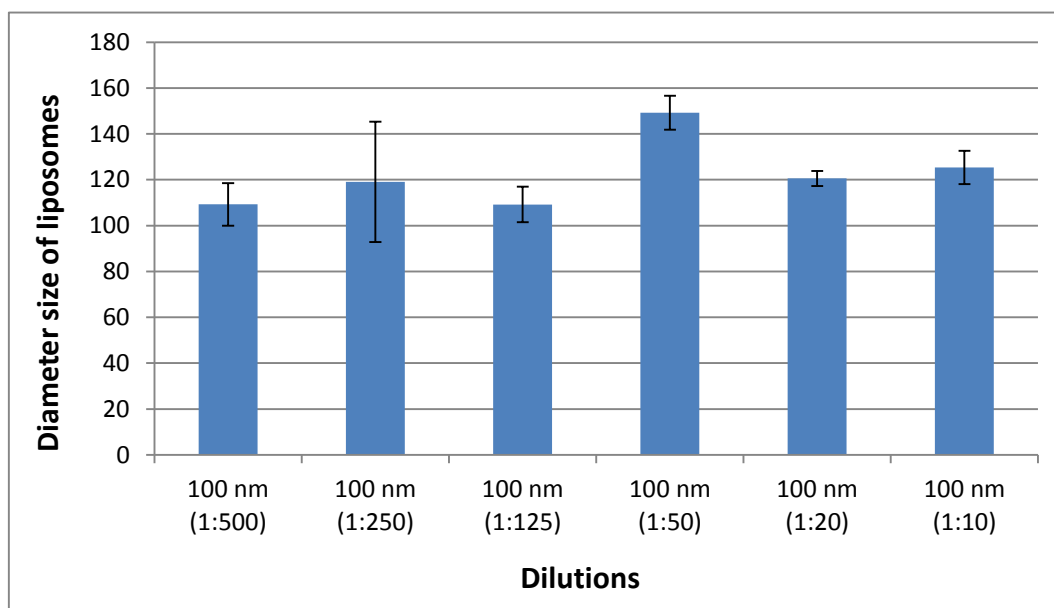


**Figure 3.9:** The graph shows the average diameter of 200 nm simple liposomes at different dilutions.

*The x-axis describes the different dilutions, while the y-axis describes the mean diameter  $\pm$  SD (n=3) recorded by DLS. A variety of values was observed at the different liposomes dilutions with the most accurate value (200.4 nm) obtained at 1:20 dilution.*

### 100 nm Simple liposomes

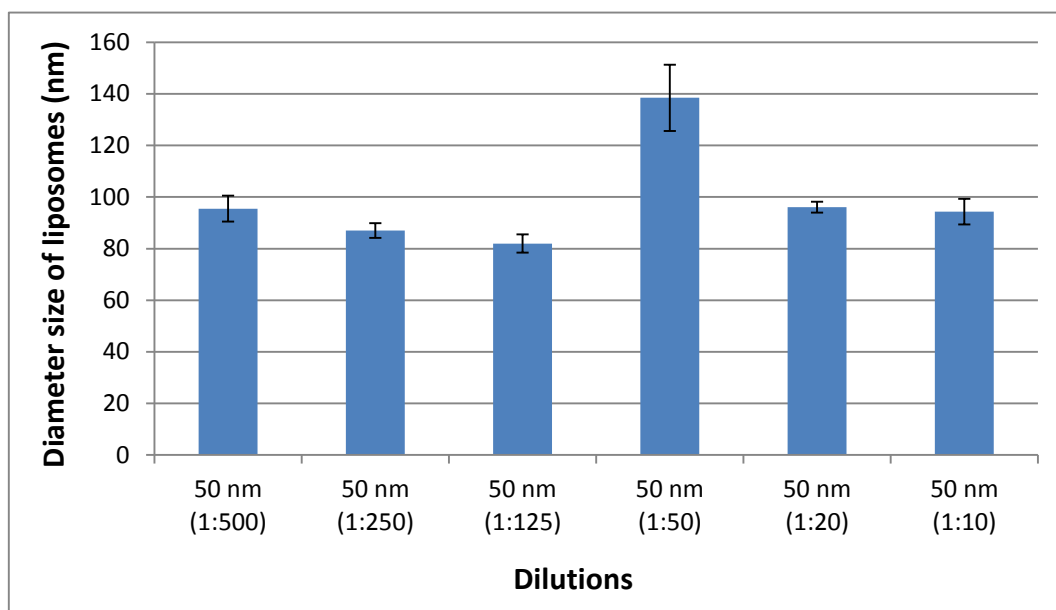
The size of 100 nm simple liposomes was also examined at different dilutions of 1:500, 1:250, 1:125, 1:50, 1:20, and 1:10 which gave mean sizes of  $109.23 \pm 9.2$  nm,  $119.1 \pm 26.2$  nm,  $109.2 \pm 7.75$  nm,  $149.2 \pm 7.4$  nm,  $120 \pm 3$  nm and  $125.3 \pm 7.2$  nm, respectively (see figure 3.10).



**Figure 3.10:** The graph shows the average diameter of 100 nm simple liposomes at different dilutions. A variety of values was observed at the different liposome dilutions with the closest to expected values (109.2 and 109.23 nm) observed at dilutions of 1:500 and 1:125.

### 50 nm Simple liposomes

The measurements for 50 nm nanoliposomes at different dilutions of 1:500, 1:250, 1:125, 1:50, 1:20, and 1:10 gave mean sizes of  $95.5 \pm 5$  nm,  $87 \pm 2.9$  nm,  $82 \pm 3.5$  nm,  $138 \pm 12.8$  nm,  $96.11 \pm 2.1$  nm and  $94.34 \pm 4.92$  nm, respectively (see figure 3.11).



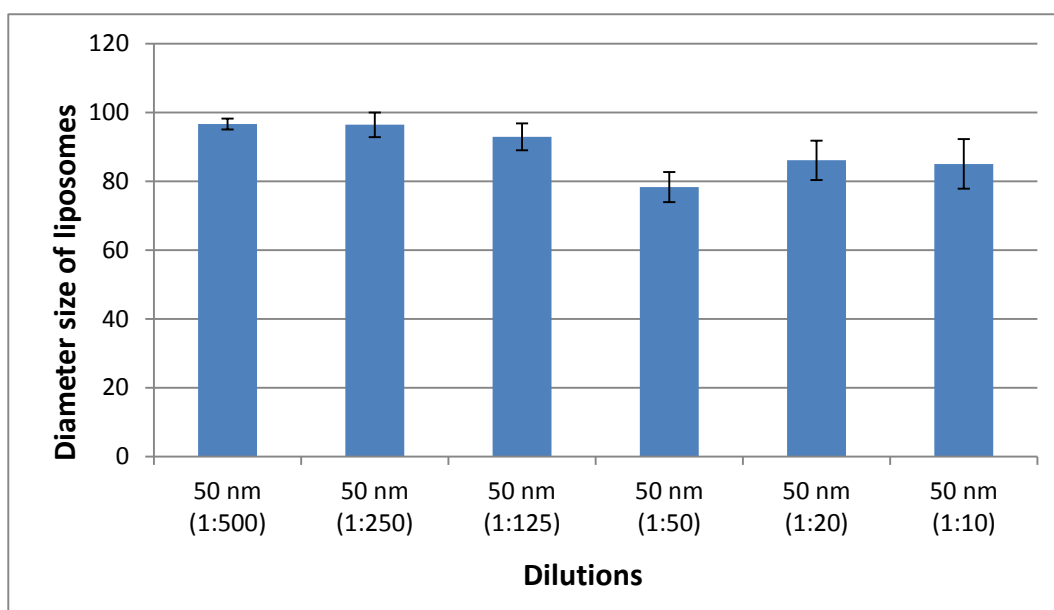
**Figure 3.11: The graph shows the average diameter of 50 nm simple liposomes at different dilutions.**

*A variety of values was observed at the different liposomes dilutions with the most accurate value (84.59 and 84.65 nm) at dilutions of 1:250 and 1:125. However, all values were slightly larger than anticipated.*

The measurements for the 50 nm simple liposomes were higher than expected, as can be observed from figure 3.11. These measurements were lower than those obtained for 100 nm liposomes, but were closer to 100 nm than 50 nm. So in order to attempt to get more reliable values (closer to 50 nm) the liposome mixture was extruded initially through a 200 nm polycarbonate membrane for 5 passages, then 5 passages through a 100 nm polycarbonate membrane, and, finally, the liposome suspension was extruded through a 50 nm polycarbonate membrane for 11 passages. Despite all these extrusions through the three different polycarbonate membranes, the mean size of the 50 nm simple liposomes did not change greatly, although a slightly decrease in diameter was observed at dilutions of 1:50, 1:20,



1:10, giving mean sizes of  $78.34 \pm 4.3$  nm,  $86.13 \pm 5.72$  nm and  $85.08 \pm 7.2$  nm, respectively (see figure 3.12).



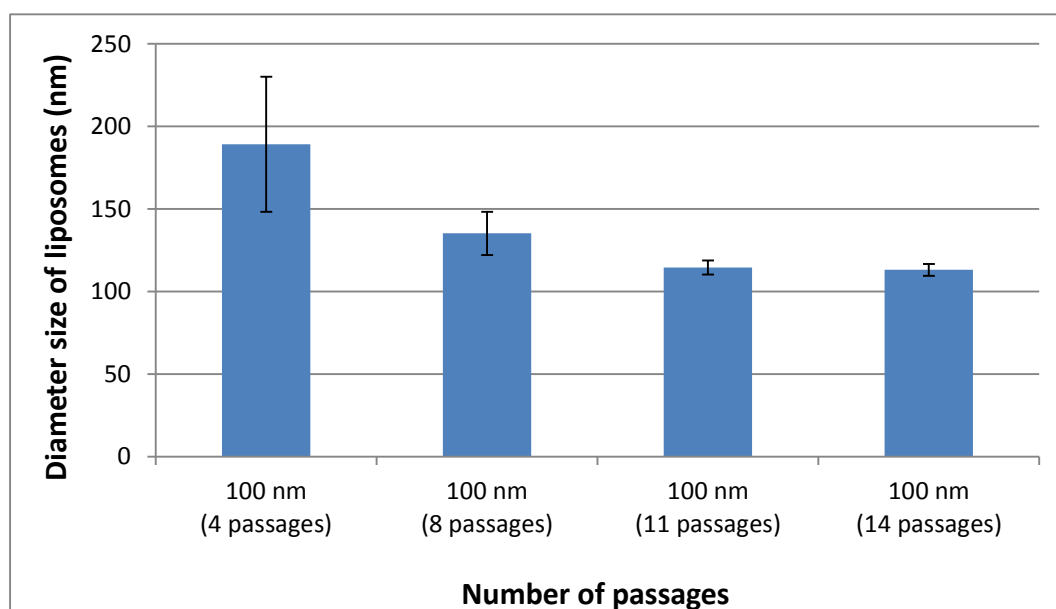
**Figure 3.12:** The graph shows the average sizes of 50 nm simple liposomes at different dilutions after extrusion through 200 nm, 100 nm and, finally, 50 nm polycarbonate membranes.

### Observations using simple liposomes

Taking into consideration the above results, it was observed that the 100 nm simple liposomes gave the most reliable results, having an average mean size in the different dilutions very close to 100 nm, with relatively low standard deviation compared to the 50 nm and 200 nm nanoliposomes. Consequently, as the 100 nm liposomes had the more reliable results, they were used for further experiments to examine their size and their polydispersity at 4, 8 and 11 passages, and also by heating the extruder block at 75°C compared to room temperature. In addition, the liposome size was examined in liposomes suspensions which had undergone sonication and a freeze and thaw process and for liposomes solutions which did not undergo sonication or freezing and thawing.

100 nm liposomes at 4, 8, 11 and 14 passages through the extruder at room temperature

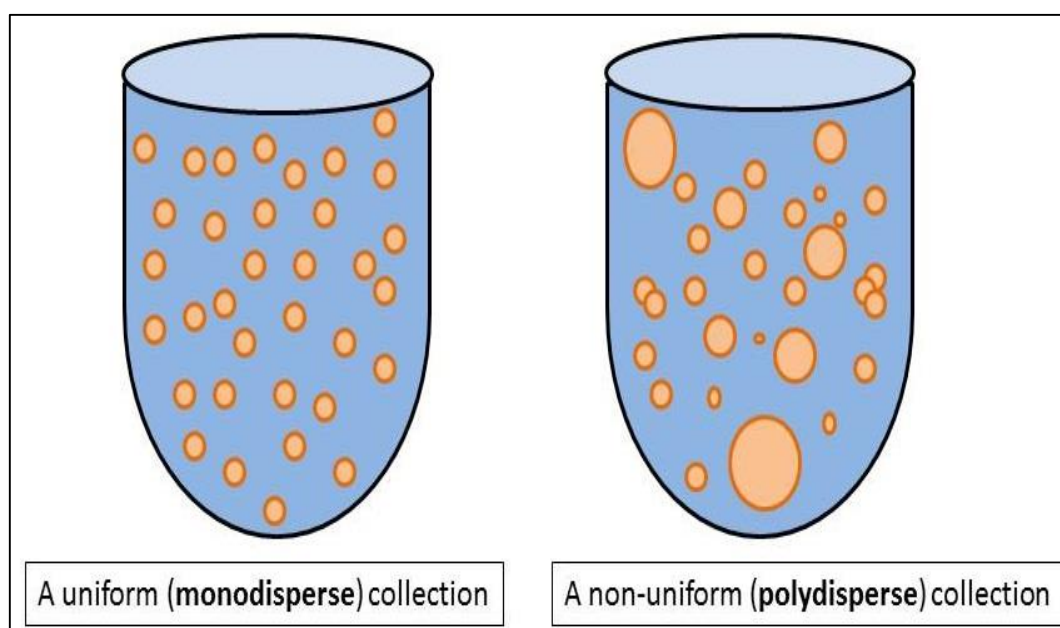
As can be seen from figure 3.13, the mean size of the 100 nm liposomes gradually decreased as the number of passages through the membranes was increased. Initially the size of liposomes at 4 passages was  $189 \pm 40.9$  nm, at 8 passages this decreased to  $135.2 \pm 13.2$  nm, while at 11 passages the size decreased again to  $114.5 \pm 4.3$  nm and finally at 14 passages the size of liposomes ( $113.1 \pm 3.61$  nm) did not change significantly from that obtained at 11 passages.



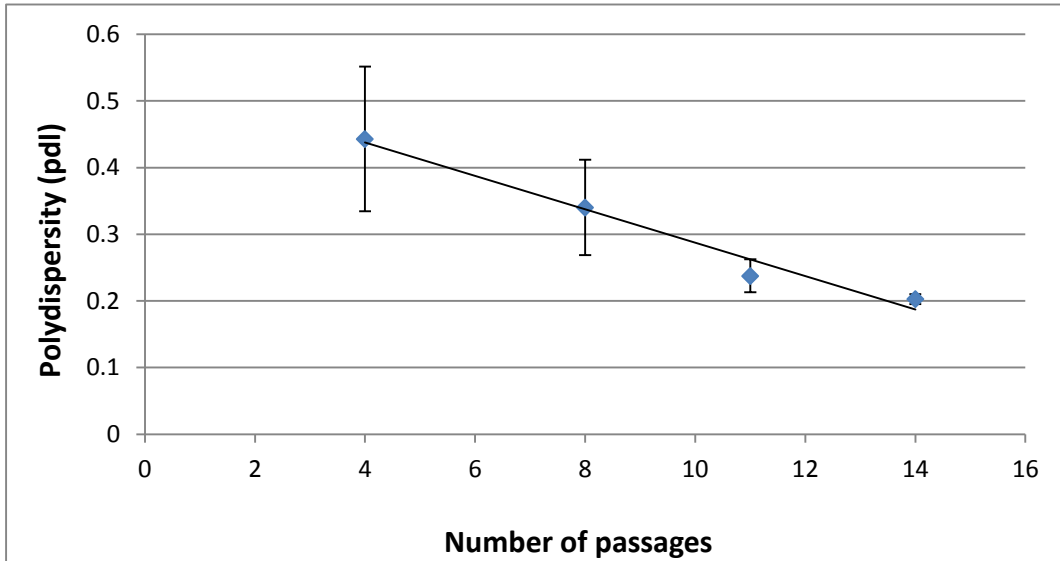
**Figure 3.13:** The graph shows and compares the average size of 100 nm simple liposomes at 4, 8, 11 and 14 passages through the Avanti's mini extruder at room temperature. The x-axis describes the number of passages through the 100 nm membrane and the y-axis describes the diameter recorded by DLS. As the number of passages increases the average diameter decreases and becomes closer to 100 nm.

Dispersity of 100 nm liposomes and number of passages through the extruder at room temperature

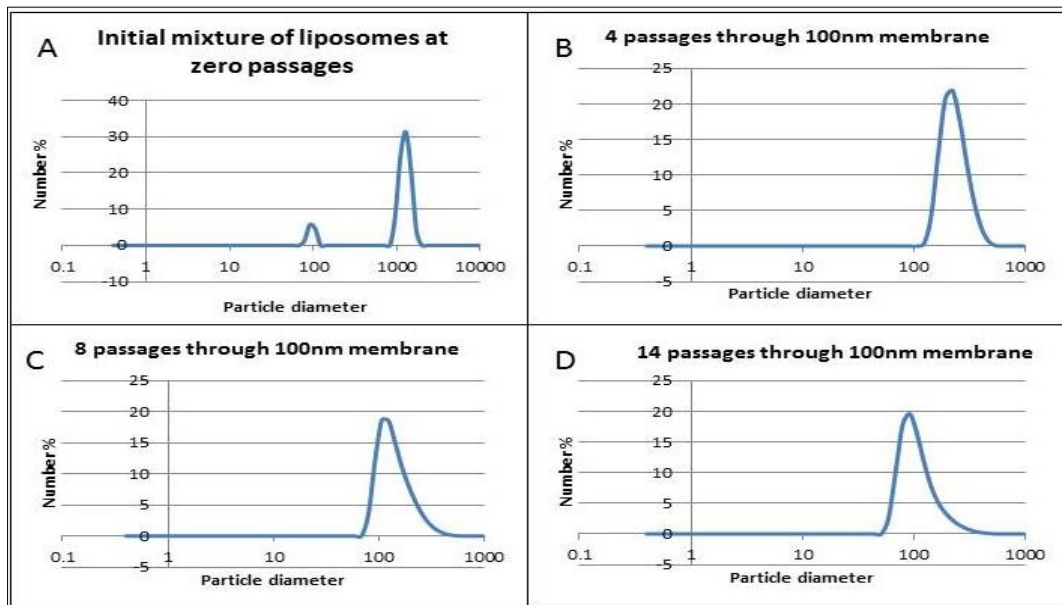
This experiment illustrates the importance of the number of extrusions of the liposome suspension, in order to give the most accurate and suitable size of liposomes, with a less polydisperse nanoliposome population. Polydispersity index (pdl) is a parameter of DLS which measures the heterogeneity of sizes of particles in a mixture (see figure 3.14). According to figures 3.15 and 3.16, it is clear that as the number of passages increases, the percentage of pdl decreases, giving a population which is more monodisperse and less polydisperse.



**Figure 3.14: Dispersity of nanoliposomes.** This illustration shows the two cases of dispersity of liposomes in a suspension. The illustration on the left shows a liposome suspension with a uniform population of liposomes (same size, mass and shape - i.e. low pdl) while the illustration on the right shows a liposome suspension with a non-uniform population of liposomes (inconsistent size, mass and shape - i.e. high pdl).

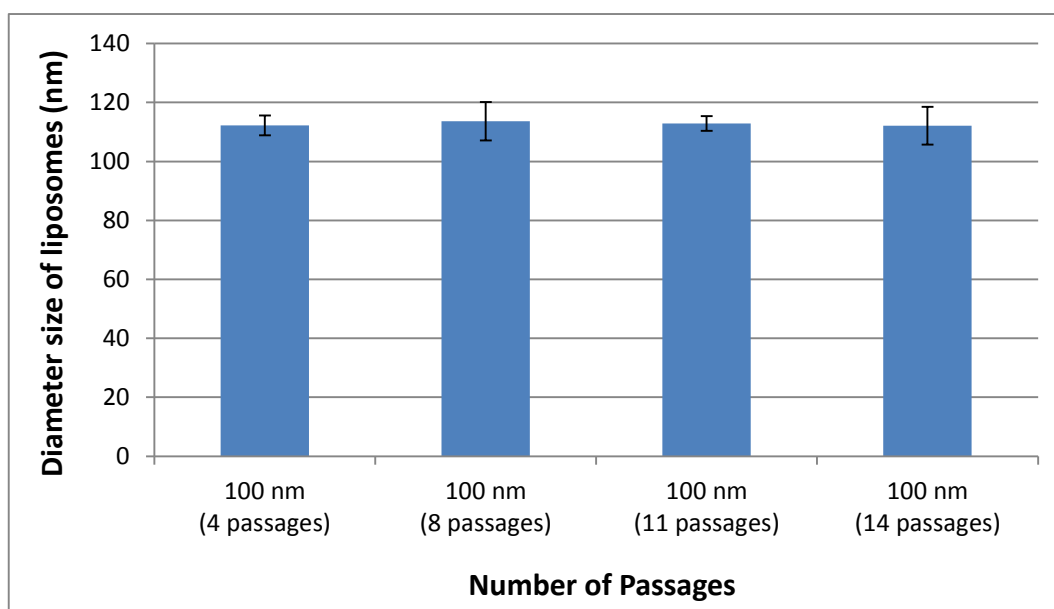


**Figure 3.15:** The graph describes the polydispersity of different populations of 100 nm simple liposomes produced by increasing number of passages through the extruder at room temperature. The calibration curve shows a near linear correlation, where the x-axis expresses the number of passages through the extruder, and the y-axis describes the recorded liposome pdl by DLS. As the number of passages increases the polydispersity decreases.

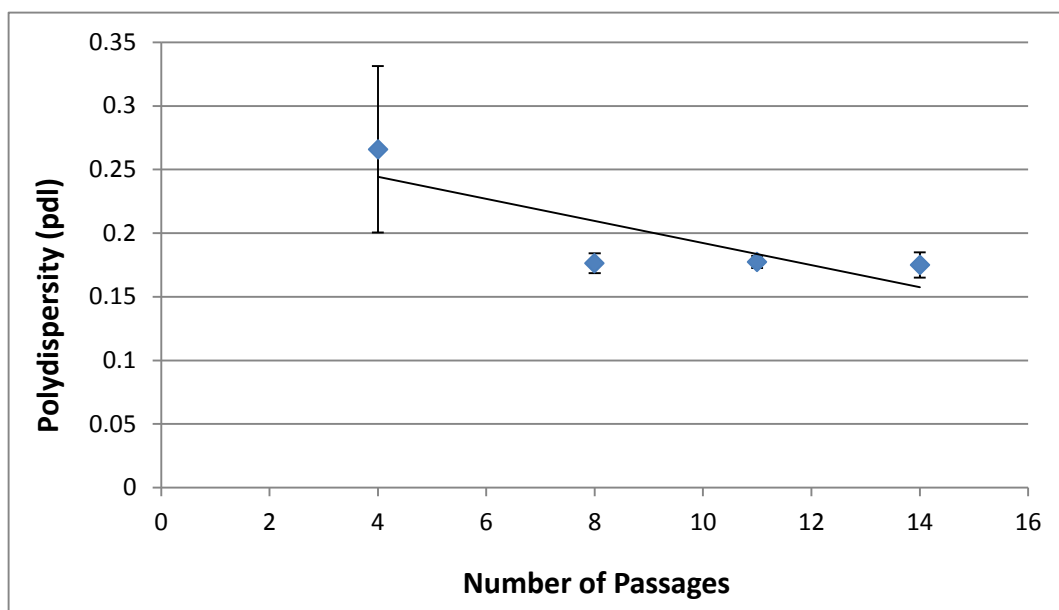


**Figure 3.16:** The graphs show the change of size distribution of 100 nm simple liposomes with increased number of passages. As the number of passages increases the population distribution of 100 nm simple liposomes becomes closer to 100 nm (A = zero passages, B = 4 passages, C = 8 passages and D = 14 passages).

On the other hand, in the case of liposome extrusion at 75°C the mean size of nanoliposomes (NL) was maintained at almost the same level for all passages. The 4<sup>th</sup> passage gave a mean size of  $112.23 \pm 3.38$  nm, compared to  $113.66 \pm 6.5$  nm at 8 passages,  $112.86 \pm 2.45$  nm at 11 passages and  $112 \pm 6.4$  nm at 14 passages (see figure 3.17). This illustrates the fact that liposome membranes become more fluid at high temperatures and so can pass more easily through the polycarbonate membrane filter, and in this case an accurate size is obtained from only the first four passages (Los and Murata, 2004).



**Figure 3.17:** The graph shows and compares the average size of 100 nm simple liposomes at 4, 8, 11 and 14 passages through the Avanti mini extruder at 75°C. The increase of temperature makes the liposomes more fluid and so they can pass through the polycarbonate membrane more easily. Consequently, from passage 4 until passage 14 the size of liposomes is approximately the same.



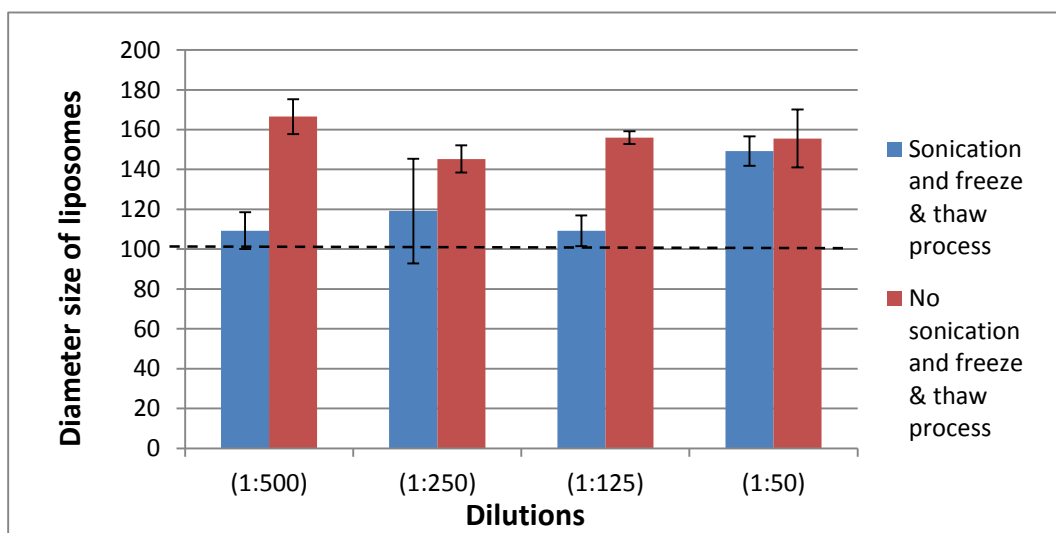
**Figure 3.18:** The graph describes the polydispersity of different populations of liposomes in a 100-nm simple liposome solution after four different passages through the extruder at 75°C. The calibration curve suggests a non-linear correlation, where the x-axis expresses the number of passages through the extruder, and the y-axis describes the polydispersity by DLS.

Furthermore, the polydispersity parameter of the liposomes was also tested for the other sizes that were investigated. With regard to the polydispersity of the three sizes of liposomes, it was found that for nanoparticles of 50 nm and 200 nm, the percentage of polydispersity after 11 passages through the appropriate polycarbonate membrane was higher than that obtained for the 100 nm liposomes. Accordingly, the populations of 50 nm and 200 nm liposomes were more polydisperse than the population of 100 nm NL (see table 3.1).

Simple liposomes at room temperature		
Expected particle size	Mean particle size $\pm$ SD	Polydispersity Index (PDI)
50 nm	75.34 nm $\pm$ 4.35	0.233
100 nm	104.2 nm $\pm$ 3.01	0.092
200 nm	214.4 nm $\pm$ 5.66	0.139

**Table 3.1:** The table shows the size and the polydispersity of different populations of 50 nm, 100 nm and 200 nm simple liposome suspensions after 11 passages through the extruder at room temperature (n=3). All values presented low percentage of polydispersity but 50 and 200 nm liposomes were more polydisperse than 100 nm liposomes.

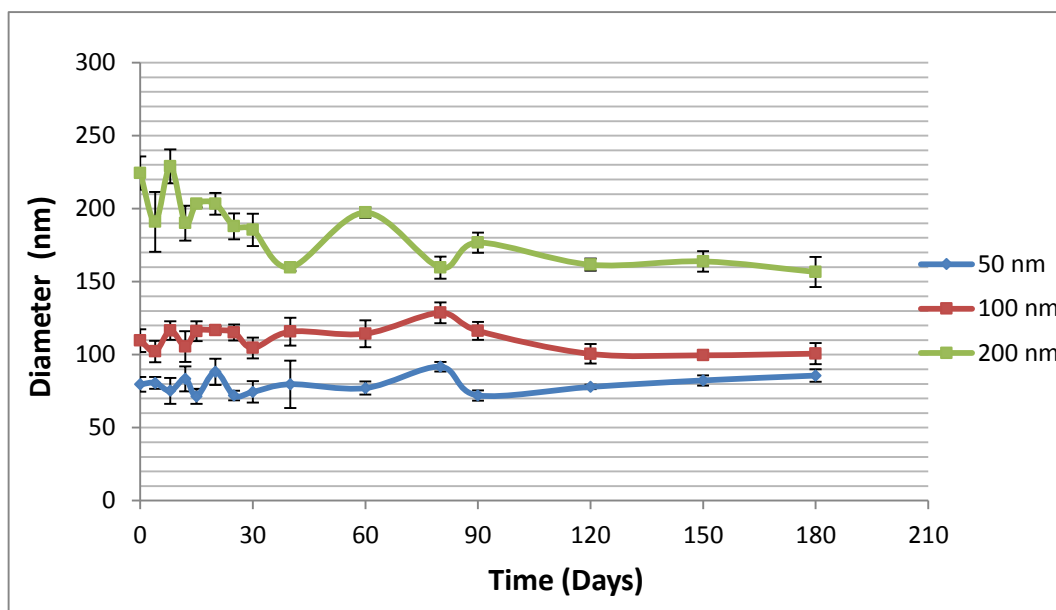
In addition, the size of NL was examined by comparing two samples of 100 nm liposomes (one of which had undergone sonication and freeze/thaw process and the other which did not), it is clearly that the liposome suspension which had undergone freeze/thawing, had a smaller diameter closer to 100 nm compared to the untreated liposome suspension. The two samples were measured by DLS at different dilutions (see figure 3.19).



**Figure 3.19:** The graph shows the average size of two liposome suspensions at different dilutions prepared with and without sonication followed by freeze/thawing. The blue bars represent the liposome suspension which had undergone sonication and a freeze/thaw process and the red bars represent the liposome suspension which did not undergo either of these two procedures. The black dashed line represents 100 nm and it can be seen that the blue bars are closer to this value.

After the evaluation of the size and the polydispersity of the three distinct sizes of simple liposomes, their stability (the ability of the liposomes to maintain a constant spherical shape and diameter) was also examined during storage for 6 months at 4°C. During first two months, the liposome suspensions were measuring at more frequent periods. The mean size for the 200 nm simple liposomes ranged from 229 nm (highest) to 159 nm (lowest), and as can be seen from figure 3.20, the mean size of liposomes during the 1<sup>st</sup> month remained close to 200 nm, but this fell to ~160 nm during months 2, 3 and 4. In contrast, the 100 nm and 50 nm liposomes appear to have a more stable size on long term storage, with the 100 nm liposomes in particular maintaining an almost constant size very close to 100 nm. The measurements for the 50 nm liposomes were relatively stable but were higher than the expected values. The mean values of 50 nm simple liposomes over six months ranged from 71 nm to 91 nm.





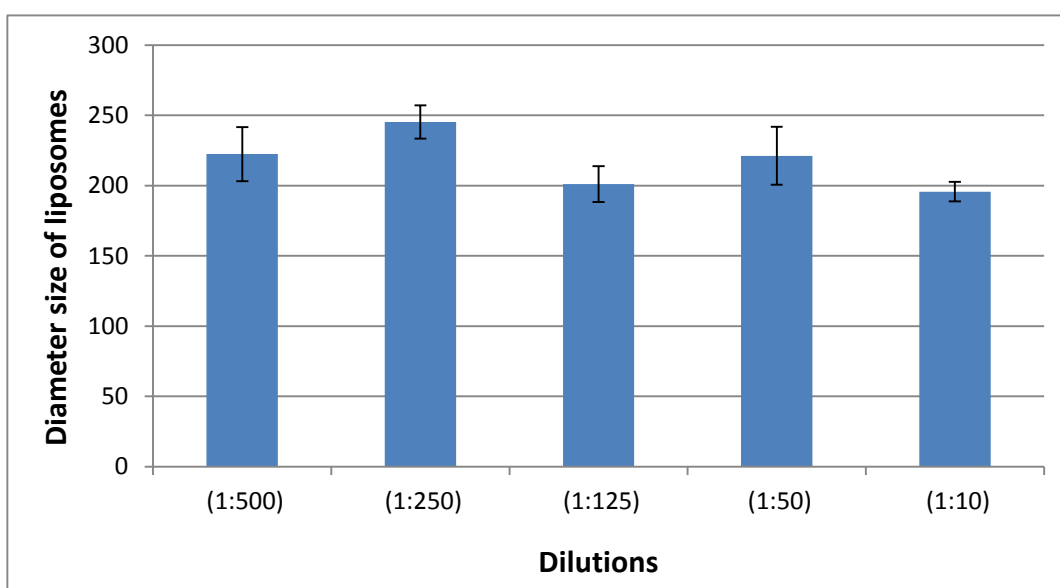
**Figure 3.20:** The graph shows the stability of the three different sizes of simple liposomes over 180 days at 4°C. The 100 nm liposomes seem to be the most stable compared to the other sizes (50 and 200 nm) and maintain their size stability for up to 6 months.

### 3.2.3 Characterization of MAL-PEG liposomes by size using DLS

PEGylated liposomes are simple liposomes which have 1,2-distearoyl-sn-glycero-3 phosphoethanolamine-N-[maleimide (polyethylene glycol)-2000] (mal-PEG-PE) incorporated into them. The inclusion of mal-PEG-PE into the liposomes offers the ability to improve their circulation times, maximize delivery, and produce PEG-lipid conjugates for the incorporation of targeting agents (Wang, et al., 2012). In the following section of the thesis, three distinct sizes (200, 100 and 50 nm) of PEGylated liposomes were produced and their size was also examined by DLS at different dilutions.

### 200 nm PEGylated liposomes

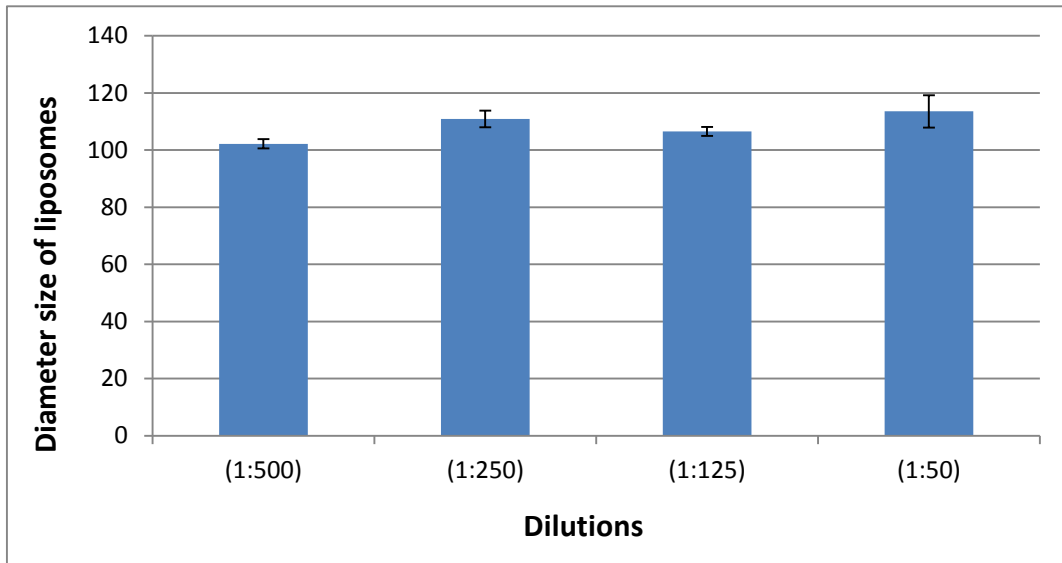
In contrast to the 200 nm diameter simple liposomes, the 200 nm PEGylated liposomes at different dilutions gave more stable mean diameter sizes, with values closer to 200 nm. Dilutions of 1:500, 1:250, 1:125, 1:50 and 1:10 gave mean ( $\pm$ SD) sizes of  $222.47 \pm 19.28$  nm,  $245.3 \pm 11.86$ ,  $201 \pm 12.7$  nm,  $221 \pm 20.6$  nm and  $195.7 \pm 6.9$  nm, respectively (see figure 3.21).



**Figure 3.21:** The graph shows the average sizes of 200 nm MAL-PEG liposomes at different dilutions. Bars show mean  $\pm$  SD ( $n=3$ ) for the different dilutions. All of them are close to the expected value, but the most accurate sizes (201.1 nm and 195.73 nm) were obtained at dilutions of 1:125 and 1:10, respectively.

### 100 nm PEGylated liposomes

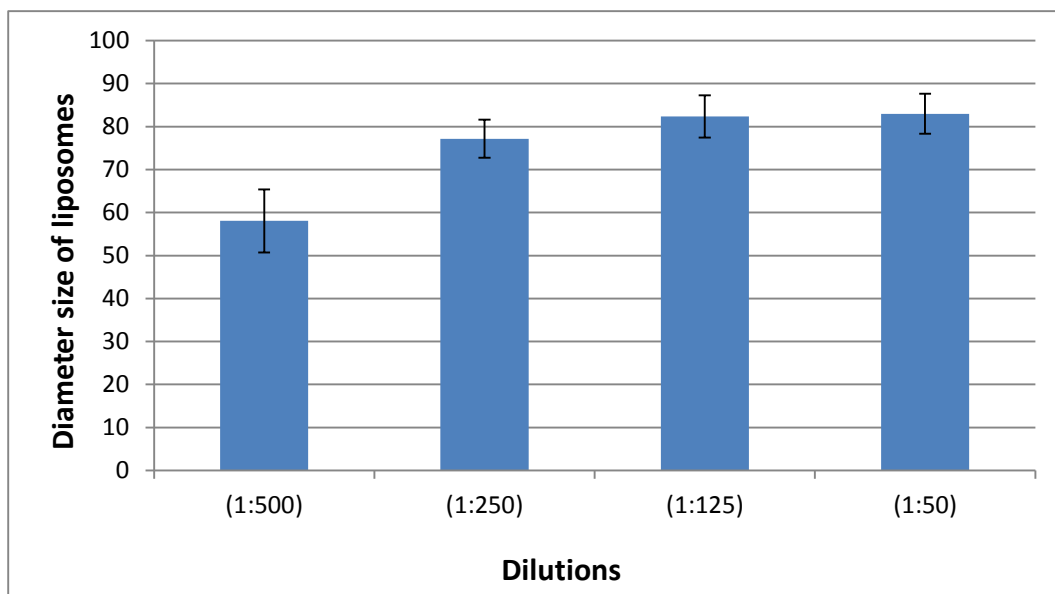
For the 100 nm PEGylated liposomes, the dilutions 1:500, 1:250, 1:50, 1:20 gave mean diameters of  $102 \pm 1.58$  nm,  $110.9 \pm 2.91$  nm,  $106.5 \pm 1.53$  nm and  $113.5 \pm 5.67$  nm respectively (see figure 3.22).



**Figure 3.22: The graph shows the average sizes of 100 nm MAL-PEG liposomes at different dilutions. Bars show mean  $\pm$  SD ( $n=3$ ) for the different dilutions. The values are similar at the different, dilutions, with the most accurate sizes (102. 2 nm and 106.53 nm) obtained at dilutions of 1:500 and 1:125, respectively.**

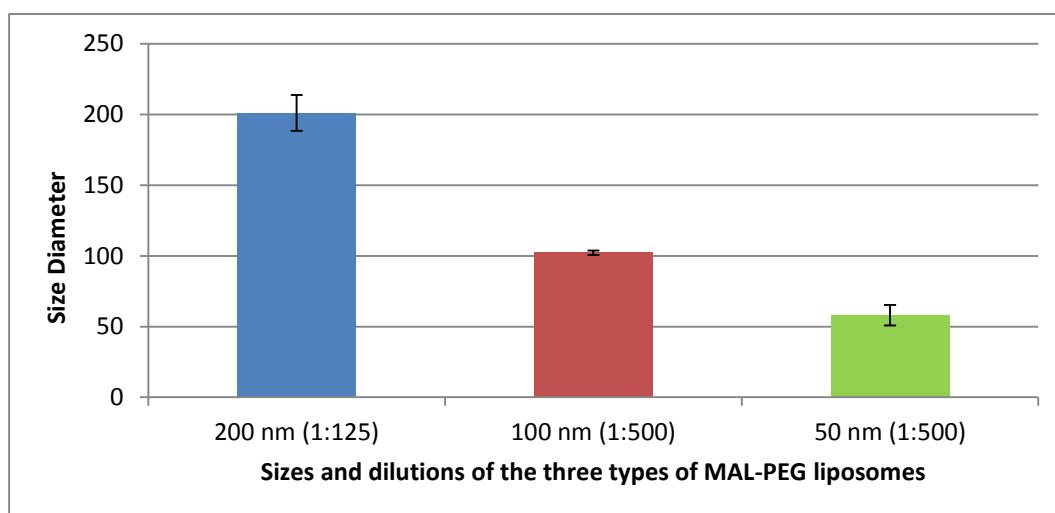
50 nm PEGylated liposomes

In the case of the 50 nm PEGylated liposomes the different dilutions of 1:500, 1:250, 1:50, 1:20 gave mean diameters of  $58 \pm 7.33$  nm,  $77.16 \pm 4.43$  nm,  $82.33 \pm 4.9$  nm and  $82.97 \pm 4.65$  nm, respectively (see figure 3.23).



**Figure 3.23:** The graph shows the average sizes of 50 nm MAL-PEG liposomes at different dilutions (n=3). Bars show  $\pm$  SD (n=3) for the different dilutions. The closest to the predicted value (58.05 nm) observed at a dilution of 1:500.

In general, the three different sizes of PEGylated liposomes gave variety of diameters at the different dilutions, which is an indication that the concentration of liposomes in a solution can affect the measurements by DLS. The closest value to the predicted size measurement of each PEGylated liposome preparation at its optimal concentration is plotted in figure 3.24, and the polydispersity of the different sizes at specific dilutions was also estimated (table 3.2).

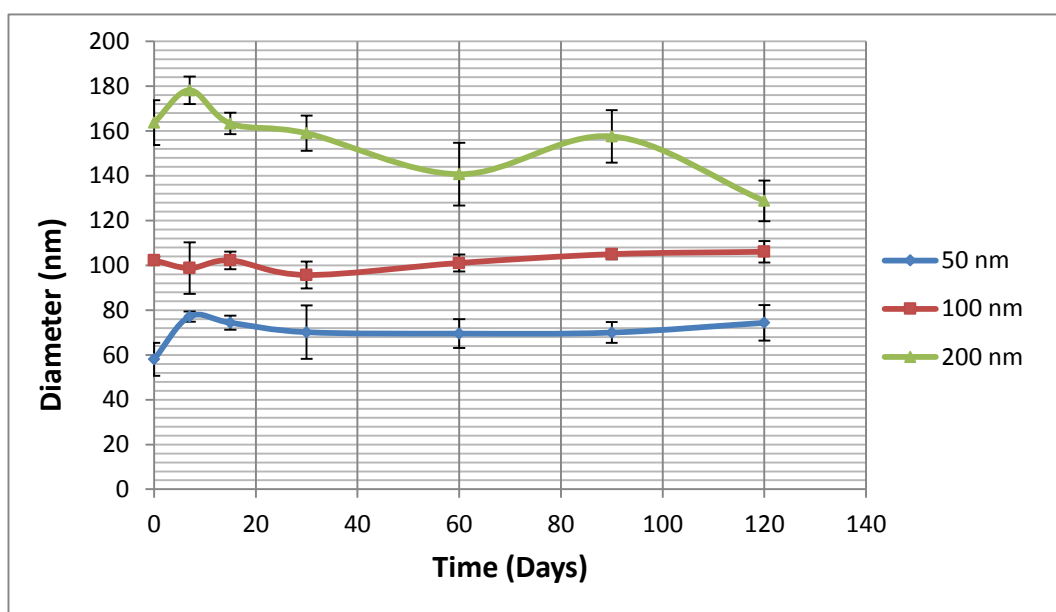


**Figure 3.24:** The graph shows the average diameters of 200, 100, and 50 nm MAL-PEG liposomes at different dilutions. Bars (mean  $\pm$  SD, n=3) show the dilutions required to give the most accurate size measurements of PEGylated liposomes of three distinct sizes.

PEGylated liposomes at room temperature		
Expected particle size	Mean particle size $\pm$ SD	Polydispersity Index (PDI)
50 nm	58.7 nm $\pm$ 7.33	0.202
100 nm	102 nm $\pm$ 1.58	0.128
200 nm	201 nm $\pm$ 12.7	0.241

**Table 3.2:** This table shows the size and the polydispersity of different populations of 50 nm, 100-nm and 200 nm PEGylated liposomes after 11 passages through the mini extruder at room temperature. The 100 nm PEGylated liposomes presented the lowest polydispersity compared to 50-nm and 200 nm PEGylated liposomes which had higher percentage of polydispersity.

As for the simple liposomes, the PEGylated liposomes were also characterized by DLS for their stability at 4°C for up to 120 days. The size and the polydispersity index indicated that sizes of liposomes with mal-PEG molecule incorporated into them remained stable for the 50 nm and 100 nm PEGylated liposomes, but decreased over time for the 200 nm PEGylated liposomes (figure 3.25). As can be seen from this figure, most stable liposome size was, again, 100 nm.



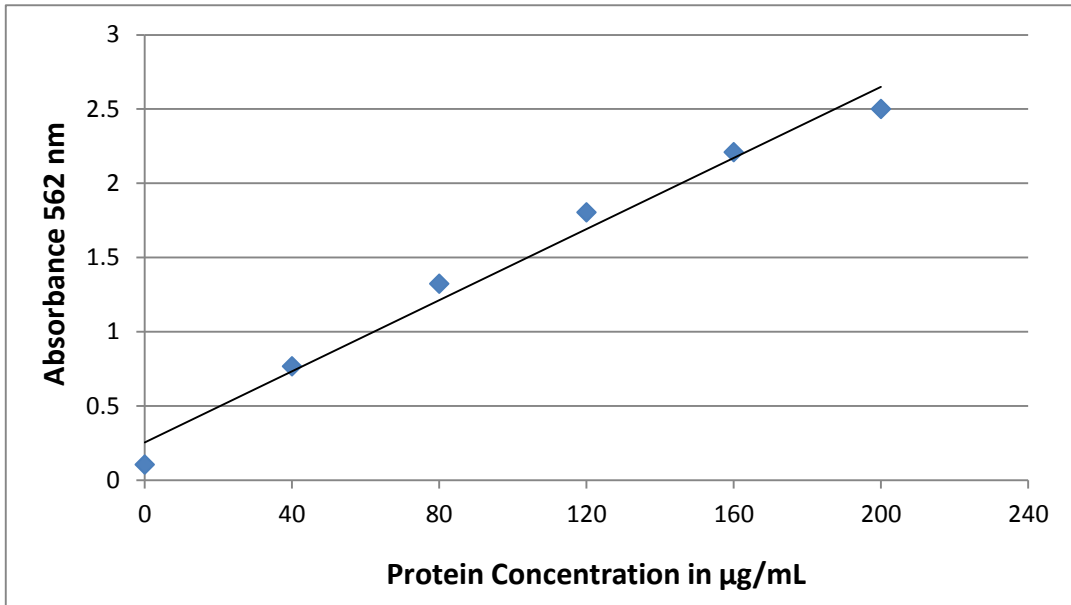
**Figure 3.25:** The graph shows the stability of the three different sizes of PEGylated liposomes over 120 days at 4°C. The 100 nm liposomes proved to be more stable and closer to their expected size than those of 100 and 200 nm diameter. The 200 nm PEGylated liposomes present a gradually decrease in size over time while the 50 nm PEGylated liposomes are maintained at a stable value that is higher than expected.

### **3.2.4 Characterization of Peptide Inhibitor Nanoparticles (PINPs) using DLS**

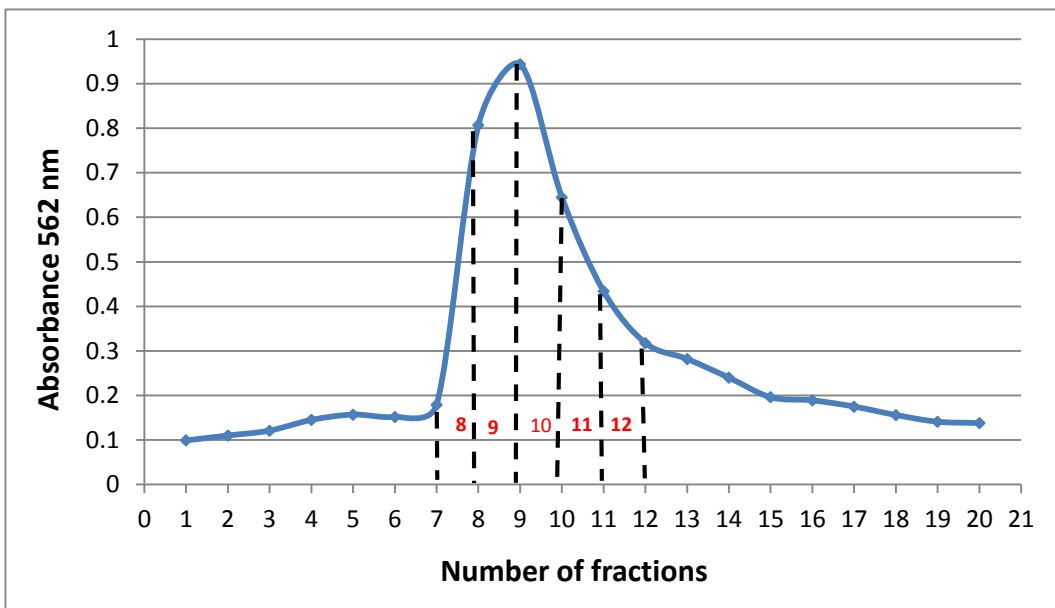
After the extrusion of PEGylated liposomes through the appropriate polycarbonate membranes, the RI-OR2-TAT-Cys peptide inhibitor was attached on the surface of the liposomes by reaction with the maliemide - PEG molecule. As the two intermediates stages of PINPs (simple and PEGylated liposomes) were measured by DLS, thus purified PINPs were also examined by DLS at different dilutions (see figures 3.29 - 3.31). Measurements of MAL-PEG liposomes and PINPs were taken in order to examine how the presence of inhibitor peptide on the MAL-PEG molecule affects the DLS measurements. The measurements of both types of more complex liposomes were compared with simple liposomes.

#### **Micro BCA protein assay**

After the purification of PINPs by gel exclusion chromatography using a sepharose 4B-CL column, the fractions were examined by a Micro BCA protein assay in order to quantify the amount of peptide bound to liposomes and identify the fractions containing the PINPs. The standard curve for this assay was plotted by the measurement of six different dilutions of Albumin (BSA), with a read out of absorbance at 562 nm (see figure 3.26). The protein content of the PINPs was measured in the same way. The initial column fractions did not contain any protein, but as the sample of liposomes (in filtered PBS) ran through the column, the PINPs started to emerge and be collected, in fractions 7-12 (see figure 3.27).



**Figure 3.26:** Standard curve for BSA in the micro plate BCA protein assay. *This curve indicates a linear correlation between protein content and absorbance (n= 1).*



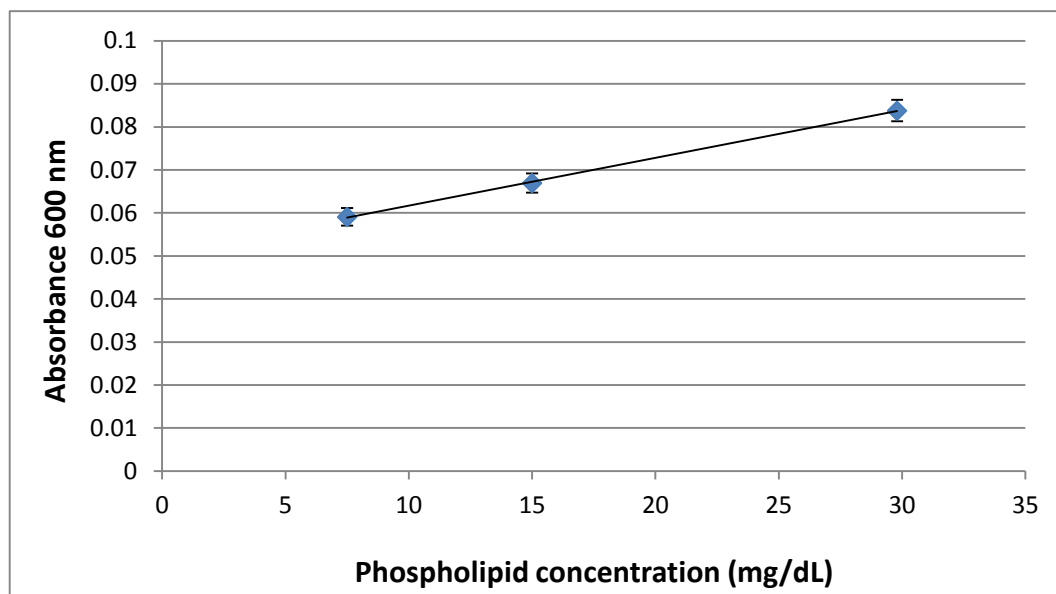
**Figure 3.27:** Elution profile following the purification of PINPs on a Sepharose 4B-CL column. *The x-axis indicates the fraction number while the y-axis gives a measure of protein concentration in BCA assay, as indicated by absorbance at 562 nm. The red numbers shows the fractions with the highest concentration of peptide inhibitor (PINPs). Fractions 8 and 9 contained the highest amount of PINPs.*

### **LabAssay Phospholipid (WAKO)**

After extrusion and column chromatography of the liposome suspension, phospholipid recovery was initially determined by phosphorous assay using the method of Stewart (Stewart, 1980). However, this method was not successful, and so another different phospholipid assay was used. This was the LabAssay (WAKO) phospholipid assay, which should determine the phospholipid content (sphingomyelin) of the liposomes, which were composed of two main lipids, cholesterol and sphingomyelin (1:1 molar ratio). This WAKO assay was more successful at determining the concentration of the lipid content of the liposomes and comparing it with the expected initial concentration (5 mM).

For example if PINPs were collected in two equal fractions, theoretically that means that each one of these two fractions has 2.5 mM of liposome suspension (2.5 mM + 2.5 mM = 5 mM). In other words, each fraction of PINPs contains 1.25 mM sphingomyelin and 1.25 mM cholesterol (molar ratio 1:1). The WAKO assay was able to quantify only the sphingomyelin based on an enzymatic reaction. Consequently, the values from the WAKO assay for each fraction, as determined from the standard curve, should give a phospholipid concentration close to 1.25 mM.

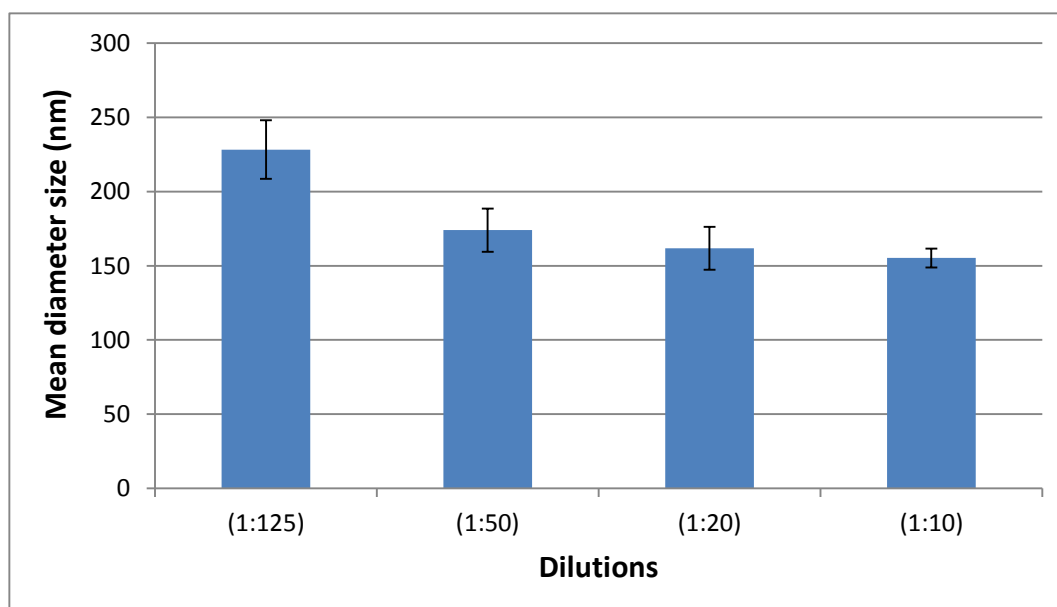




**Figure 3.28:** The graph shows the absorbance (600 nm) of the three phospholipid standards ( $n= 1$ ) as a function of phospholipid concentration (mg/dL) in the WAKO LabAssay.

### 200 nm PINPs

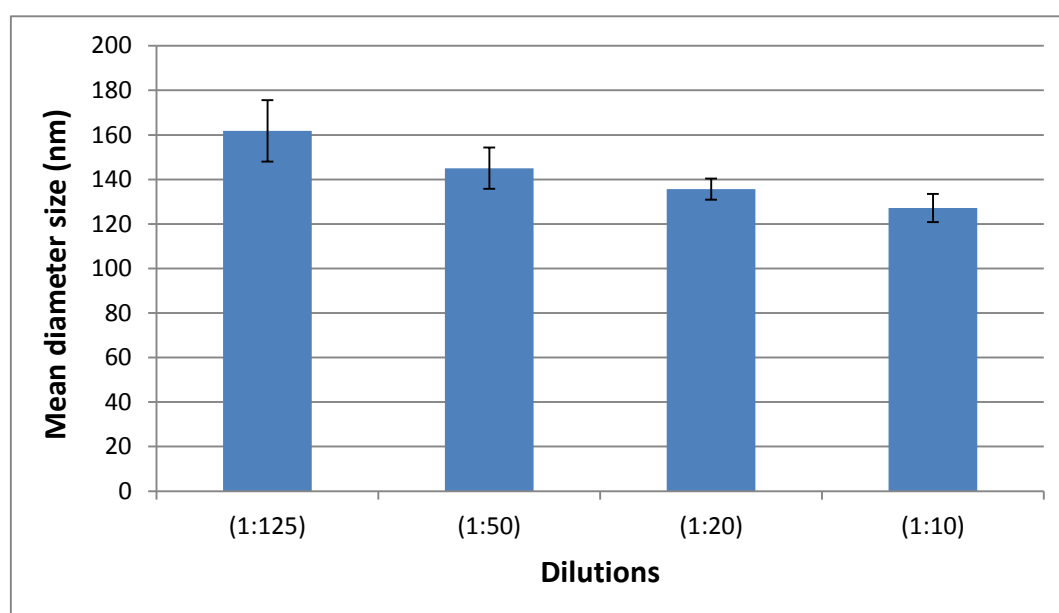
The 200 nm PINPs at different dilutions of 1:125, 1:50, 1:20 and 1:10 gave a mean size of  $228.27 \pm 19.77$  nm,  $174 \pm 14.57$  nm,  $161.8 \pm 14.43$  nm and  $155.23 \pm 6.34$ nm, respectively (see figure 3.29).



**Figure 3.29:** The graph shows the average sizes of 200 nm PINPs at different dilutions, as determined by DLS. Bars (mean  $\pm$  SD,  $n=3$ ) show a variety of values at the different liposome dilutions, with the most accurate values (228.27 and 174 nm) observed at dilutions 1:125 and 1:50, respectively.

### 100 nm PINPs

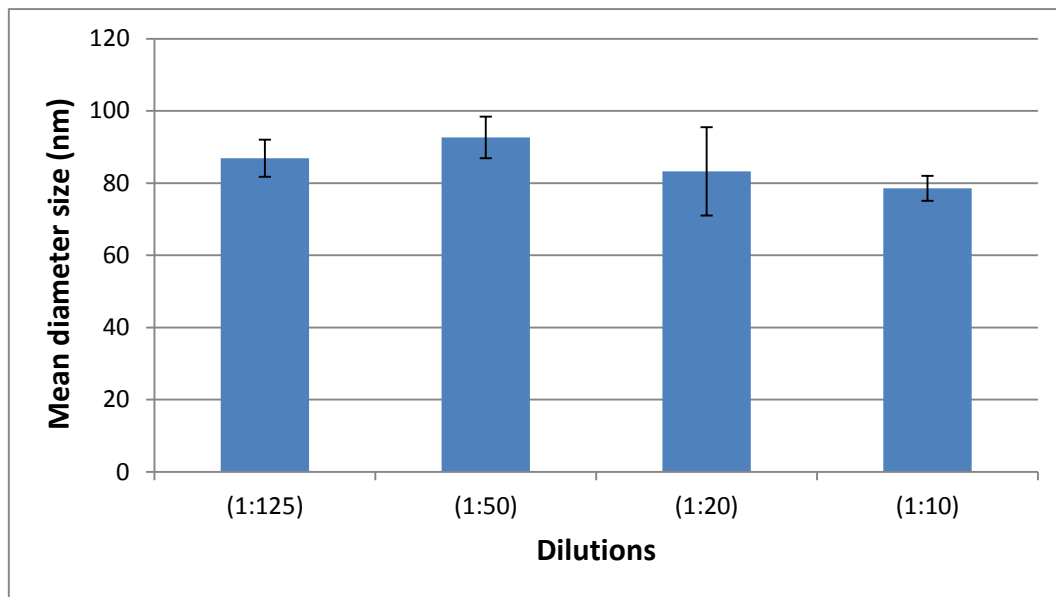
The 100nm PINPs were examined at different dilutions using DLS, but, as can be observed from the figure 3.30, their size estimates gave higher values than those obtained for 100 nm simple and PEGylated liposomes. For the dilutions of 1:125, 1:50, 1:20, and 1:10, DLS gave a mean diameter of  $161.77 \pm 13.8$  nm,  $145.03 \pm 9.2$  nm,  $135.6 \pm 4.75$  nm and  $127.1 \pm 6.32$  nm respectively.



**Figure 3.30:** The graph shows the average diameter of 100 nm PINPs at different dilutions, as determined by DLS. A variety of values (mean  $\pm$  SD,  $n=3$ ) were observed at the different liposome dilution with the most accurate values (135.6 and 127.1 nm) at dilutions of 1:20 and 1:10. However, all values were slightly larger than the anticipated.

### 50 nm PINPs

In the case of 50 nm PINPs the different dilutions of 1:125, 1:50, 1:20, 1:10 gave mean diameters of  $86.92 \pm 5.13$  nm,  $92.65 \pm 5.73$  nm,  $83.26 \pm 12.25$  nm and  $78.57 \pm 3.46$  nm, respectively (see figure 3.31).

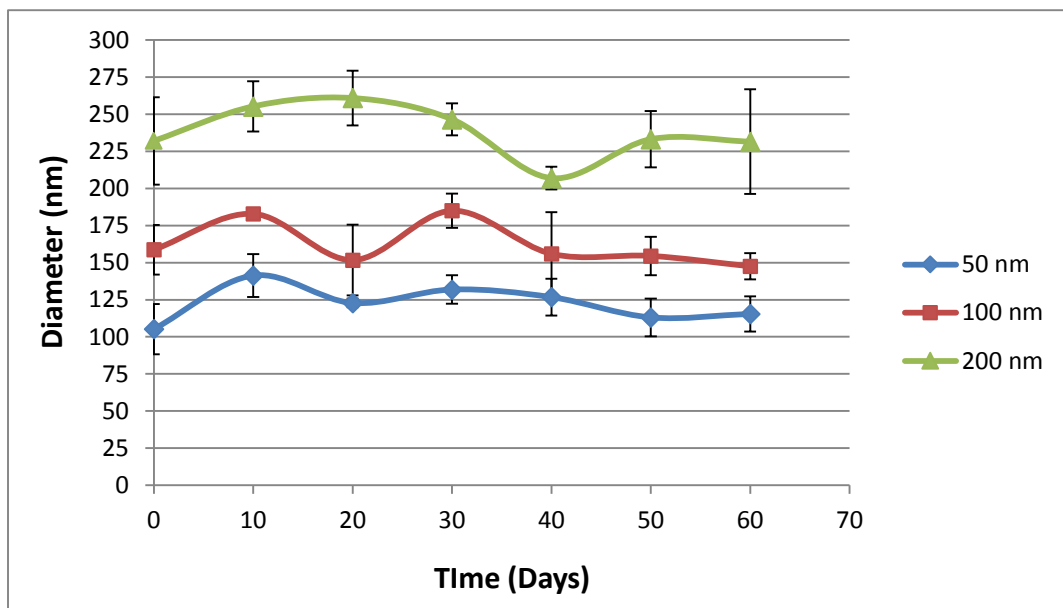


**Figure 3.31:** The graph shows the average sizes of 50 nm PINPs at different dilutions as determined by DLS. A variety of values (mean  $\pm$  SD,  $n=3$ ) was observed at the different liposome dilutions with the most accurate value (78.57 nm) obtained at a dilution of 1:10. However, all values were slightly larger than the anticipated.

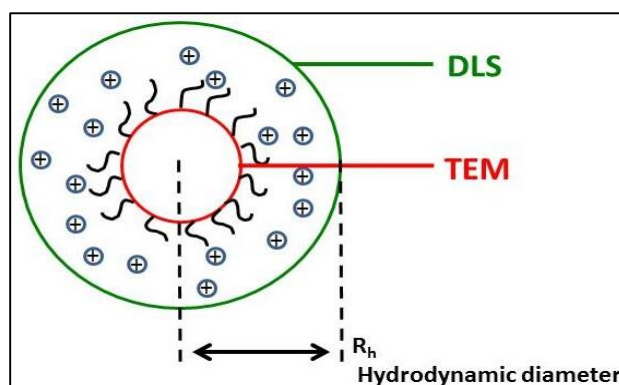
### Stability assay for PINPs

A stability assay for PINPs was also carried out in order to test if the presence of the peptide inhibitor on the surface of the liposomes could affect their size stability by DLS. The three different sizes of PINPs were examined for two months at 4°C. The liposome suspensions were measured every 10 days and for this stability test the same dilution of 1:20 was used throughout. The PINPs showed higher values using DLS compared to simple and PEGylated liposomes, and their polydispersity values were also greater. As can be seen from figure 3.32, the size measurements of PINPs were not as stable and reproducible as those of simple and PEGylated liposomes. Consequently, comparing the three stability assays for the three different types of liposomes, we can conclude that the peptide inhibitor may affect the DLS

measurements. A possible explanation of what happens with PINPs at different dilutions is given in the diagram below (see figure 3.33). Due to the fact that peptide inhibitor RI-OR2-TAT, and specifically the TAT region of the peptide has a high positive charge, this may affect the electrical conductivity of the liquid and so create a larger hydrodynamic diameter ( $R_h$ ) than the simpler liposomes, and this is detected and measured by DLS instead of the normal hydrodynamic diameter.



**Figure 3.32:** The graph shows a stability test of the three different sizes of PINPs for 2 months using dilution of 1:500 at 4°C. The three different sizes of PINPs gave variety of values during the two months and also DLS gave higher values than the expected for all sizes.



**Figure 3.33: Hydrodynamic diameter.** This diagram indicates how the electrical charge of a PINP can affect the measurement of its size using DLS and TEM. DLS, measures the hydrodynamic diameter ( $R_h$ ) of the nanoparticle and as result would be anticipated to give a larger value than with TEM which measures the physical diameter.

### Conclusion (using Dynamic Light Scattering DLS)

DLS was one of the techniques used in this project in order to characterize and compare the sizes of the three types of liposomes. As can be observed from the data above, DLS proved to be a rapid and easy technique for the measurement of wet nanoparticles with diameters of 200 nm or less. Furthermore, as the three different types of liposomes gave varying size measurements at different concentrations it was shown that concentration is an important factor which can affect the measurement of the diameter of nanoliposomes. It is important to mention that in order to obtain the above results I carried out many measurements of the liposomes suspensions, as the values from DLS varied each time. In addition, the presence of the PEG molecule and the peptide on the surface of the liposomes resulted in slight changes in diameter compared with simple liposomes. However, DLS does not give any direct information on the shape and morphology of the liposomes, and so further examination of the ultrastructure of liposomes was carried out using Transmission Electron Microscope (TEM).

## **CHAPTER FOUR - TEM RESULTS**

### **4.1 Ultrastructural characterization of liposomes by size and shape using Transmission Electron Microscope (TEM)**

In this chapter the morphology and the size of the three types of NLPs was investigated using a powerful imaging technology, TEM. TEM cannot reveal any chemical or behavioral differences between plain, MAL-PEG and PINP liposomes, but is able to characterize them by their size and shape.

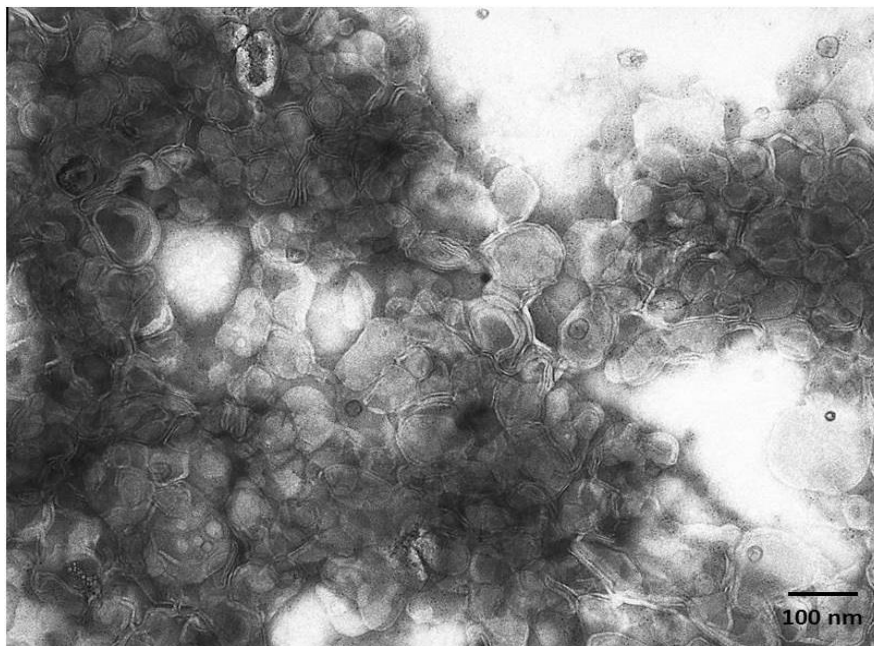
#### **4.1.1 Morphology and ultrastructure of simple liposomes**

The samples underwent negative staining (liposomes in filtered PBS) and were examined under TEM by Dr. Nigel Fullwood. Negative staining is a fast and relatively easy procedure. The ultrastructure of different types of liposomes using TEM can reveal not only their shape, but also their lamellarity which is an important aspect of their structure and consequent properties. So, in order to evaluate the importance of a freeze and thaw process and bath sonication method during the preparation of liposomes (by the thin film method) and how this can affect their lamellarity we prepared samples in which both of these the two techniques were applied, and some samples without. According to the negative staining micrographs, the majority of simple liposomes of different sizes, prepared without freeze-thaw and sonication processes have a multilamellar structure (e.g. see figure 4.3). Initially, the TEM samples were prepared using 5 mM liposomes (total lipid content), but as can be seen in some images (figures 4.1 and 4.3) these liposomes were much too concentrated and could not be examined properly. Subsequent samples used a less

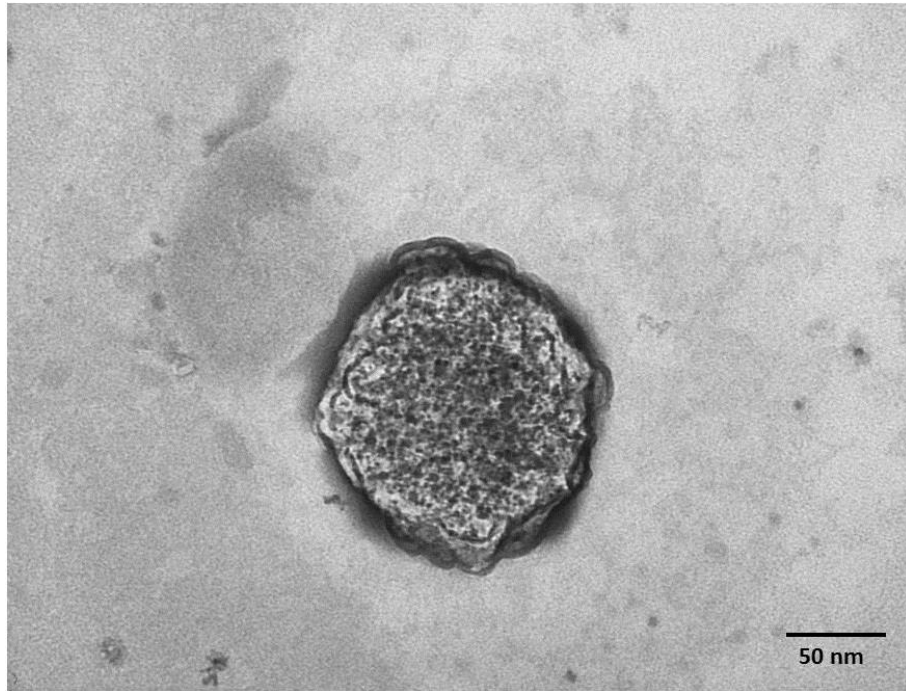
concentrated suspension of liposomes (1 mM) to avoid their dense accumulation. However, even though a lower concentration of liposomes was used, under the TEM, the liposomes were still seen to congregate in large clumps. In addition, some of them have a typical ring shape (unilamellar) (see figure 4.2) but the majority of them gave an unstable shape with an onion layer (multilamellar) (see figure 4.3) structure.

### **100 nm simple liposomes**

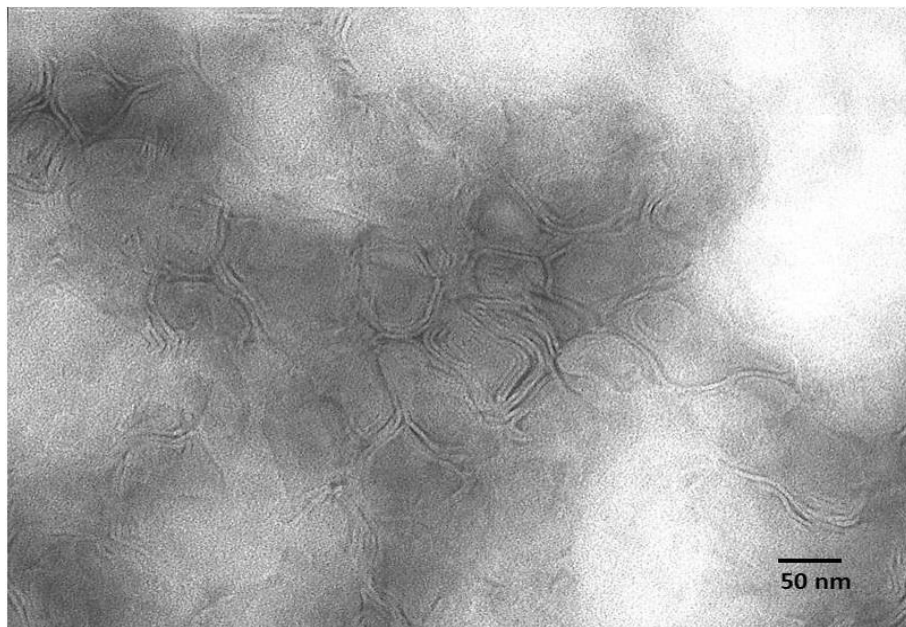
The following negative staining micrographs represent simple liposomes of 100 nm diameter which did not use a freeze and thaw process and bath sonication during their preparation. As can be observed from the micrographs, the majority of these liposomes have an irregular shape and almost all of them are multilamellar vesicles (onion layer structure).



**Figure 4.1: 100 nm simple liposomes in filtered PBS at 5 mM.** *The negative staining micrograph shows a sample of 100 nm simple liposomes. The liposomes can be seen as being rounded in shape but their size varies in the range of 40-200 nm. Scale bar = 100 nm.*



**Figure 4.2: 100 nm simple liposome in filtered PBS.** *The negative staining micrograph shows a sample of 100 nm simple liposomes. This single liposome can clearly be seen as being rounded in shape, at high magnification. Scale bar = 50 nm.*

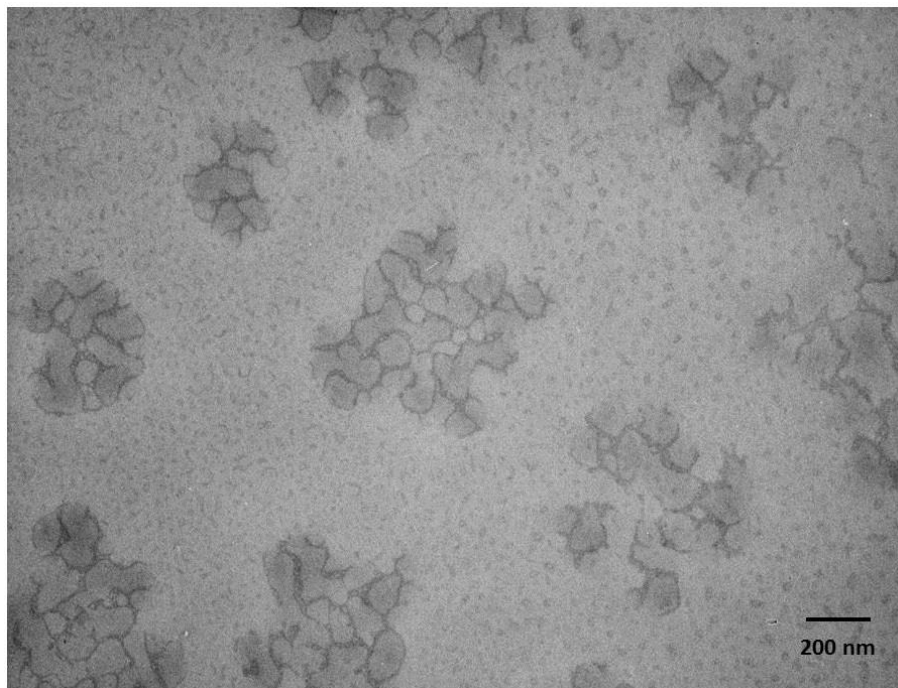


**Figure 4.3: 100 nm simple liposome in filtered PBS at 5 mM.** *The negative staining micrograph shows a sample of 100 nm simple liposomes. The liposomes can clearly be seen as being rounded in shape but the majority of them are multilamellar structures (onion structure). Scale bar = 50 nm.*



### **50 nm simple liposomes**

The following negative staining micrographs represent simple liposomes of 50-nm diameter which were not subjected to the freeze and thaw process and bath sonication during their preparation. As can be seen from the images below, the liposomes present an irregular shape and they form clumps (see figure 4.4). The images were taken at low magnification in order to see how the liposomes are arranged in the space.

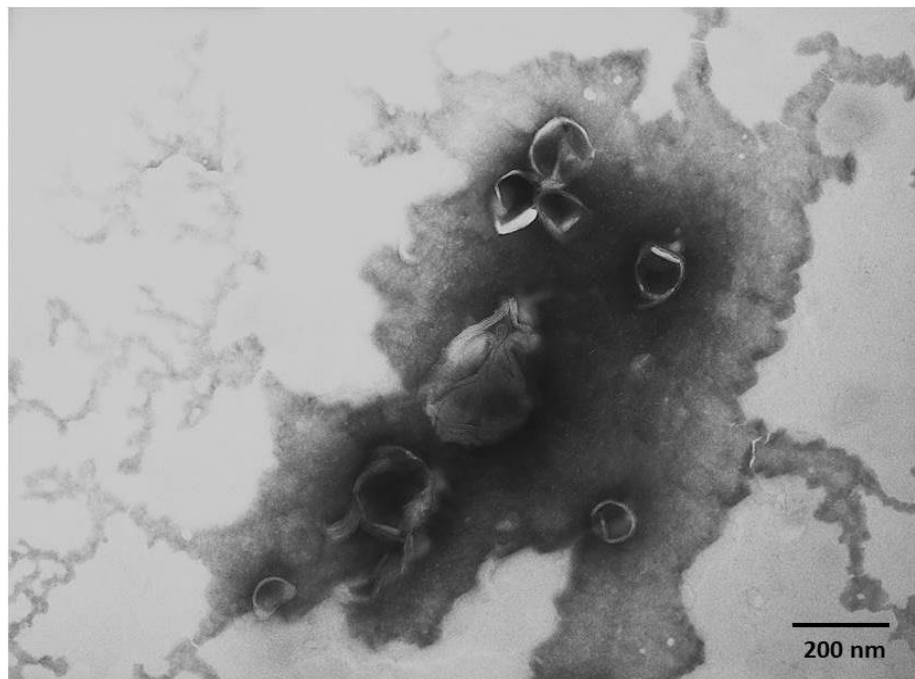


**Figure 4.4: 50 nm simple liposomes in filtered PBS at 1 mM:** *The negative staining micrograph shows a sample of 50 nm simple liposomes. The liposomes can clearly be seen as being rounded in shape with their diameter being close to 50 nm. Liposomes attract each other, creating clumps. Scale bar = 200-nm.*

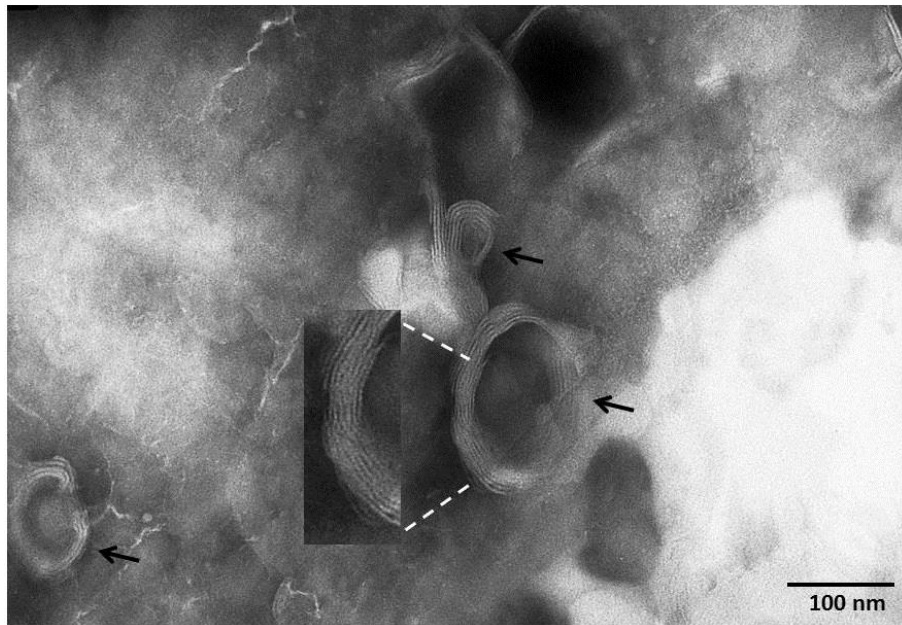
#### 4.1.2 Morphology and ultrastructure of PEGylated liposomes using TEM

##### 100 nm PEGylated liposomes

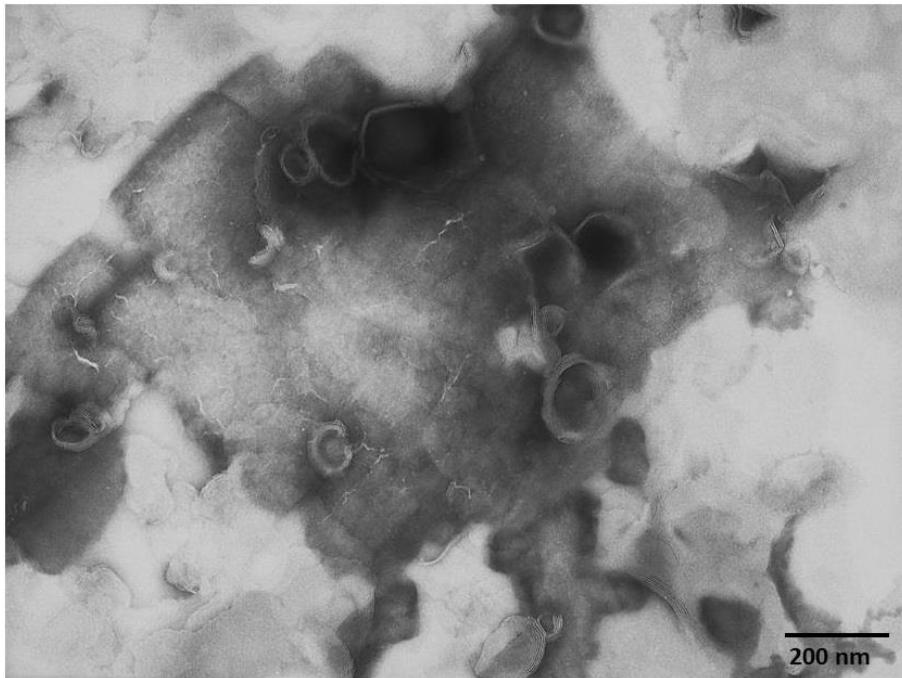
The following negative staining micrographs represent PEGylated liposomes of 100 nm diameter which were not subjected to a freeze and thaw process and bath sonication during their preparation. As can be observed from the micrographs below, the majority of liposomes have an irregular shape and almost all of them have multilamellar structures (onion layer structure) (see figures 4.6 and 4.8).



**Figure 4.5: 100 nm PEGylated liposomes in filtered PBS at 1 mM.** *The negative staining micrograph shows a sample of 100 nm PEGylated liposomes. The micrograph shows a heterogeneous population of vesicles which have a distorted shape and vary in size. The majority of them have multilamellar structures (onion layer structure). Scale bar = 200 nm.*



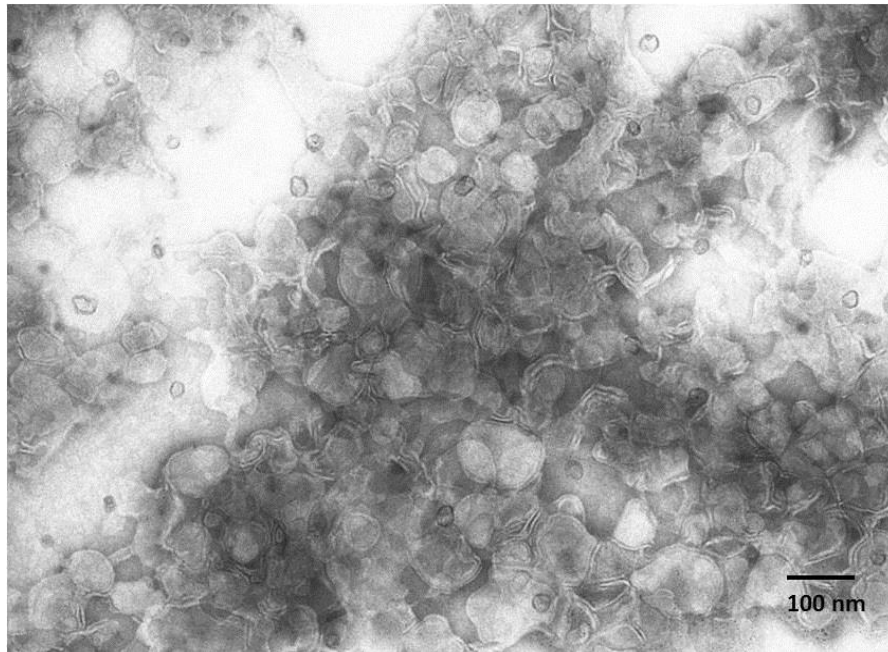
**Figure 4.6: 100 nm PEGylated liposomes in filtered PBS at 1 mM.** *The negative staining micrograph shows a sample of 100 nm PEGylated liposomes. The liposomes can clearly be seen as being rounded in shape (see arrows) but the majority of them are multilamellar structures (onion layer structure). The dashed lines show the multiple layers of the liposome at higher magnification. Scale bar = 100 nm.*



**Figure 4.7: 100 nm PEGylated liposomes in filtered PBS at 1 mM.** *The negative staining micrograph shows a sample of 100 nm PEGylated liposomes in filtered PBS. The micrograph shows a heterogeneous population of vesicles which have a distorted shape and vary in size. Scale bar = 200 nm.*



**Figure 4.8: 100 nm PEGylated liposomes in filtered PBS at 1 mM.** *The negative staining micrograph shows a sample of 100 nm PEGylated liposomes at high magnification. The liposomes were clustered together creating a clump of liposomes. Multilamellar structures are also visible. Scale bar = 50 nm.*

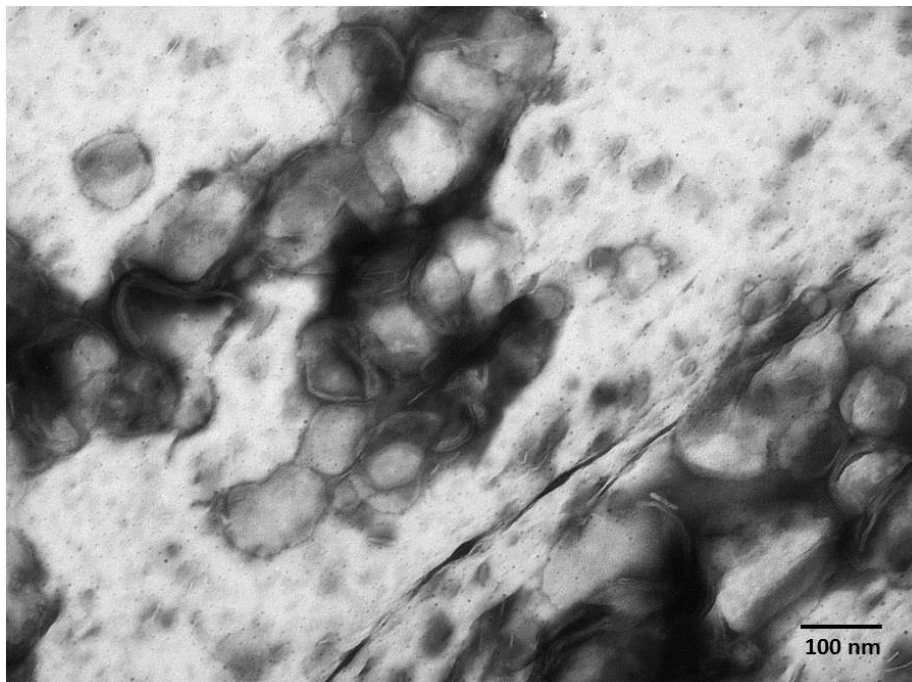


**Figure 4.9: 100 nm PEGylated liposomes in filtered PBS at 2.5 mM.** *The negative staining micrograph shows a concentrated sample (2.5 mM) of 100 nm PEGylated liposomes. The liposomes can clearly be seen as being rounded in shape. The micrograph shows a heterogeneous population of vesicles which have a distorted shape and vary in size. Scale bar = 100 nm.*

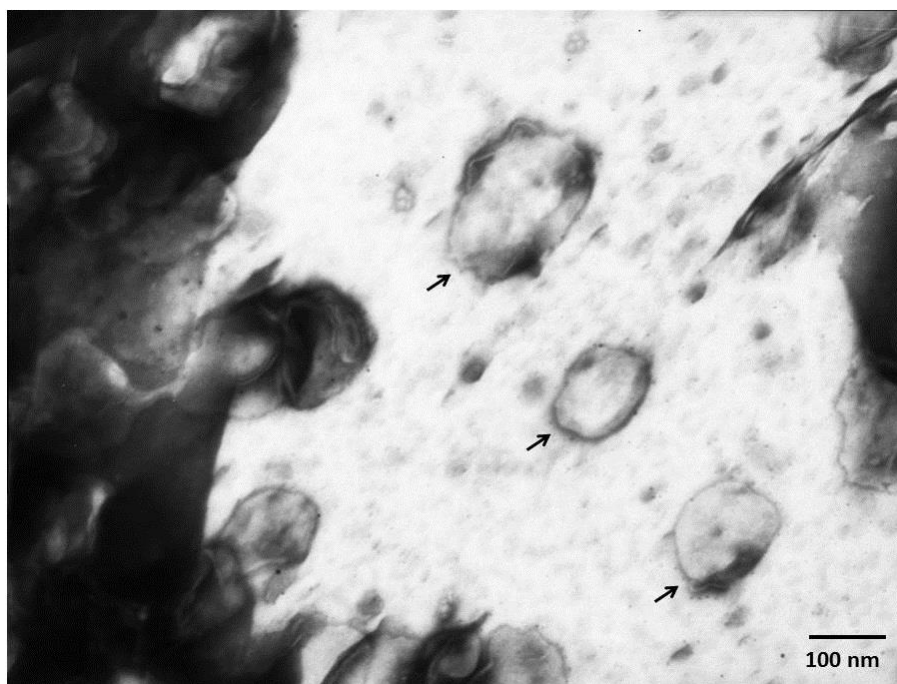
### 4.1.3 Morphology and ultrastructure of PINPs using TEM

#### 200 nm PINPs

For vesicles larger than 100 nm in diameter, the procedures of freeze and thaw and bath sonication are not recommended because this will decrease their diameter, something that must be avoided in this case. So, in this case, the samples of 200 nm liposomes were prepared without either of these two procedures. The following negative staining micrographs represent a heterogeneous population of PINPs with unstable size and shape (see figures 4.10 and 4.11).



**Figure 4.10:** 200 nm PINPs in filtered PBS at 1 mM. *The negative staining micrograph shows a sample of 200 nm PINPs. The liposomes were clustered together, creating clumps. Scale bar = 100 nm.*

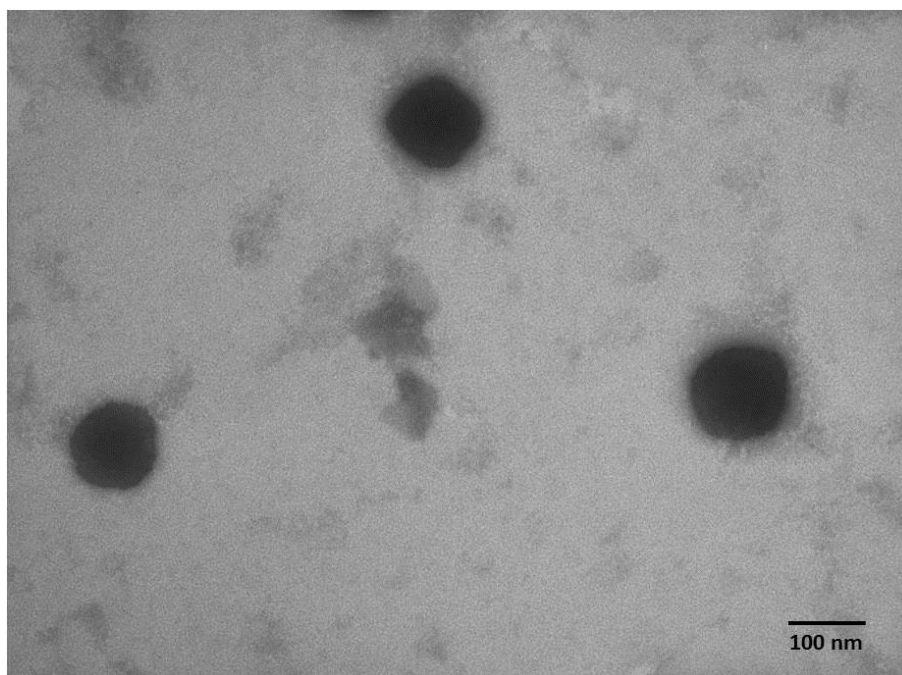


**Figure 4.11: 200 nm PINPs in filtered PBS at 1 mM.** *The negative staining micrograph shows a sample of 200 nm PINPs diluted in filtered PBS. The liposomes can clearly be seen as being rounded in shape while a heterogeneous mixture of PINPs with a diameter range of 100-200 nm was observed (see arrows). Scale bar = 100 nm.*

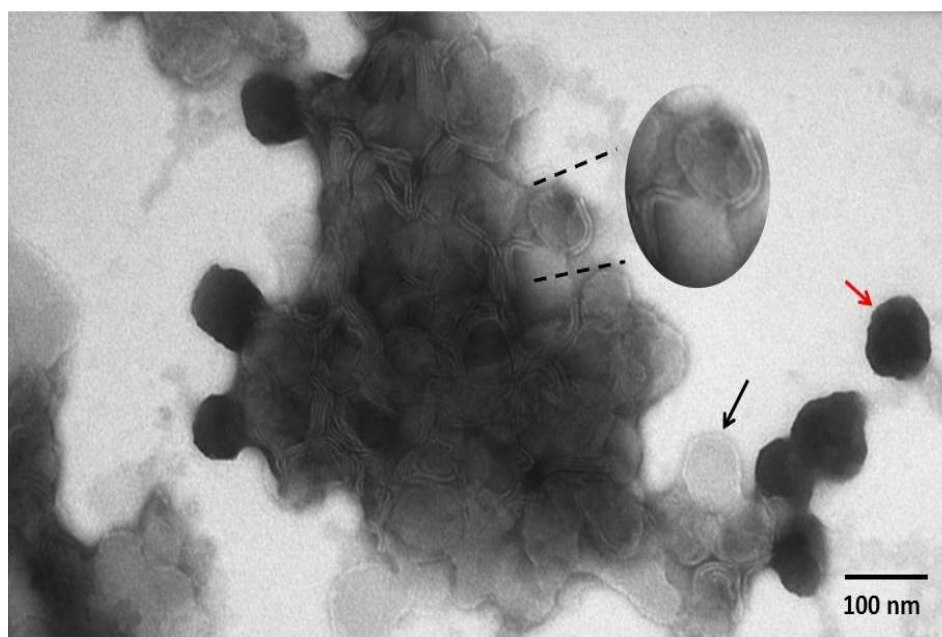
### **100 nm PINPs**

The following negative staining micrographs represent PINPs of 100 nm which were subjected to a freeze and thaw process and bath sonication during their preparation. As can be observed from the micrographs below, the majority of these liposomes have a more stable and rounded shape, close to their expected size (100-nm) and they now have a unilamellar structure. In addition, in the following negative staining micrographs (see figures 4.12 and 4.13) some of the liposomes were stained positively while some others negatively.





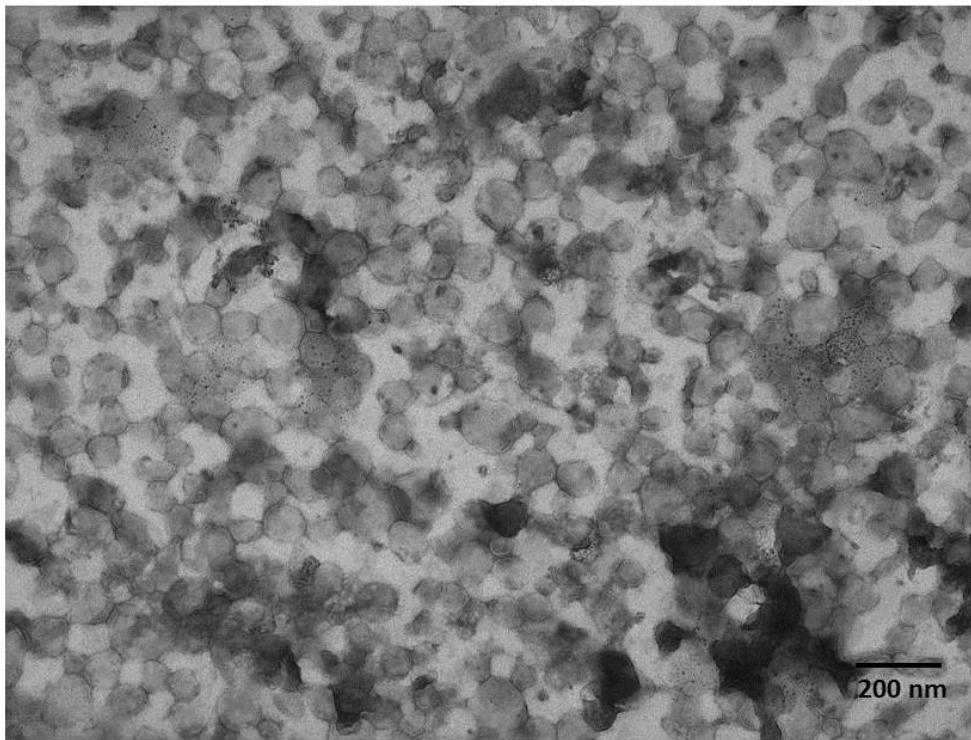
**Figure 4.12: 100 nm PINPs in filtered PBS at 1 mM.** *The negative staining micrograph shows a sample of 100- nm PINPs. The liposomes can clearly be seen as being rounded in shape and they vary only slightly in size. Scale bar = 100 nm.*



**Figure 4.13: 100 nm PINPs in filtered PBS at 1 mM.** *The negative staining micrograph shows a sample of 100 nm PINPs. The liposomes were clustered together creating clumps. The red arrow shows a liposome with positive staining while the black arrow shows a liposome with negative staining. The dashed lines show the enlargement of a liposome with two layers. Scale bar = 100 nm.*

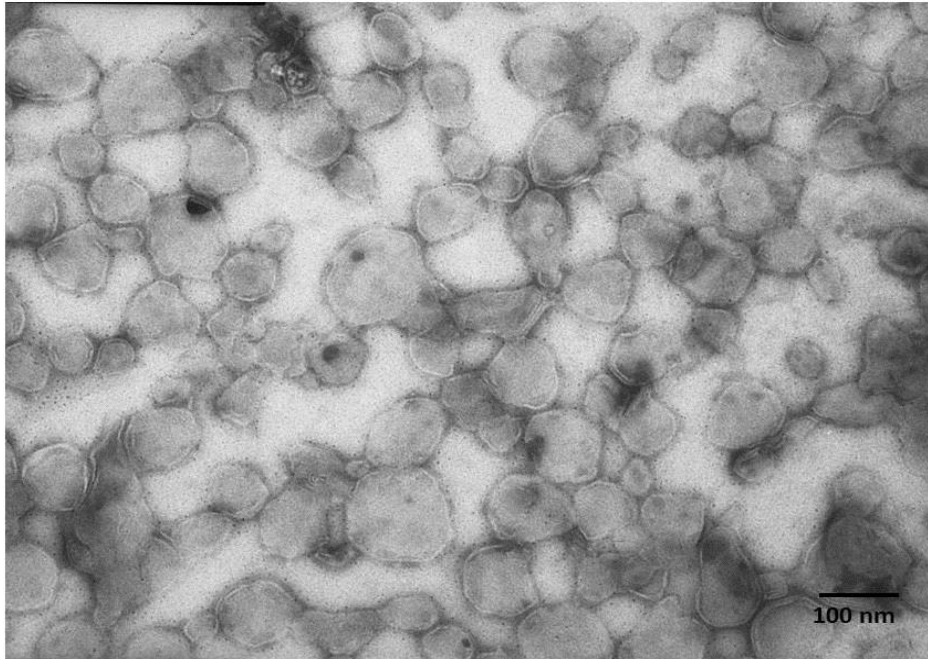
## **50 nm PINPs**

The following negative staining micrographs represent a sample of 50 nm PINPs where the freeze and thaw process using liquid nitrogen and bath sonication was applied during their preparation. As can be seen, these two methods are responsible for the transformation of multilamellar vesicles to unilamellar (single layer) vesicles. As can be observed from the micrographs below (see figures 4.14 - 4.17), most of these liposomes have a more stable and rounded shape, and they also have a unilamellar structure.

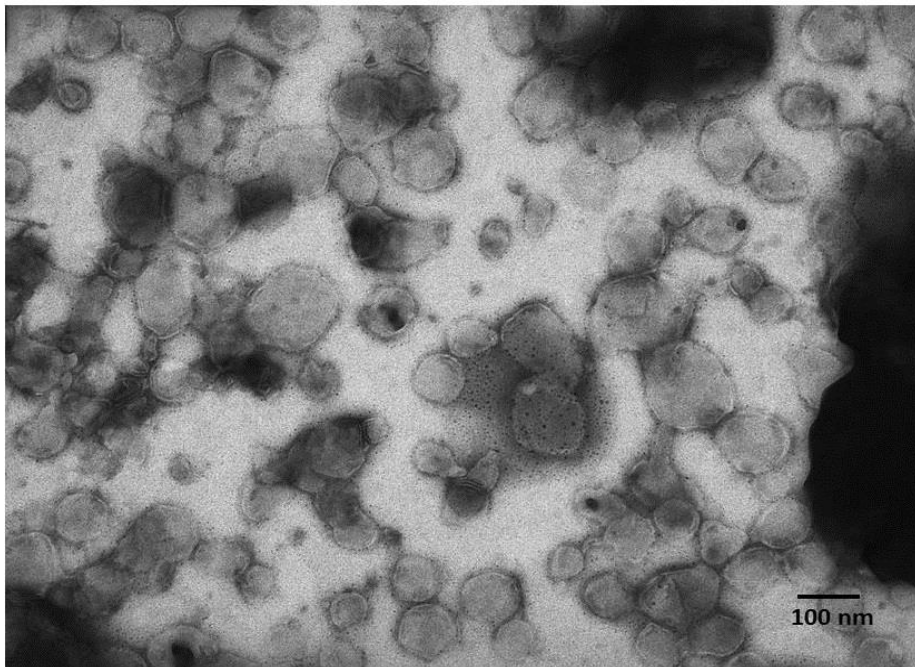


**Figure 4.14: 50 nm PINPs in filtered PBS at 1 mM.** Here the PINPs were prepared with freeze-thawing and bath sonication. The negative staining micrograph shows a sample of 50 nm PINPs liposomes at low magnification. Scale bar = 200 nm.

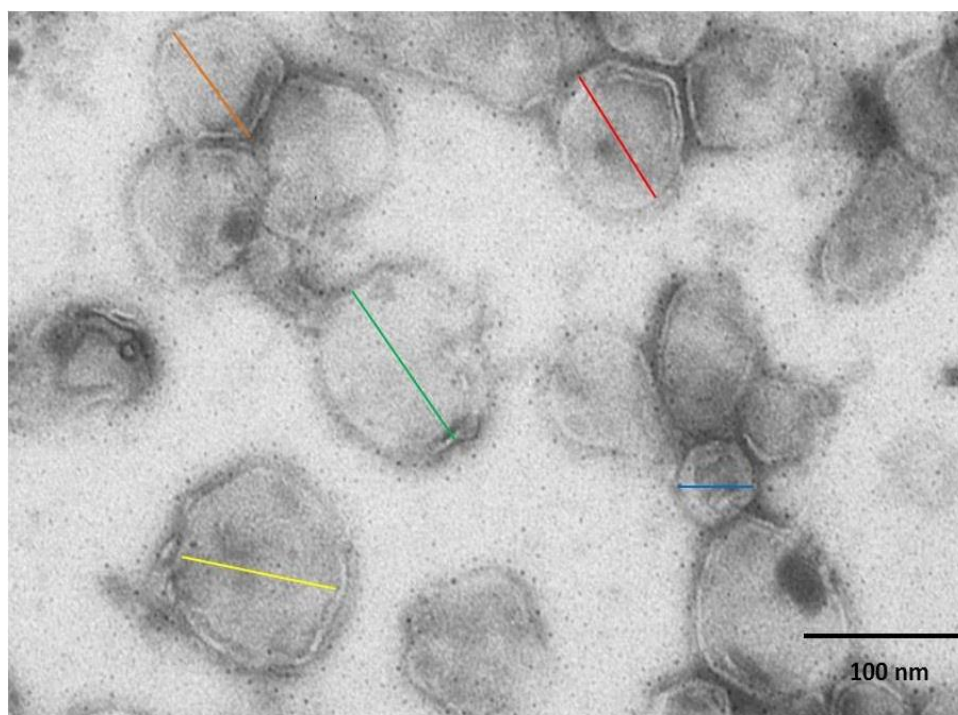




**Figure 4.15: 50 nm PINPs in filtered PBS at 1 mM.** *The negative staining micrograph shows a sample of 50 nm PINPs. While a heterogeneous mixture of PINPs with a diameter range of ~ 30-130 nm was observed they can clearly be seen as being rounded in shape, with a unilamellar structure. Scale bar = 100 nm.*



**Figure 4.16: 50 nm PINPs in filtered PBS at 1 mM.** *The negative staining micrograph shows a sample of 50 nm PINPs. A heterogeneous heterogeneous mixture of PINPs with a diameter range of 50-130 nm was observed. Scale bar = 100 nm.*



**Figure 4.17: 50 nm PINPs in filtered PBS at 1 mM.** *The negative staining micrograph shows a sample of 50 nm PINPs at high magnification. The liposomes can be seen clearly as rounded in shape with unilamellar structures while a heterogeneous mixture of PINPs was observed. The different diameters of liposomes are shown using different colours of lines (yellow, green, blue, orange and red). Scale bar = 100 nm.*

### **Conclusion using TEM**

TEM was the second technique which was used for the characterization of liposomes. It is important to note that the current study is based on the production of liposomes using the lipid thin film method, and variations in this method can greatly affect their characteristics. Some of these characteristics, notably liposome morphology and ultrastructure, including lamellarity (production of unilamellar or multilamellar vesicles), are not revealed by DLS, but could be determined here by using TEM. In addition, another characteristic of liposomes which cannot be revealed

by DLS, but is revealed by TEM, is how the liposomes are arranged in space. We found that the shape, size range, degree of clumping, and lamellarity of the liposomes are all affected by the preparation technique. This is not surprising, because it has already been well established that, the preparation of liposomes, their environment can greatly affect these characteristics. Often, during the preparation of liposomes, their free enthalpy is not stable, and as a result this creates liposomes which can change in size, shape and lamellarity with time (Chetanachan et al., 2008; Ran and Yalkowsky 2003; Zasadzinski, 1986). In particular, the lamellarity of liposomes preparation is very important, and is impossible to examine by DLS. In order to produce unilamellar liposomes, which are a prerequisite for the production of PINPs, it is essential, based on the TEM results presented here, to include the freeze-thawing and sonication steps in their preparation protocol.

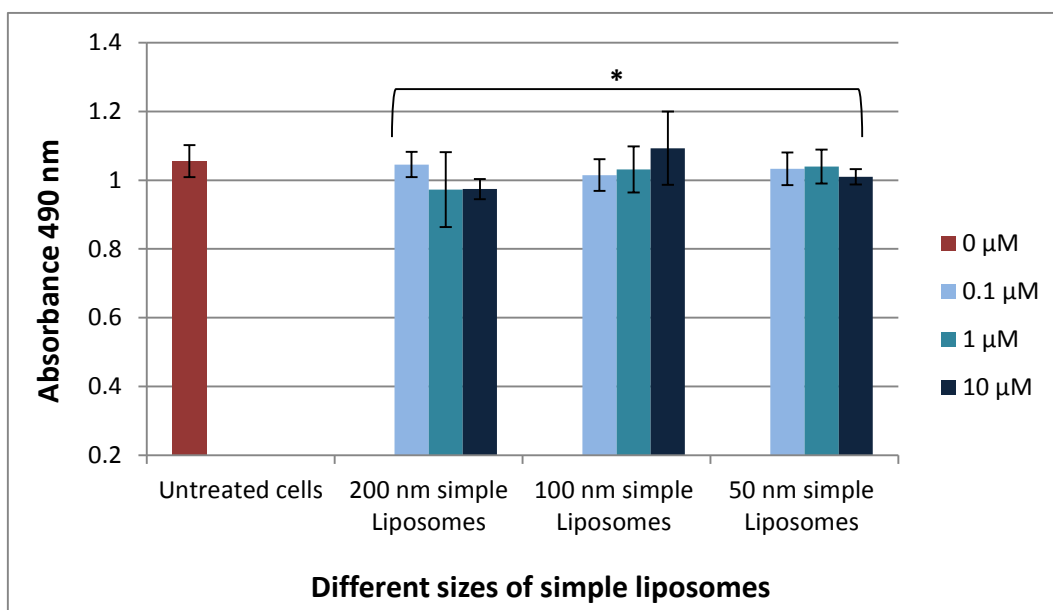
## **CHAPTER FIVE – CELL TOXICITY AND CELL PENETRATION RESULTS**

### **5.1. Cell toxicity using the three different types of liposomes**

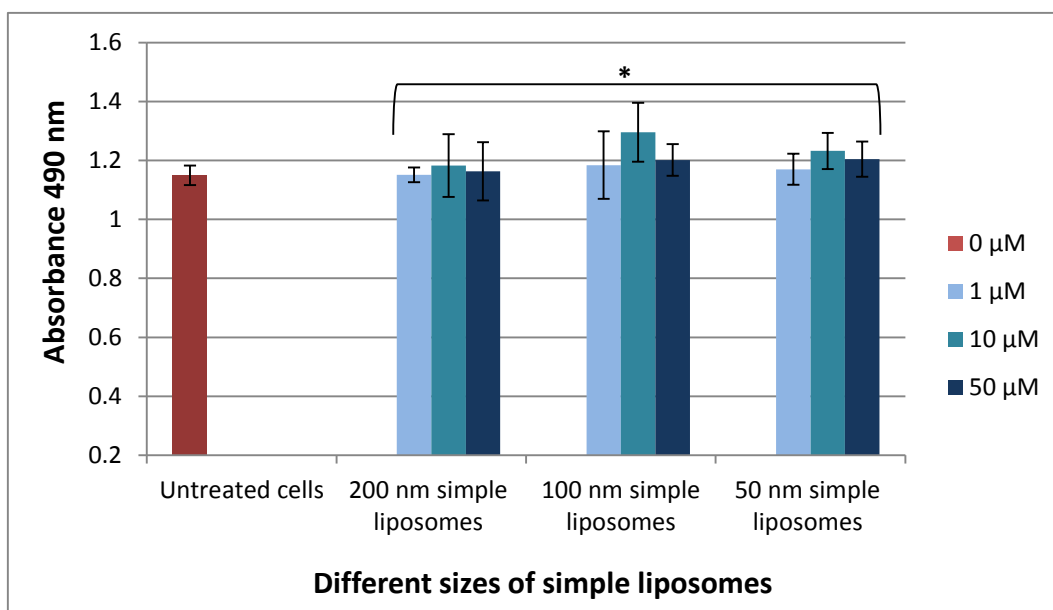
After the characterization of liposomes based on their size and shape, NLS were also characterized based on their toxicity to neuroblastoma cells because for a drug delivery system it is obviously important to be non-toxic. In order to examine the toxicity of the three types of liposomes (simple, PEGylated liposomes and PINPs), at three distinct sizes of 200 nm, 100 nm and 50 nm, a MTS cell toxicity assay was performed. Here, these different liposomes were tested for their toxicity effects on SHSY-5Y neuroblastoma cells grown in culture, using each type of liposome at four different concentrations (50  $\mu$ M, 10  $\mu$ M, 1  $\mu$ M and 0.1  $\mu$ M).

#### **5.1.1 Simple liposomes**

In the case of simple liposomes, as can be observed from figures 5.1 and 5.2, there was no loss in the viability of neuroblastoma cells at any of the four different concentrations (50  $\mu$ M, 10  $\mu$ M, 1  $\mu$ M and 0.1  $\mu$ M), with liposomes in DMEM, giving almost the same absorbance (measure of viability) as control cells with no liposomes (represented by the dark red coloured bar to the left of the graph), after 24 h incubation at 37°C. This experiment was performed twice and the results for both assays are shown below.



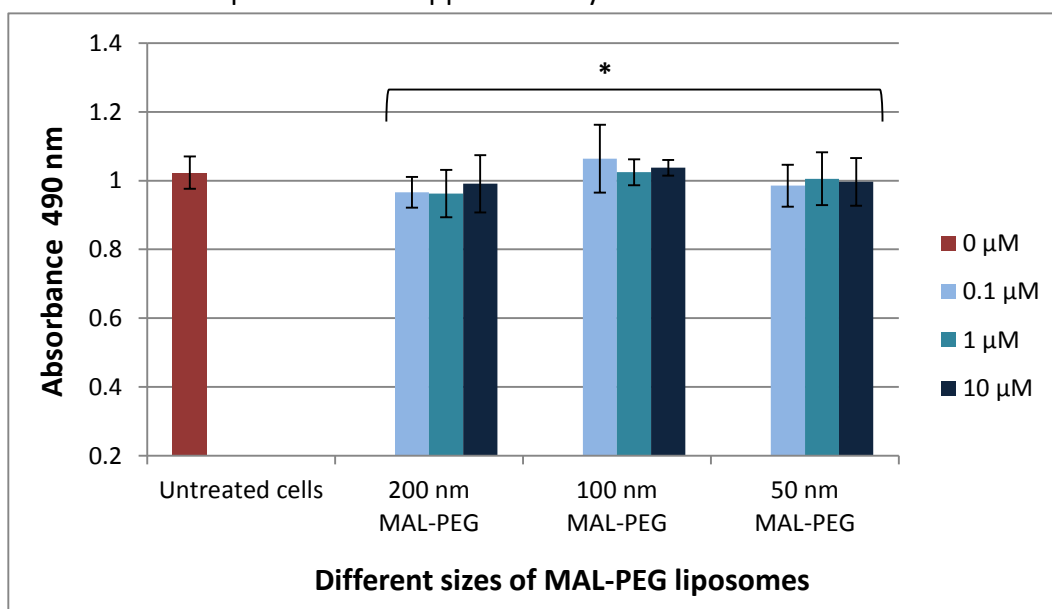
**Figure 5.1: Simple liposomes are not toxic to cells.** The graph shows a MTS cell viability assay (mean  $\pm$ SD, n=4) of SHSY-5Y neuroblastoma cells grown in the presence of three different sizes of simple liposomes at different concentrations (0.1, 1, 10  $\mu$ M) for 24 h. The bars with star (all) are not statistically significant from the untreated cells.  $*=P>0.05$  by Student's t-test.



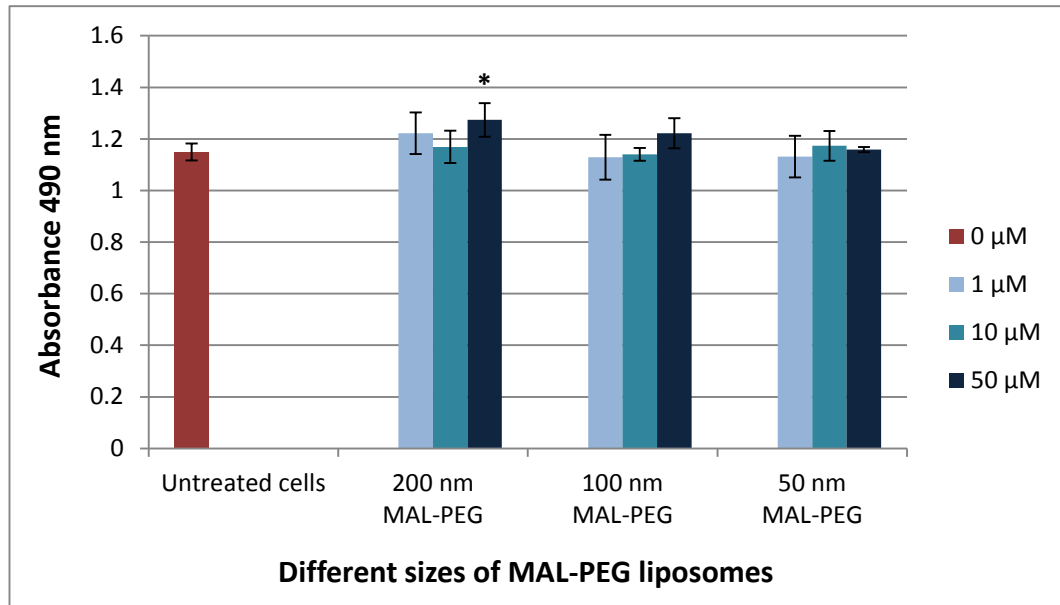
**Figure 5.2: Simple liposomes are not toxic to cells.** The graph shows a MTS cell viability assay of SHSY-5Y neuroblastoma cells (mean  $\pm$  SD, n=4) grown in the presence of three different sizes of simple liposomes at different concentrations (1, 10, 50  $\mu$ M) for 24 h. The bars with star (all) are not statistically significant from the untreated cells.  $*=P>0.05$  by Student's t-test.

### 5.1.2 PEGylated liposomes and PINPs

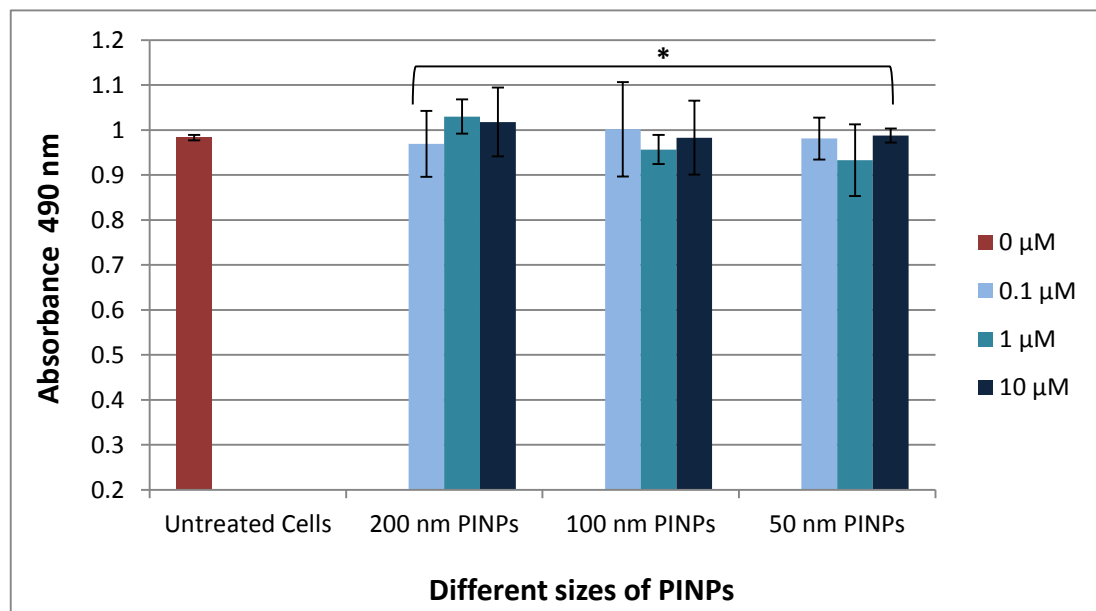
In the case of PEGylated liposomes and PINPs, exactly the same experiments with SHSY-5Y neuroblastoma cells were carried out as for the simple liposomes, and they also did not affect the viability of these cells. It can be concluded that neither the MAL-PEG liposomes nor PINPs are toxic towards SHSY-5Y neuroblastoma cells, despite the presence of the MAL-PEG molecule on their surface (for PEGylated liposomes) and the presence of RI-OR2-TAT peptide (in the case of PINPs). As can be seen from figures 5.3 to 5.6, the different concentrations of PEGylated liposomes and PINPs, after exposure to SHSY-5Y neuroblastoma cells for 24 h, produced no loss in viability of the cells. The red bar to the left of the graphs represents the viability of control cells without liposomes, and the blue bars represent the different concentrations of liposomes. The viability of untreated cells compared to cells incubated with liposomes was approximately the same.



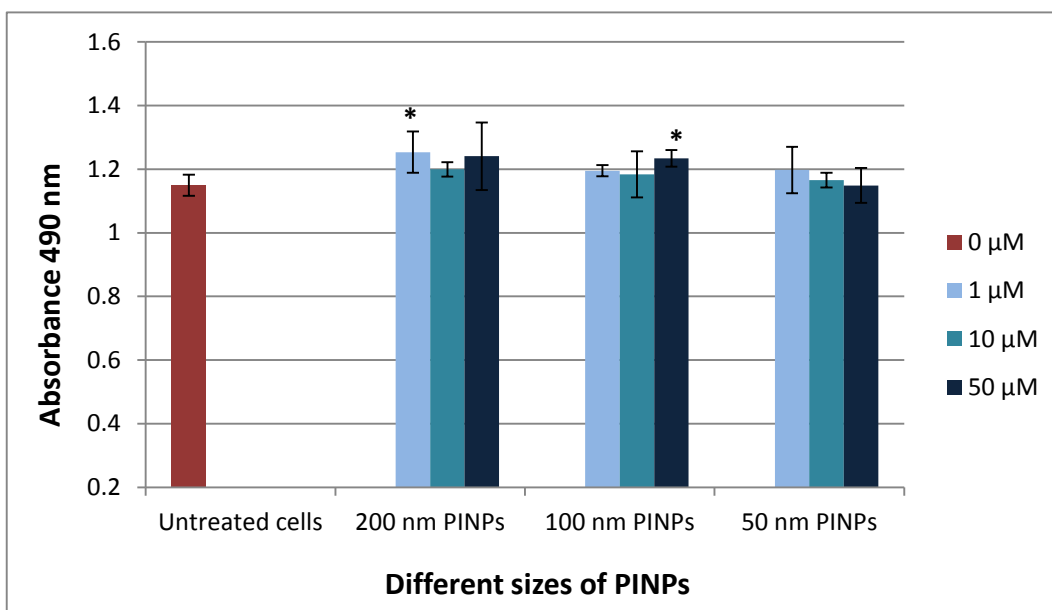
**Figure 5.3: PEGylated liposomes are not toxic to cells.** The graph shows a MTS cell viability assay (mean  $\pm$ SD,  $n=4$ ) of SHSY-5Y neuroblastoma cells grown in the presence of three different sizes of PEGylated liposomes at different concentrations (0.1, 1, 10  $\mu$ M) for 24 h. \* = $P>0.05$  by Student's t-test.



**Figure 5.4: PEGylated liposomes are not toxic to cells.** The graph shows a MTS cell viability assay (mean  $\pm$ SD, n=4) of SHSY-5Y neuroblastoma cells grown in the presence of three different sizes of PEGylated liposomes at different concentrations (1, 10, 50  $\mu$ M) for 24 h. Only the bar with star is statistically significant from untreated cells.  $*=p<0.05$  by Student's t-test.



**Figure 5.5: PINPs are not toxic to cells.** The graph shows a MTS cell viability assay (mean  $\pm$ SD, n=4) of SHSY-5Y neuroblastoma cells grown in the presence of three different sizes of PINPs at different concentrations (0.1, 1, 10  $\mu$ M) for 24 h. The bars with star (all) are not statistically significant from untreated cells.  $*=P>0.05$  by Student's t-test.



**Figure 5.6: PINPs are not toxic to cells.** The graph shows a MTS cell viability assay (mean  $\pm$ SD,  $n=4$ ) of SHSY-5Y neuroblastoma cells grown in the presence of three different sizes of PINPs at different concentrations (1, 10, 50  $\mu$ M) for 24 h. The bars with star only are statistically significant from untreated cells.  $*=p<0.05$  by Student's t-test.

## 5.2 Statistical analysis of cell viability results using T-test

A statistical analysis of the above cell viability data using the Student t-test was carried out in order to confirm that the liposomes were not toxic towards SHSY-5Y neuroblastoma cells (null hypothesis). T-test is used to determine if two sets of data (the untreated cells and the different concentrations of different types of liposomes) are significantly different from one another. The t-test analysis is shown in the tables below. Also, the significant values are higher than controls - i.e. more healthy. This is probably because we are supplying them with lipids, which acts as an addition 'food source'.

<b>Key for tables with T-tests</b>	
<b>P value</b> (Probability) = 0.05	*If T-test > 0.05 $\rightarrow$ <b>NO</b> significant difference
	*If T-test < 0.05 $\rightarrow$ <b>YES</b> significant difference



SHSY-5Y cell viability using simple liposomes						
Concentration ( $\mu\text{M}$ )	200 nm T-test values	Significant difference	100 nm T-test values	Significant difference	50 nm T-test values	Significant difference
0.1	0.74	NO	0.25	NO	0.52	NO
1	0.94	NO	0.6	NO	0.5	NO
10	0.59	NO	0.055	NO	0.068	NO
50	0.81	NO	0.162	NO	0.17	NO

**Table 5.1: Different concentrations of simple liposomes Vs untreated cells.** This table shows an analysis of simple liposomes of three different sizes (200, 100 and 50 nm) and different concentrations (0.1, 1, 10 and 50  $\mu\text{M}$ ) comparing them with the untreated cells according to the Student t-test ( $P$  value). None of the differences between treated and control cells are statistically significant ( $P > 0.05$ ).

SHSY-5Y cell viability using PEGylated liposomes						
Concentration ( $\mu\text{M}$ )	200 nm T-test values	Significant difference	100 nm T-test values	Significant difference	50 nm T-test values	Significant difference
0.1	0.39	NO	0.6	NO	0.58	NO
1	0.39	NO	0.98	NO	0.8	NO
10	0.65	NO	0.81	NO	0.69	NO
50	0.02	YES	0.088	NO	0.61	NO

**Table 5.2: Different concentrations of PEGylated liposomes Vs untreated cells.** This table shows an analysis of PEGylated liposomes of three different sizes (200, 100 and 50 nm) and different concentrations (0.1, 1, 10 and 50  $\mu\text{M}$ ) compared with untreated cells, according to the Student t-test ( $P$  value). None of the differences between treated and control cells are statistically significant ( $P > 0.05$ ) except for the 200 nm PEGylated liposomes (50  $\mu\text{M}$ ) which gave a higher MTS cell viability value ( $P < 0.05$ ) than untreated cells.

SHSY-5Y cell viability using PINPs						
Concentration ( $\mu\text{M}$ )	200 nm PINPs T-test values	Significant difference	100 nm PINPs T-test values	Significant difference	50 nm PINPs T-test values	Significant difference
0.1	0.72	NO	0.74	NO	0.93	NO
1	0.04	YES	0.064	NO	0.29	NO
10	0.055	NO	0.43	NO	0.46	NO
50	0.18	NO	0.0077	YES	0.98	NO

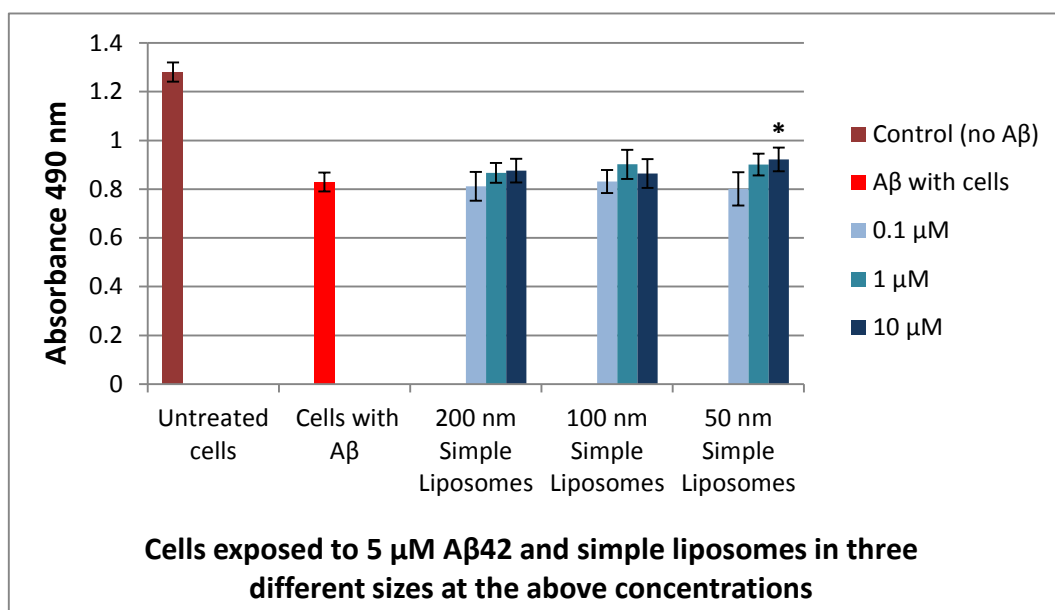
**Table 5.3: Different concentrations of PINPs Vs untreated cells.** This table shows an analysis of PINPs of three different sizes (200, 100 and 50 nm) and different concentrations (0.1, 1, 10 and 50  $\mu\text{M}$ ) compared with untreated cells, according to the Student t-test ( $P$  value). None of the differences between treated and control cells are statistically significant ( $P > 0.05$ ), except for the 200 nm and 50 nm PINPs (1 and 50  $\mu\text{M}$ ) which gave a higher MTS cell viability value ( $P < 0.05$ ) than untreated cells.

### **5.3 Ability of liposomes to rescue SHSY-5Y cells in the presence of A $\beta$**

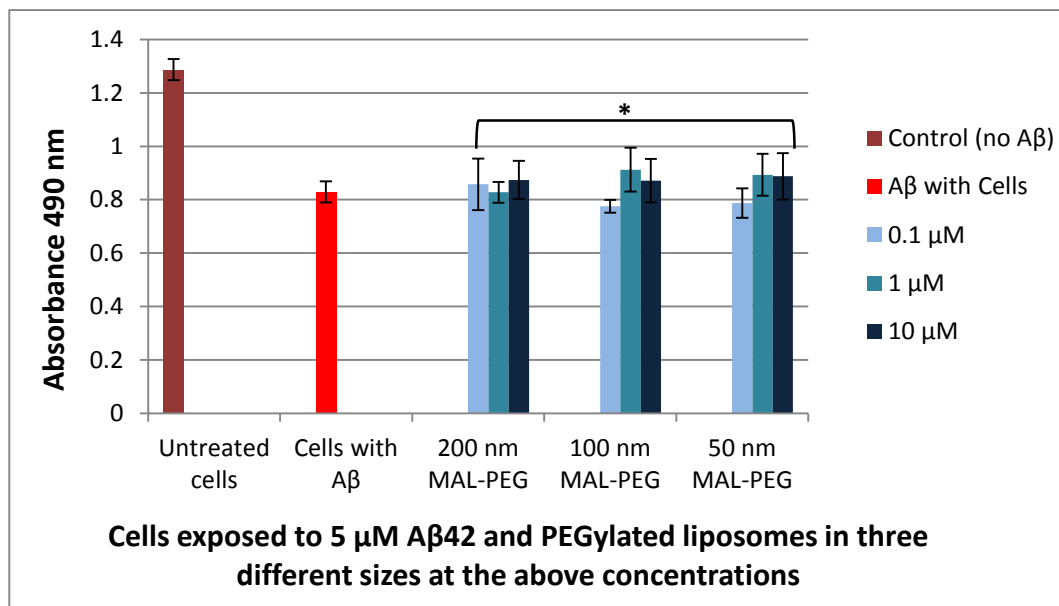
In addition, using the MTS assay, the three different types of liposomes were examined in order to test for their ability to rescue SHSY-5Y cells from the toxic effect of A $\beta$ , which was pre-aggregated for 24 h. The SHSY-5Y cells were exposed to 5  $\mu$ M A $\beta$  and using several concentrations of the three types of liposomes we examine their ability to block the toxic effects of A $\beta$ . The first column to the left (control – no A $\beta$ ) in figures 5.7 and 5.8 shows data for cells which were not exposed to A $\beta$ , i.e. the viability of healthy SHSY-5Y cells, while the red bar represents the negative effect on cell viability of the presence of 5  $\mu$ M A $\beta$ . As can be seen from the graphs, the viability of the A $\beta$ -treated cells was decreased by approximately 36% in relation to the healthy control value.

#### **5.3.1 Simple and PEGylated liposomes**

Figures 5.7 and 5.8 show cell viability data for effects of the three different sizes of simple and PEGylated liposomes on SHSY-5Y cells which were exposed to 5  $\mu$ M A $\beta$  at three different concentrations of liposomes (0.1, 1, 10  $\mu$ M). Both types of liposomes were unable to rescue the cells from the toxicity of A $\beta$ , but were themselves not toxic to the cells. For both types of liposomes, the MTS values obtained for all three sizes of liposomes were very close to the red bar, which represents the negative effect on cell viability obtained in the presence of A $\beta$ .



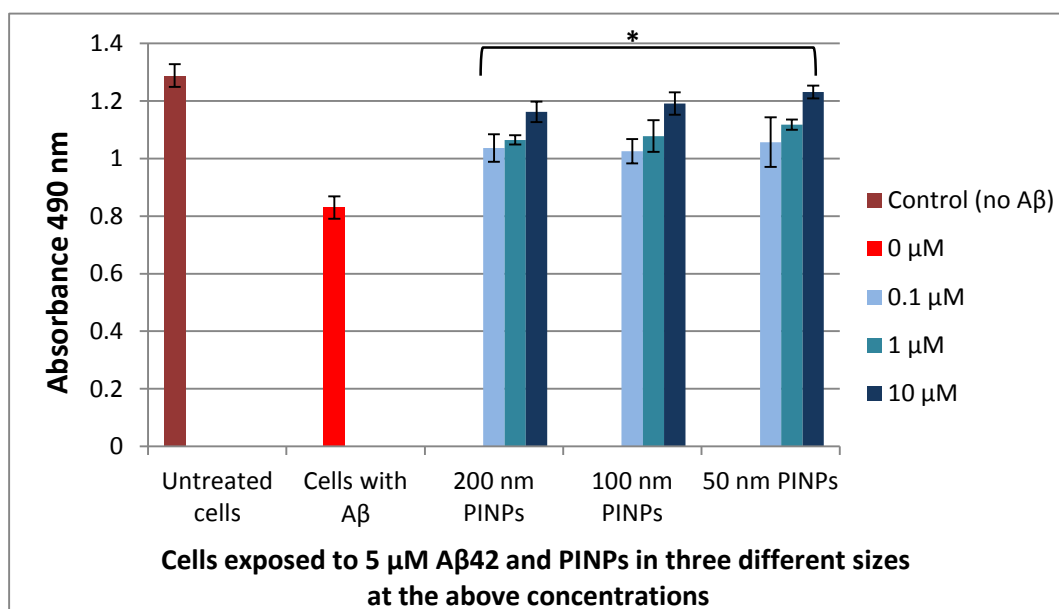
**Figure 5.7: Simple liposomes cannot block the toxic effect of A $\beta$ .** The graph shows the inability of simple liposomes of three different sizes and concentrations (0.1, 1, 10  $\mu\text{M}$ ) to rescue SHSY-5Y neuroblastoma cells from the toxic effect of 5  $\mu\text{M}$  of pre-aggregated A $\beta$ . Only the bar with star is statistically significant from cells with A $\beta$ .  $^* = p < 0.05$  by Student's t-test.



**Figure 5.8: PEGylated liposomes cannot block the toxic effect of A $\beta$ .** The graph shows the inability of PEGylated liposomes of three different sizes and concentrations (0.1, 1, 10  $\mu\text{M}$ ) to rescue SHSY-5Y neuroblastoma cells from the toxic effect of 5  $\mu\text{M}$  of pre-aggregated A $\beta$ . The bars with star (all) are not statistically significant from cells with A $\beta$ .  $^* = P > 0.05$  by Student's t-test.

### 5.3.2 PINPs

According to the graph below (figure 5.9), all concentrations and sizes of PINPs were able to rescue the SHSY-5Y cells from the toxic effect of A $\beta$ . The three different concentrations of PINPs of all sizes maintain the viability of the cells to almost the same value as the control cells with no A $\beta$ . As the concentration of PINPs is increased, the amount of rescued cells increased as well, while at the lower concentrations of PINPs, the amount of viable cells is lower.



**Figure 5.9: PINPs block the toxic effect of A $\beta$ .** The graph shows the ability of PINPs of three different sizes and concentrations (0.1, 1, 10  $\mu$ M) to rescue SHSY-5Y neuroblastoma cells from the toxic effect of 5  $\mu$ M of pre-aggregated A $\beta$ . The bars with star are statistically significant from cells with A $\beta$ .  $^* = P < 0.05$  by Student's *t*-test.

#### 5.4 Statistical analysis of the ability of liposomes to rescue SHSY-5Y cells in the presence of A $\beta$ using T-test

As above, a statistical Student t-test was carried out in order to confirm that both, simple and PEGylated liposomes were unable to block the toxic effect of A $\beta$ , while PINPs were able (null hypothesis). The tables below (table 5.4-5.6) represent the statistical analysis of the ability of the three types of liposomes to rescue SHSY-5Y cells in the presence of A $\beta$  using Student t-test.

Cells exposed to A $\beta$ Vs cells exposed to simple liposomes						
Concentration ( $\mu$ M)	200 nm T-test values	Significant difference	100 nm T-test values	Significant difference	50 nm T-test values	Significant difference
0.1	0.64	NO	0.95	NO	0.5	NO
1	0.23	NO	0.096	NO	0.051	NO
10	0.25	NO	0.36	NO	0.02	YES

**Table 5.4: Different concentrations of simple liposomes Vs cells exposed to A $\beta$ .** This table shows an analysis of simple liposomes of three different sizes (200, 100 and 50 nm) and different concentrations (0.1, 1 and 10  $\mu$ M) comparing them with the cells exposed to A $\beta$  according to the Student t-test (*P* value). None of the differences between cells exposed to A $\beta$  and cells exposed to simple liposomes are statistically significant (*P*>0.05), except for the 50 nm simple liposomes (10  $\mu$ M) which gave a higher MTS value (*P*<0.05) than cells exposed to A $\beta$ .

Cells exposed to A $\beta$ Vs cells exposed to PEGylated liposomes						
Concentration ( $\mu$ M)	200 nm T-test values	Significant difference	100 nm T-test values	Significant difference	50 nm T-test values	Significant difference
0.1	0.62	NO	0.065	NO	0.26	NO
1	0.95	NO	0.135	NO	0.21	NO
10	0.3	NO	0.4	NO	0.28	NO

**Table 5.5: Different concentrations of PEGylated liposomes Vs cells exposed to A $\beta$ .** This table shows an analysis of PEGylated liposomes of three different sizes (200, 100 and 50 nm) and different concentrations (0.1, 1 and 10  $\mu$ M) comparing them with the cells exposed to A $\beta$  according to the Student t-test (*P* value). None of the differences between cells exposed to A $\beta$  and cells exposed to PEGylated liposomes are statistically significant (*P*>0.05).

Cells exposed to A $\beta$ Vs cells exposed to PINPs						
Concentration ( $\mu$ M)	200 nm T-test values	Significant difference	100 nm T-test values	Significant difference	50 nm T-test values	Significant difference
0.1	0.0065	YES	0.0005	YES	0.0075	YES
1	0.0038	YES	0.00051	YES	0.00013	YES
10	1.64E-05	YES	1.22E-05	YES	1.44E-05	YES

**Table 5.6: Different concentrations of PINPs Vs cells exposed to A $\beta$ .** *This table shows an analysis of PINPs of three different sizes (200, 100 and 50 nm) and different concentrations (0.1, 1 and 10  $\mu$ M) comparing them with the cells exposed to A $\beta$  according to the Student t-test (P value). All of the differences between cells exposed to A $\beta$  and cells exposed to PINPs are statistically significant ( $P < 0.05$ ).*

### 5.5 Conclusion applying cell toxicity assay (MTS)

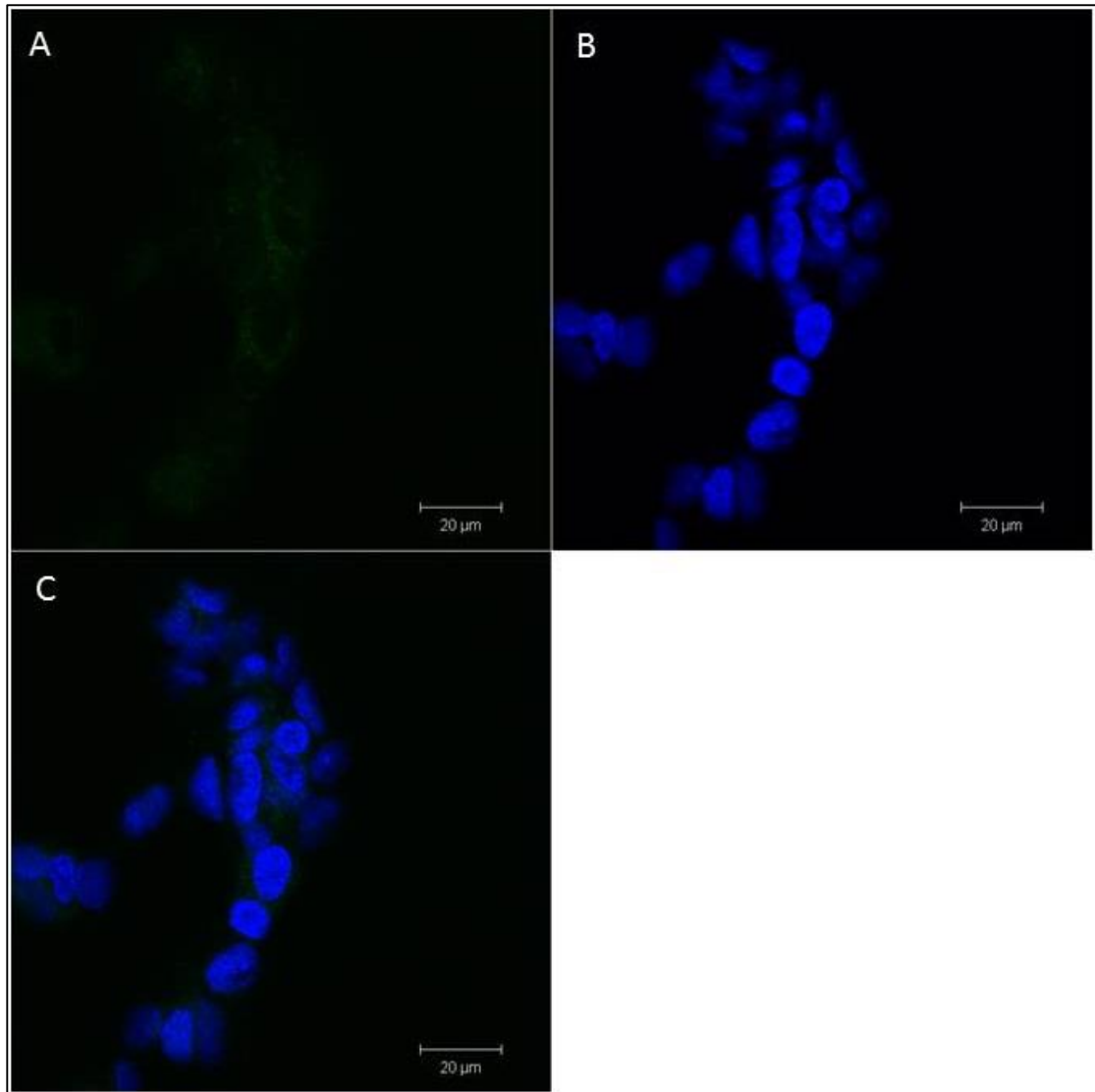
The use of the MTS assay to measure cell toxicity was divided in two experiments: (a) to test whether the liposomes were toxic to SHSY-5Y neuroblastoma cells, and (b) to examine the ability of the three types of liposomes to affect A $\beta$  aggregation and protect against A $\beta$  cytotoxicity. Both of them revealed important information for the three types of NPs. First of all, according to the results for part A, we can conclude that the three types of liposomes are not toxic towards SHSY-5Y cells at the concentrations tested, which is positive in terms of the requirements for development of a non-toxic drug (PINPs). These results confirm the fact that the lipids themselves are not toxic, which is anticipated given that they are basic components of the membranes of cells. Based on part B, the results revealed that both simple and PEGylated liposomes were not able to rescue the SHSY-5Y cells from A $\beta$  cytotoxicity, while the presence of PINPs resulted in rescue of the cells, even at low PINP concentrations (0.1  $\mu$ M).

## **5.6 Cell penetration assay – Fluorescent microscopy using 200 nm of PEGylated liposomes and PINPs**

Based on previous studies, the site where A $\beta$  is generated is not clear, but Takahashi et al. (2002) have determined that compartments called ‘multivesicular bodies’ are responsible for the release of proteins from the interior side of the cell to the exterior side. Also, there is some evidence that A $\beta$  aggregation begins inside cells, suggesting that the prevention of intracellular aggregation of A $\beta$  is a feasible target for drug development. For this to happen, the drug must be able to penetrate into the cells and inhibit A $\beta$  aggregation or prevent its release from the inside to the outside of the cell. It is believed that the inhibition of A $\beta$  accumulation is easier inside the cell instead rather than after its release to the exterior (Takahashi et al., 2002). It is also necessary to find a way to get the drug from the bloodstream across the BBB (the BBB is a layer of cells with tight junctions between them that prevents access of many molecules to the brain). In the following assay, 200 nm fluorescent bodipy PEGylated liposomes and PINPs (emission wavelength 507 nm and excitation wavelength 495 nm) at different concentrations (0.1  $\mu$ M, 1  $\mu$ M and 10  $\mu$ M) were incubated in standard mammalian cell culture conditions with SHSY-5Y neuroblastoma cells for an hour and their ability to penetrate into cells was investigated using a confocal microscope (LSM 510 – Laser Module – ZEISS).

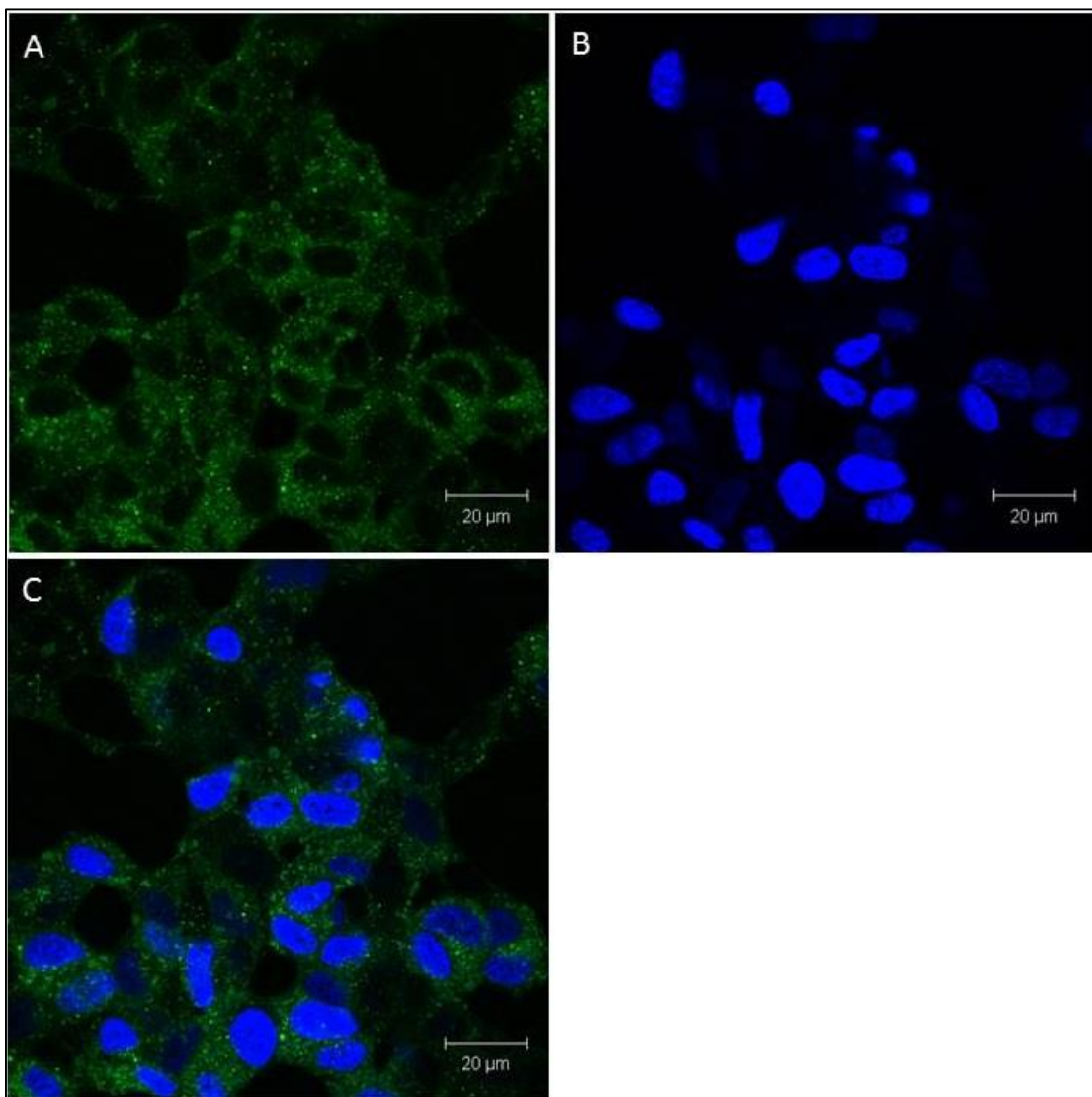
According to the fluorescent images below, as the concentration of fluorescent bodipy PINPs or PEGylated liposomes was increased, so the amount of green fluorescence also increased, which is an indication that more PINPs or PEGylated liposomes have penetrated into the cells. In the figure 5.10, which represents a

sample with neuroblastoma cells only, we did not expect to observe green fluorescence (no bodipy liposomes) but in some cases the cells appear to produce a signal due to auto-fluorescent properties of the cells themselves.

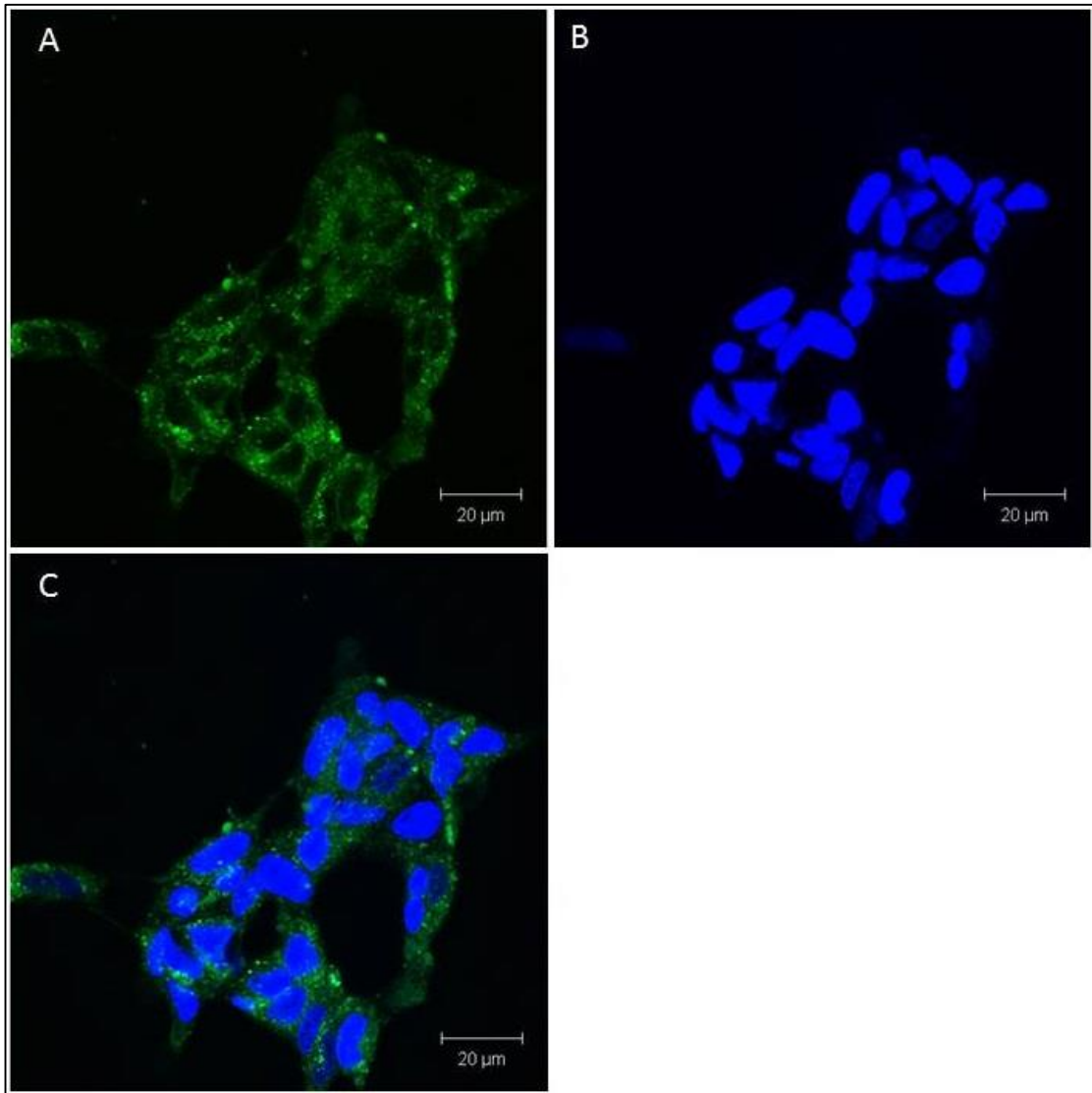


**Figure 5.10:** A confocal image of SHSY-5Y cells grown on glass coverslips with filtered PBS and incubated for an hour (Control). Panels A, B and C present the same section of a slide, under different filters. A: The green fluorescent colour emitted by the cells themselves is due to auto-fluorescence. B: DAPI-staining – 405 nm DNA (blue) - in the nucleus of SHSY-5Y cells. C: Merging of both images (A+B) shows the blue colour (nucleus of cells) together with green auto-fluorescence. Scale bar = 20 µM.

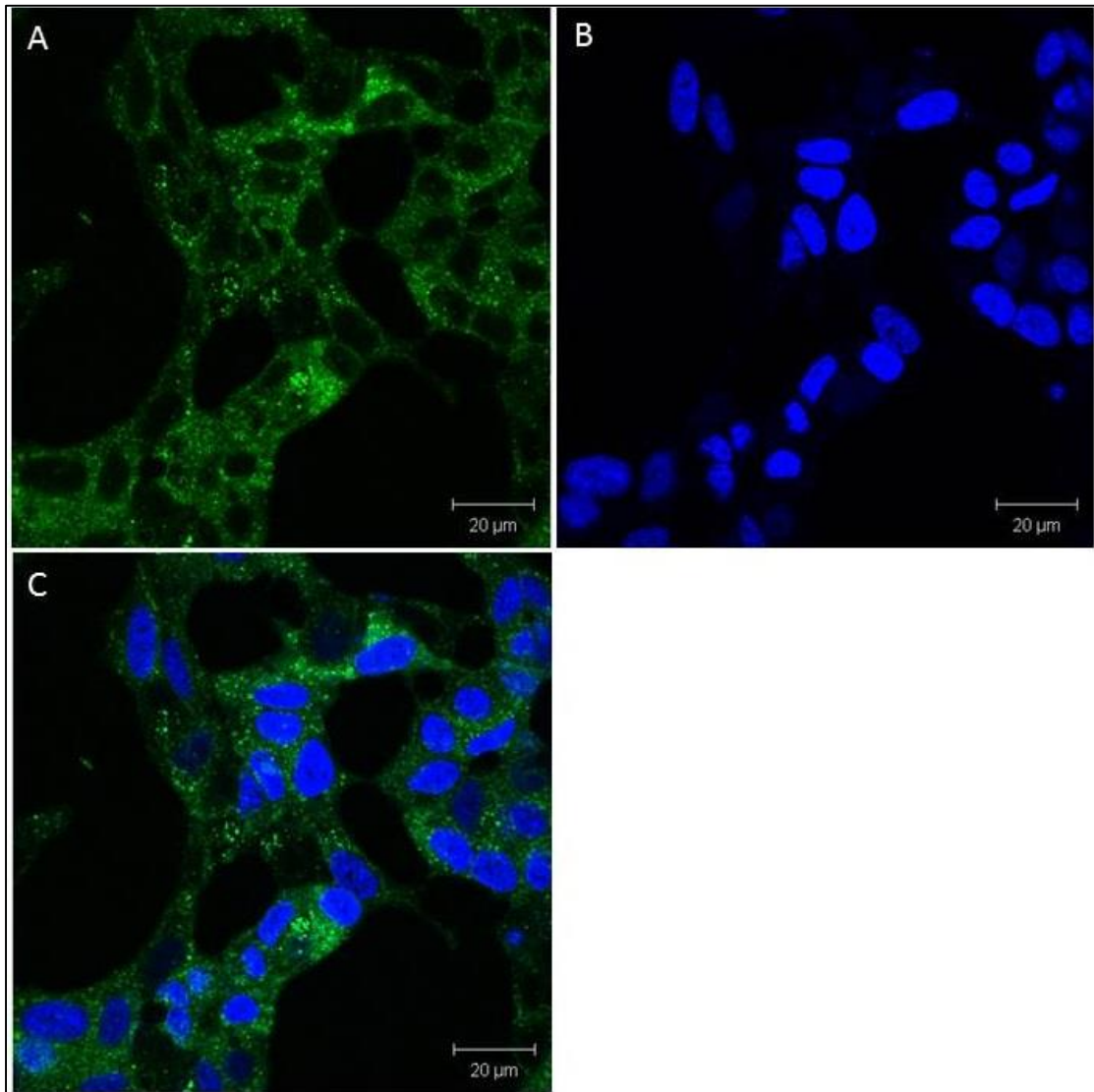




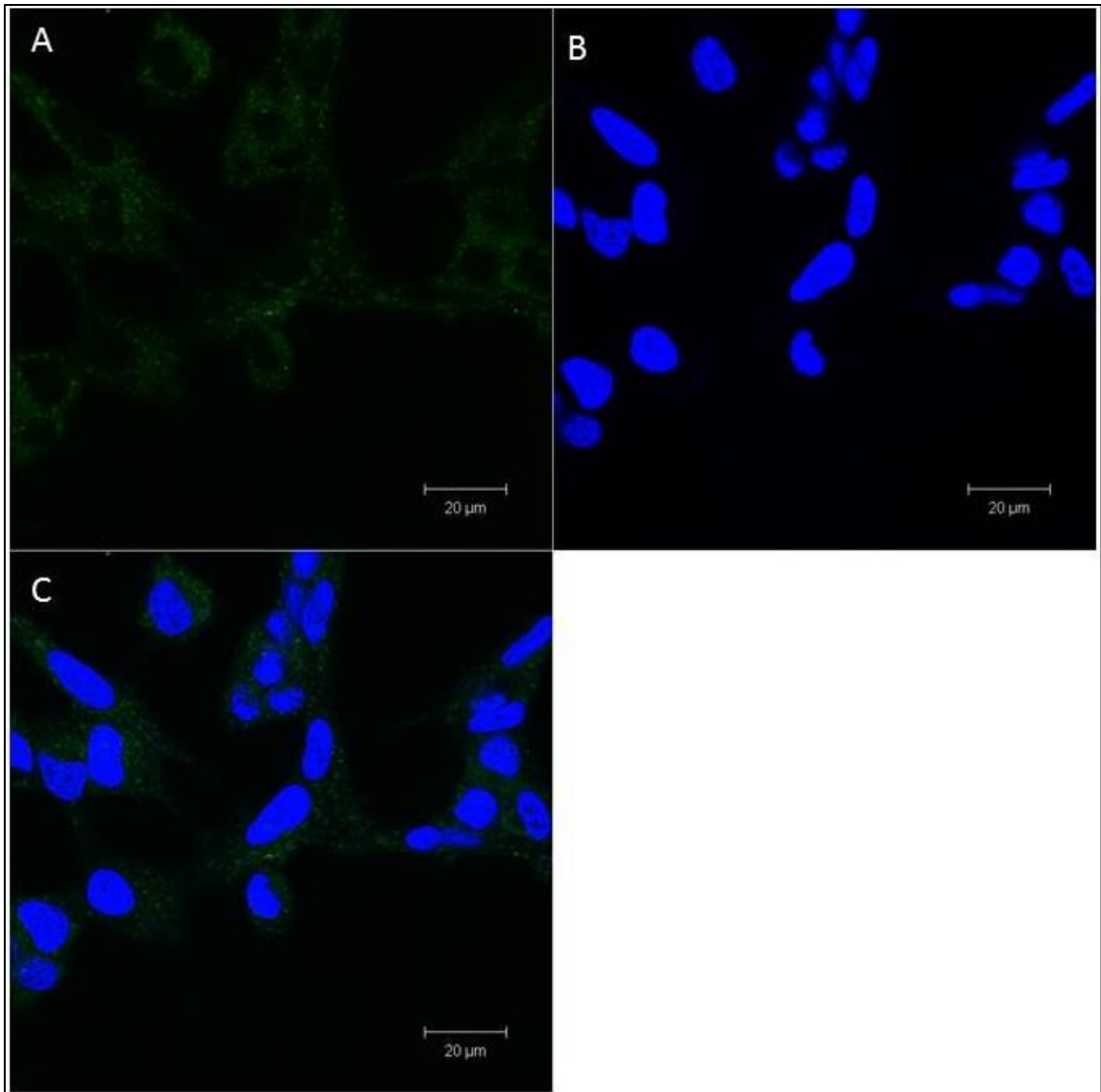
**Figure 5.11:** A confocal image of SHSY-5Y cells grown on glass coverslips and incubated for an hour with fluorescent (bodipy) PINPs at 0.1 µM. Panels A, B and C present the same section of a slide, under different filters. A: Alexa-fluor-488 nm shows that PINPs have penetrated the membranes of SHSY-5Y cells (green). B: DAPI-stained – 405 nm DNA (blue) - nucleus of SHSY-5Y cells. C: Merging of both images (A+B) shows the nucleus of cells (blue) and the fluorescent PINPs (green). The intensity of the green fluorescent colour is increased in relation to the control sample, which is an indication that the PINPs are able to penetrate into the cells. Scale bar = 20 µM.



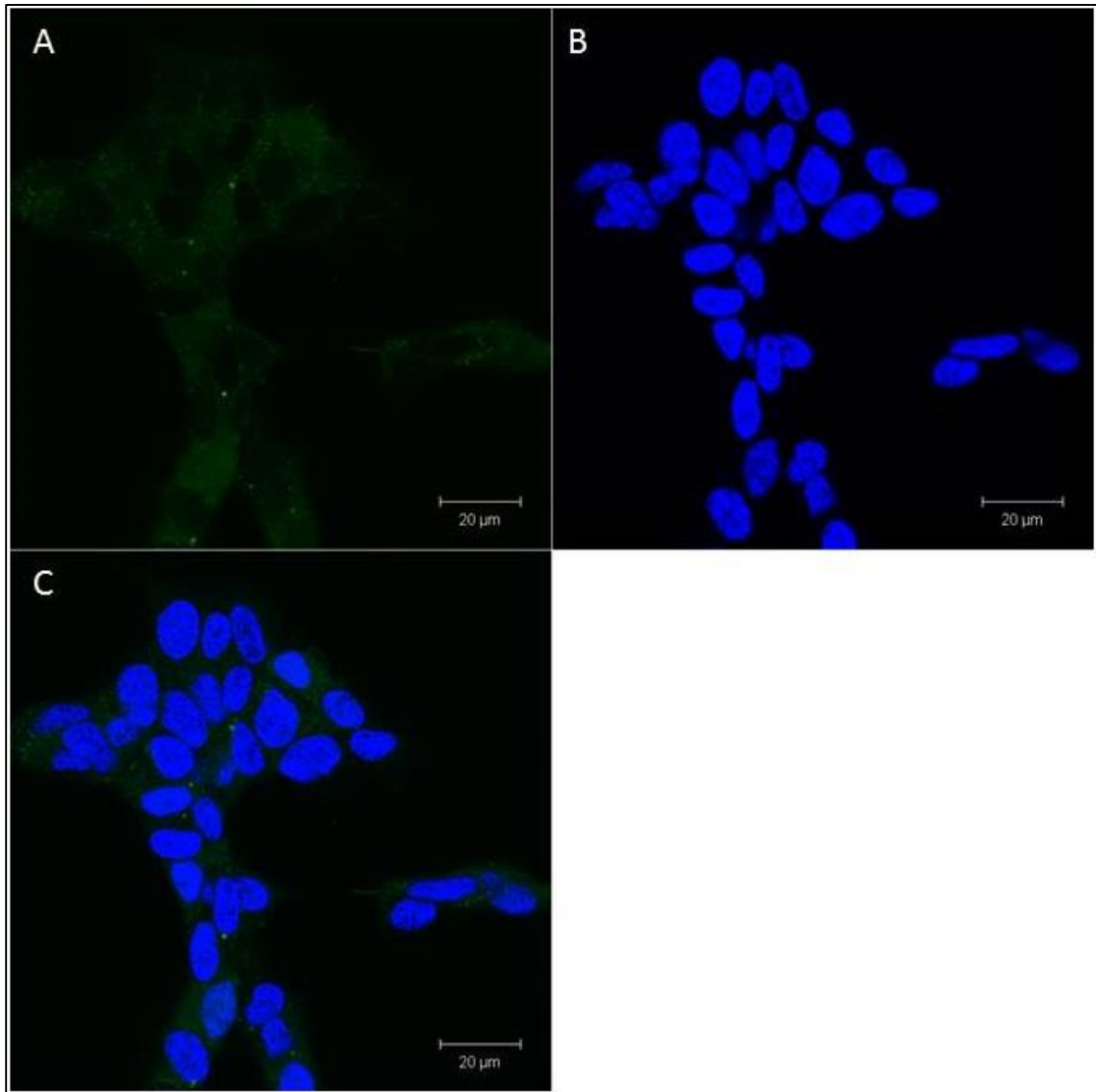
**Figure 5.12:** A confocal image of SHSY-5Y cells grown on glass coverslips and incubated for an hour with fluorescent (bodipy) PINPs at 1  $\mu\text{M}$ . Panels A, B and C present the same section of a slide, under different filters. A: Alexa-fluor-488 nm shows that PINPs have penetrated the membranes of SHSY-5Y cells (green). B: DAPI-stained – 405 nm DNA (blue) - nucleus of SHSY-5Y cells. C: Merging of both images (A+B) shows the nucleus of cells (blue) and the fluorescent PINPs (green). The intensity of the green fluorescence is increased in relation to 0.1  $\mu\text{M}$  of PINPs, showing that more of the PINPs at a concentration of 1  $\mu\text{M}$  are able to penetrate into the cells. Scale bar = 20  $\mu\text{M}$ .



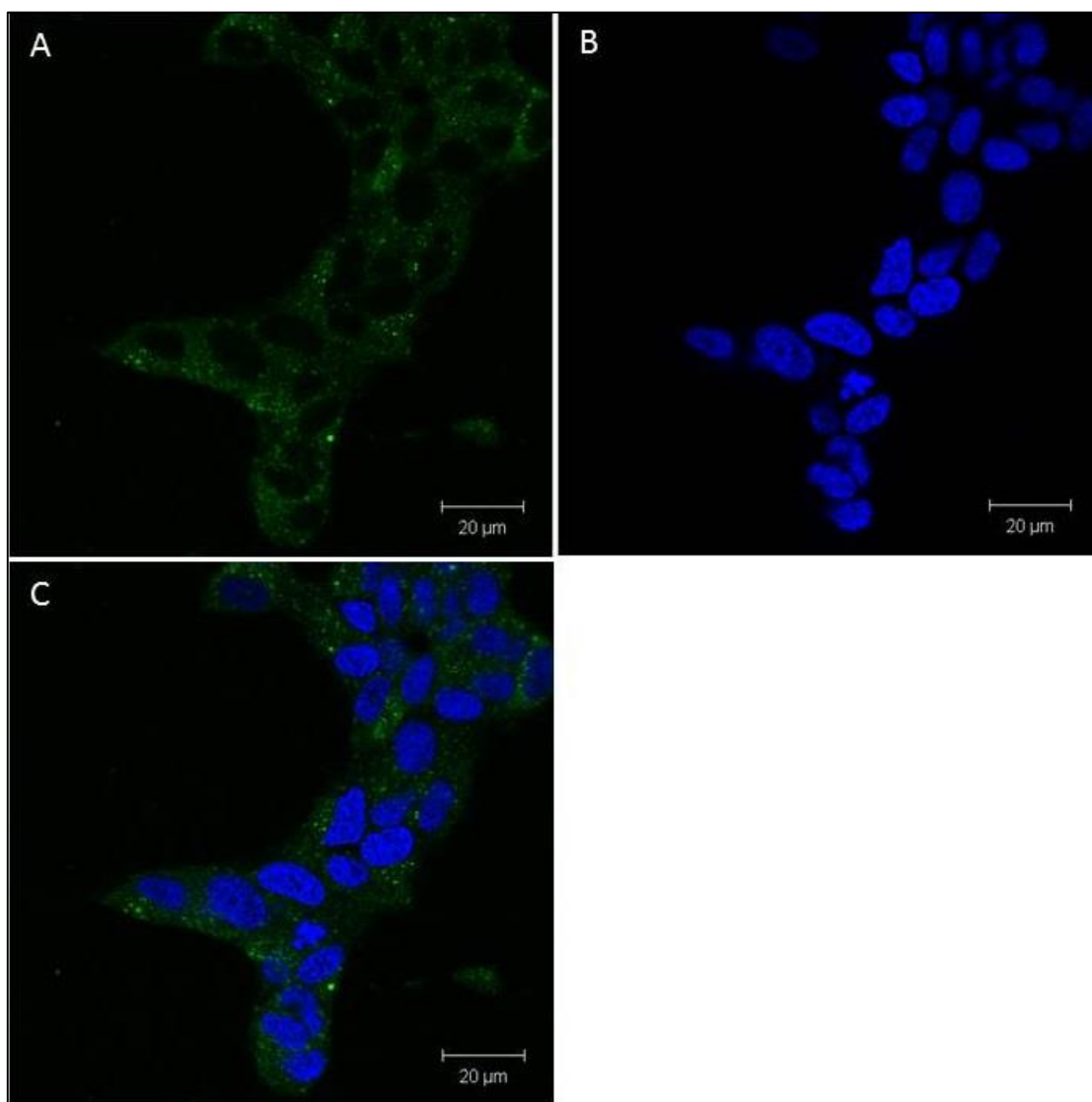
**Figure 5.13:** A confocal image of SHSY-5Y cells grown on glass coverslips and incubated for an hour with fluorescent (bodipy) PINPs at 10  $\mu\text{M}$ . Panels A, B and C present the same section of a slide, under different filters. A: Alexa-fluor-488 nm shows that PINPs have penetrated the membranes of SHSY-5Y cells (green). B: DAPI-stained – 405 nm DNA (blue) - nucleus of SHSY-5Y cells. C: Merging of both images (A+B) shows the nucleus of cells (blue) and the fluorescent PINPs (green). The intensity of the green fluorescence is increased in relation to 1  $\mu\text{M}$  of PINPs, showing that even more of the PINPs at a concentration of 10  $\mu\text{M}$  are able to penetrate into the cells. Scale bar = 20  $\mu\text{M}$ .



**Figure 5.14:** A confocal image of SHSY-5Y cells grown on glass coverslips and incubated for an hour with fluorescent (bodipy) PEGylated liposomes at 0.1 μM. Panels A, B and C present the same section of a slide, under different filters. A: Alexa-fluor-488 nm shows the PEGylated liposomes which penetrated the membrane of SHSY-5Y cells (green). B: DAPI-stained – 405 nm DNA (blue) - nucleus of SHSY-5Y cells. C: Merging of both images (A+B) shows the nucleus of cells (blue) and the fluorescent PEGylated liposomes (green). The intensity of the green fluorescent colour is increased in relation to the control sample which is an indication that PEGylated liposomes at the concentration of 0.1 μM are able to penetrate the cells. Scale bar = 20 μM.

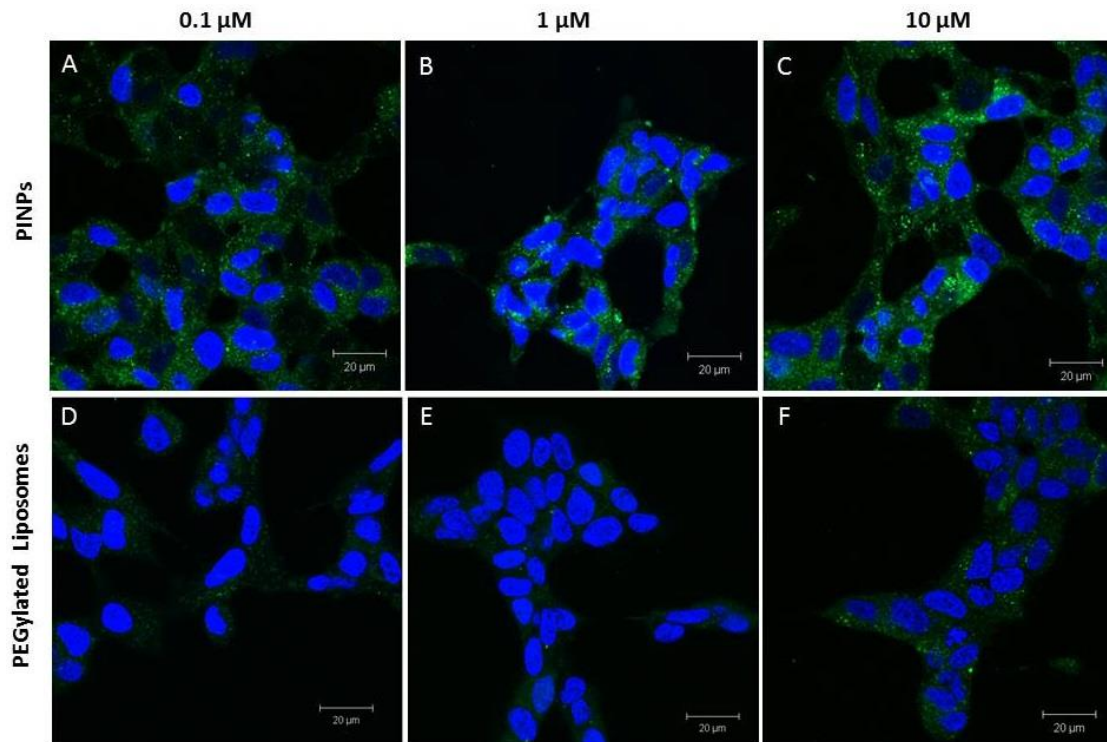


**Figure 5.15:** A confocal image of neuroblastoma SHSY-5Y cells grown on glass coverslips and incubated for an hour with fluorescent (bodipy) PEGylated liposomes at 1 µM. Panels A, B and C present the same part of a slide, under different filters. A: Alexa-fluor-488 nm shows the PEGylated liposomes which have penetrated the membrane of SHSY-5Y cells (green). B: DAPI-stained – 405 nm DNA (blue) - nucleus of SHSY-5Y cells. C: Merging of both images (A+B) shows the nucleus of cells (blue) and the fluorescent PEGylated liposomes (green). The intensity of the green fluorescent colour is increased in relation to 0.1 µM PEGylated liposomes, which is an indication that more of the PEGylated liposomes at a concentration of 1 µM were able to penetrate the cells. Scale bar = 20 µM.



**Figure 5.16:** A confocal image of SHSY-5Y cells grown on glass coverslips with fluorescent (bodipy) and incubated for an hour with PEGylated liposomes at 10  $\mu\text{M}$ . Panels A, B and C present the same section of a slide, under different filters. A: Alexa-fluor-488 nm shows the PEGylated liposomes which have penetrated the membrane of SHSY-5Y cells (green). B: DAPI-stained – 405 nm DNA (blue) - nucleus of SHSY-5Y cells. C: Merging of both images (A+B) shows the nucleus of cells (blue) and the fluorescent PEGylated liposomes (green). The intensity of green fluorescent colour increased in relation to 1  $\mu\text{M}$  of PEGylated liposomes, which is an indication that more PEGylated liposomes at the concentration of 10  $\mu\text{M}$  are able to penetrate the cells. Scale bar = 20  $\mu\text{M}$ .





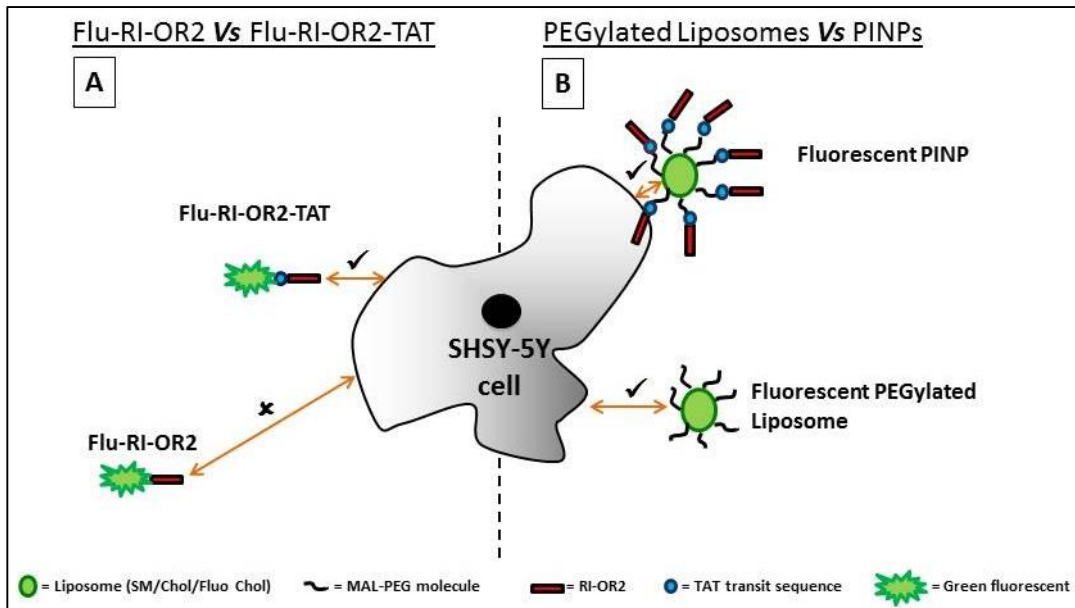
**Figure 5.17: Neuroblastoma SHSY-5Y cells grown on glass coverslips with fluorescent (bodipy) at different concentrations of PINPs and PEGylated liposomes. A-C micrographs show confocal images of SHSY-5Y cells incubated with PINPs at different concentrations for 1 h, while D-F micrographs show confocal images of SHSY-5Y cells incubated with PEGylated liposomes at different concentrations for 1 h. Comparing the same concentrations of the two types of liposomes (PINPs and PEGylated) (i.e. compare A with D; B with E; and C with F) we can observe that both types of liposomes are able to penetrate into cells. However, the PINPs penetrate into cells with greater efficiency than PEGylated liposomes.**

### 5.6.1 Conclusion cell penetration assay

The cell penetration assay was an experimental procedure which was carried out in order to examine the ability of our drug (PINPs) to penetrate into neuroblastoma SHSY-5Y cells. The results were positive: the successful penetration of PINPs into the cells is shown from the figures above. However, under the same conditions we found out that the PEGylated liposomes (even in the absence of the cell penetrating 'TAT' sequence of RI-OR2-TAT) have some ability to penetrate into neuroblastoma cells. According to a previous study (Parthsarathy et al., 2013), two types of the peptide inhibitors Flu-RI-OR2-TAT and Flu-RI-OR2 were tested for their ability to enter cultured SHSY-5Y cells, and the results revealed that only Flu-RI-OR2-TAT was able to penetrate the cells.

However, in the current thesis we examined both fluorescent PINPs and PEGylated liposomes to see if they were able to enter the cultured SHSY-5Y cells, and our results have revealed that both types of liposomes have the ability to penetrate into these cells (see figures above). This is another indication of how potent the liposomes themselves are as a drug delivery system, without any peptide attached on their surface to be taken up by the cells. For this reason further experiments are required to confirm the mechanism of how liposomes are taken up by neuroblastoma cells. However, we can conclude that the conjugation of the peptide inhibitor onto the surface of PEGylated liposomes has resulted in the creation of a more potent drug (PINPs) compared to Flu-RI-OR2-TAT.



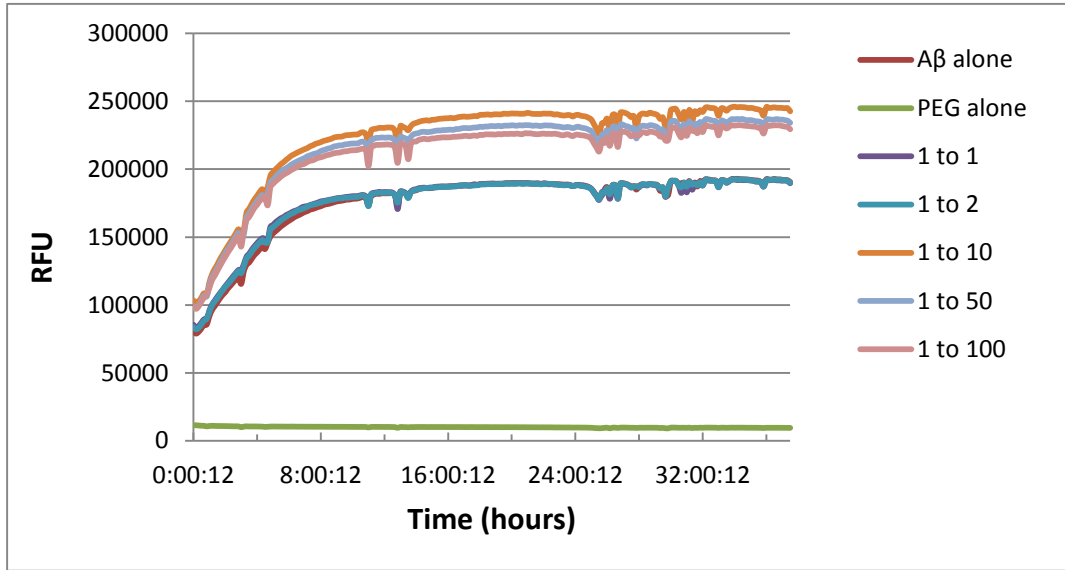


**Figure 5.18: Cell penetration.** This illustration shows the ability of different versions of the peptide inhibitor and PEGylated liposomes to enter SHSY-5Y neuroblastoma cells. The left part (A) of the figure represents an experiment which compares the ability of Flu-RI-OR2-TAT and Flu-RI-OR2 to penetrate the cultured cells. Due to the presence of the TAT sequence attached to the peptide, Flu-RI-OR2-TAT is able to enter cells, while Flu-RI-OR2 is not. The right part (B) of the figure represents an experiment which compares the ability of fluorescent PINPs and fluorescent PEGylated liposomes to enter the cells. In this case both types of liposomes can penetrate the cells, but the PINPs do so with enhanced efficiency because of the presence of the TAT transit sequence. However, fluorescent PEGylated liposomes are more effective at entering cells than Flu-RI-OR2.

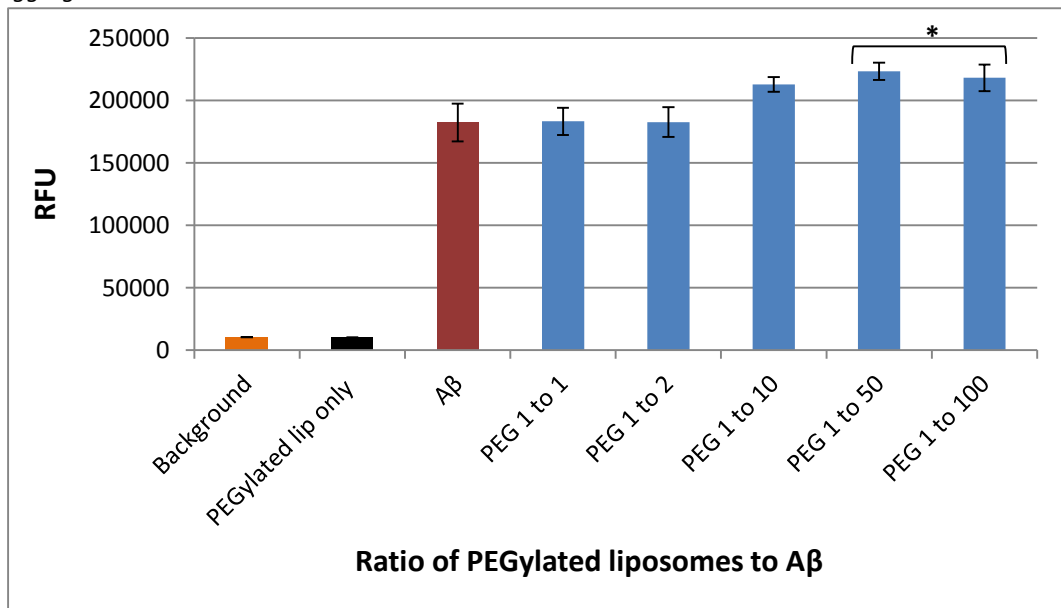
## 5.7 PINPs are potent aggregation inhibitors (Th-T assay)

A Th-T assay was used in order to determine if PINPs can block or inhibit the aggregation of A $\beta$ . In the following figures, Th-T data are presented for A $\beta$ 42 incubated for approximately two days with various molar ratios of PEGylated liposomes and PINPs (total lipids): A $\beta$ , ranging from 1:1 to 1:100. In the case of PEGylated liposomes the assay was stopped after 37 h instead of 48 h because the readings had reached a steady state. In these Th-T assays, we did not get the expected results. We (our team) tried the current experiment with PINPs from our collaborators in Italy and with PINPs which were prepared in our laboratory more than 5 times and we did not manage to get the expected results (see figures 5.19-5.22) for some reasons. The reasons for this are not clear, but could include the fact that amyloid aggregation experiments employing the Th-T assay are very variable, and if the nanoliposomes (PINPs) are not mixed well with A $\beta$  and Th-T this can give a poor result. However, the PINPs did show some inhibition of aggregation of A $\beta$ , comparing with the PEGylated liposomes which did not have any effect (see figure 5.22).

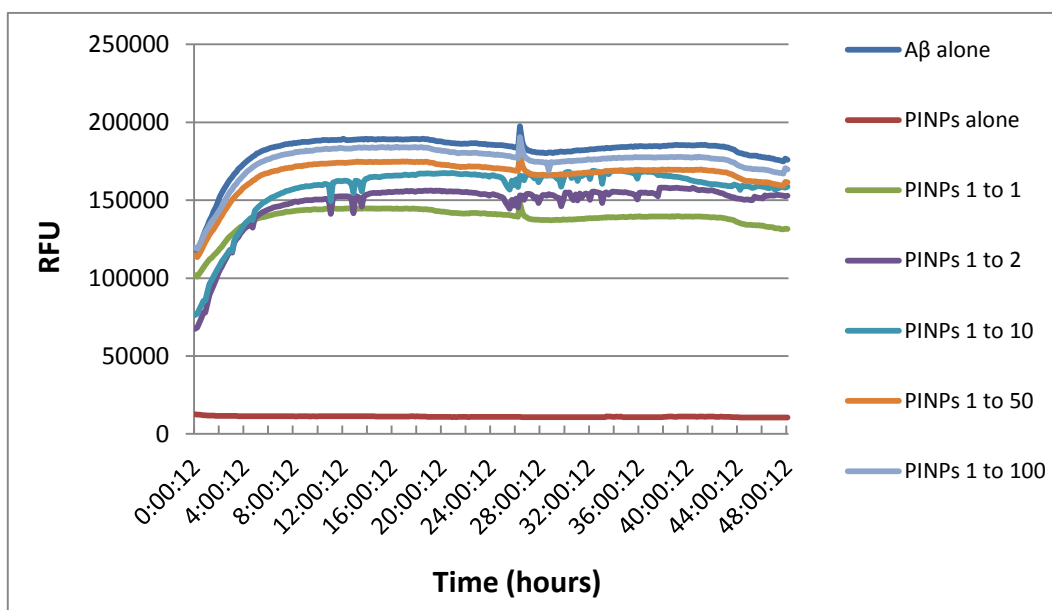
According to Gregori et al., 2015 (manuscript submitted) carried out the same experiment and they revealed that 50% inhibition occurs at around a 1:50 molar ratio of lipid to A $\beta$ 1-42 or, as the inhibitory peptide is only ~2.5% of total lipids, ~1:2000 of RI-OR2-TAT to A $\beta$ 1-42. On the other hand, PEGylated liposomes were also tested for their ability to inhibit the A $\beta$  aggregation at higher ratios (1:1 and 1:2) but without any important effect (Gregori et al., 2015 manuscript submitted).



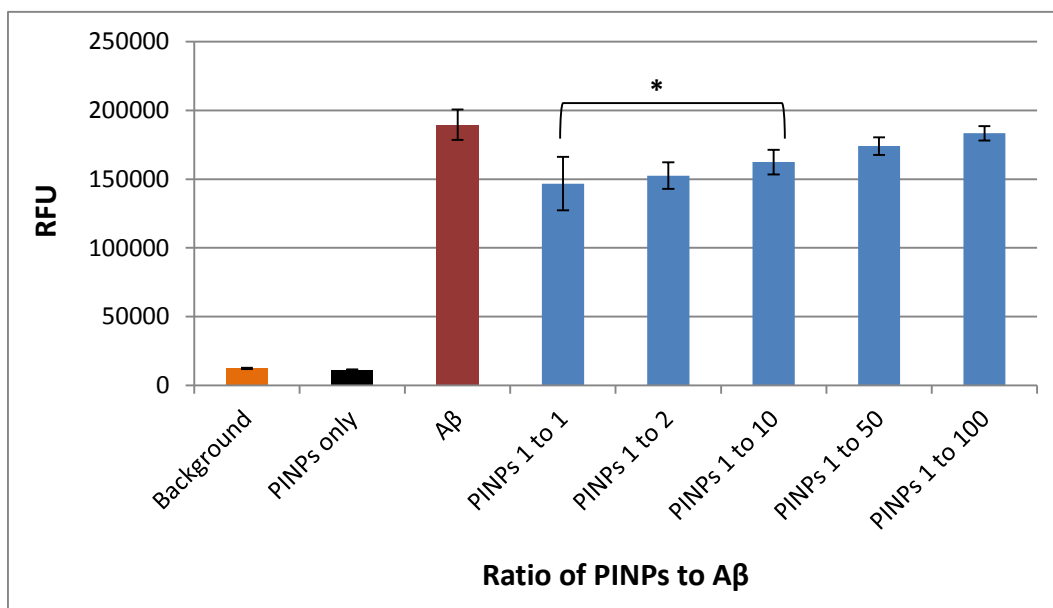
**Figure 5.19:** The graph shows a time course of Aβ-42 aggregation in the presence of PEGylated liposomes with various ratios incubated for 37 h. None of the dilutions showed any inhibition of Aβ aggregation. So the PEGylated liposomes are not considered suitable for the inhibition of Aβ aggregation.



**Figure 5.20:** PEGylated liposomes do not inhibit the aggregation of Aβ42. This graph represents Th-T data for Aβ42 with various molar ratios of PEGylated liposomes for 37 h incubation: "Background" is buffer only, "Aβ" (red bar) is Aβ42 incubated at 25 μM for 37 h without inhibitor, the blue bars represent the different concentrations of PEGylated liposomes (1 to 1 = 25 μM) which were incubated with Aβ42 for 37 h and the black bar is PEGylated liposomes only with no Aβ. The bars with star only are statistically significant from Aβ. \*= $p < 0.05$  by Student's t-test.



**Figure 5.21:** The graph shows a time course of A $\beta$ -42 aggregation in the presence of PINPs with various ratios incubated for 48 h. The dilutions 1 to 1 up to 1 to 10 showed important inhibition of A $\beta$  aggregation and dilutions 1 to 50 and 1 to 100 showed slight inhibition. Therefore, more diluted samples of PINPs (1 to 500 and 1 to 1000) did not show any inhibition of A $\beta$  aggregation (date not shown).



**Figure 5.22:** PINPs inhibit the aggregation of A $\beta$ 42. This graph represents Th-T data for A $\beta$ 42 with various molar ratios of PINPs for 48 h incubation: “Background” (orange bar) is buffer only, “PINPs only” are PINPs only without A $\beta$ , “A $\beta$ ” (red bar) is A $\beta$ 42 incubated at 25  $\mu$ M for 48 h without inhibitor, the blue bars represent the different concentrations of PINPs (1 to 1 = 25  $\mu$ M) which are incubated with A $\beta$ 42 for 48 h. The bars with star only are statistically significant from A $\beta$ .  $\ast = p < 0.05$  by Student’s t-test.

## CHAPTER SIX - DISCUSSION

### 6.1 Background

AD is the most common neurodegenerative disease and is characterized by the accumulation of senile plaques, containing fibrils composed of the protein A $\beta$ , and neurofibrillary tangles made of the protein Tau (Blennow et al., 2006). It is estimated that around 1 in 3 people will have this condition by the end of their life, and this is a problem that will become even more common with the growing ageing population. Many scientists have tried to develop new drugs to treat this fatal neurodegenerative disease. Recent studies have indicated that the retro-inverso peptide 'RI-OR2-TAT' could be a successful treatment for AD, with suitable drug like properties, and, potentially, with promising prospects for the future. In previous studies, RI-OR2-TAT has been shown to effectively inhibit the formation of both A $\beta$  oligomers and fibrils, as demonstrated by several different *in vitro* and *in vivo* experimental systems. Apart from its ability to inhibit the formation of A $\beta$  oligomers, some other important properties of this RI-peptide are its ability to pass through the BBB, and its stability in the blood circulation due to its high resistance to proteolysis (Parthsarathy et al., 2013).

In the current project, the main objective was to establish a nano carrier technology for our RI-peptide inhibitors. Previously, we have developed a promising new drug which we call a Peptide Inhibitory NanoParticle (PINP). This consists of cholesterol/sphingomyelin PEGylated nanoliposomes to which the retro-inverted peptide RI-OR2-TAT (Ac-rGffvlkGrrrrqrrkkrGyc-NH<sub>2</sub>) has been attached by '*click chemistry*'. Previous work has indicated that PINPs are able to block the formation of

aggregated forms of A $\beta$  *in vitro* and *in vivo* (Gregori et al., 2015 manuscript submitted). The initial development of these PINPs was carried out by a group in Milan, Italy, at the University of Milano-Bicocca, led by Prof. Massimo Masserini and Dr. Maria Gregori, and one of the main objectives of this work was to transfer the technology needed to make these PINPs to our group at Lancaster. This project was approached in three distinct stages, involving the manufacture and characterization of simple liposomes, PEGylated liposomes, and, finally, the PINPs themselves. Each type of liposome was developed in three different sizes (50, 100 and 200 nm). These various types of liposomes were characterized by size using DLS, shape-ultrastructure using TEM, and were also examined for their ability to affect A $\beta$  aggregation, and to protect against A $\beta$  cytotoxicity.

The use of PINPs as a potential drug for the treatment of AD, instead of the free peptide, was an attempt to improve the efficacy of the peptide inhibitor. In previous experiments by Dr. Mark Taylor at Lancaster University, the potency of the two types of drugs (RI-OR2-TAT and PINPs) was tested and compared, and the results suggested that the PINPs had more potency and increased efficacy against A $\beta$  aggregation. There are several reasons as to why this might be the case.

The presence of multiple copies of the RI-peptide on the surface of the nanoliposomes, would allow their simultaneous interaction with oligomeric forms of A $\beta$ , and this should result in more potent inhibition of aggregation, due to the effects of multivalency. According to a previous study, Chafekar and his colleagues observed that four KLVFF linked together by a dendrimer scaffold inhibit A $\beta$  aggregation more effectively than the monomeric KLVFF peptide. Consequently, in the case of PINPs, where there are many more copies of the RI-peptide, this inhibition is

expected to be even more effective (Chafekar et al., 2007). Another possible explanation for the increase potency of PINPs is based on their electrical charge. We have calculated that each PINP with approximately 100 nm has ~ 1690 RI-OR2-TAT molecules attached onto its surface, and this RI-peptide contains many positively charged amino acids residues. This means that the surface of each PINP would have a high positive charge which could help to attract and capture A $\beta$  monomers or multimers (Gregori et al., 2015 manuscript submitted). Additionally, it is possible that, once captured, A $\beta$  inserts into the lipid component of the liposomes, and so is effectively removed from solution. It is well known that A $\beta$  oligomers and pre-fibrils of A $\beta$  1-42 insert into the lipid component of cell membranes (Morita et al., 2012).

## **6.2 Findings of the study**

The main goal of this project was the creation of simple liposomes, which were then combined with the peptide inhibitor RI-OR2-TAT to create the PINPs. However, the part of this study most in common with other published work is based on development of the preparation method for the liposomes, and their subsequent characterization, based on their size and shape-ultrastructure. Previous investigators have reported that DLS is a quick and easy method to measure the size of liposomes, ranging from 50 nm to 200 nm, which is why we chose it as a suitable technique in the current project (Matsuzaki et al., 2000; Morton et al., 2012). TEM with negative staining is also a well-established method for determining the size, ultrastructure, as well as the lamellarity of liposomes (Chetanachan et al., 2008) and in our study this technique also proved to be a suitable for revealing the ultrastructure of liposomes.

### **6.2.1 Creation of liposomes in three distinct sizes**

For the manufacture of the three different sizes (50, 100, 200 nm) of liposomes, the use of polycarbonate membranes (PM) of different pore sizes was necessary. After the extrusion of the liposome suspensions through these PMs, they were examined by DLS. These DLS measurements confirmed that three different sizes of nanoliposomes were produced. Furthermore, the measurements of standard gold nanoparticles showed DLS is able to measure the size of nanoparticles reasonably accurately, including those with a small diameter (figure 3.8).

In the current study, hydration of a thin lipid film was applied for the preparation of liposomes: i.e. the Bangham method. In other studies, alternative methods have been used, such as: the reverse-phase evaporation (REV) technique; the solvent (ether or ethanol) injection technique; and detergent dialysis (Laouini et al., 2012; Akbarzadeh et al., 2013). According to (Meure et al., 2008; Dua et al., 2012) all of the above techniques have their advantages and disadvantages. Some of the main drawbacks of all of the above techniques are: they are time consuming, they have sterilization issues, they result in a high percentage of heterogeneity with regard to the size of the vesicles, and large amount of organic solvent is required. Furthermore, the ethanol/ether injection and reverse-phase evaporation (REV) techniques present some further limitations, such as: low drug stability, unsuitable for drug encapsulation, low yield, as well as poor entrapment efficiency. On the other hand, hydration of a thin lipid film by the Bangham method, despite its limitations, is one of the most widely used and simple techniques for the preparation of liposomes.



With regard to the extrusion of liposomes, Morton and colleagues have used a Liposofast LF-50 extruder, instead of Avanti's mini extruder which was used in our study (Morton, et al., 2012). The use of the Liposofast LF-50 extruder has some advantages since it is, practically, an easier and more effective technique. Two of the most important advantages of this extruder are, firstly, that specific and reproducible nitrogen pressure is used for each pore size (e.g. 25 psi for 400 nm liposomes, 125 psi for 100- nm liposomes, and 400-500 psi for 30 nm liposomes), while Avanti's mini extruder is operated by hand. Secondly, the Liposofast LF-50 extruder allows the preparation of liposomes up to 50 mL in volume, while the maximum volume of liposomes that can be prepared using Avanti's mini extruder is only 1 mL (Morton et al., 2012). Clearly, the replacement of our extrusion method with the Liposofast LF-50 extruder would be advantageous.

### **6.2.2 DLS investigation**

DLS enabled us to examine the size of the three types of liposomes. Following techniques published previously using DLS (Santos et al., 2010; Cho et al., 2013), the ideal number of passages (11 passages) required to achieve a correct and consistent size of liposomes was defined in our study. An increase in number of up to 14 passages was tried, but without any significant change compared with liposomes which underwent 11 passages (see figure 3.13).

Additionally, by the use of DLS, it was possible to investigate how the different concentrations of the liposome suspensions might affect their size measurement. Furthermore, DLS also revealed that the measurement of nanoparticles which are

positively charged, in our case, can affect the final results by giving an erroneous value from their normal size due to their increased hydrodynamic diameter. DLS also helped us to examine the stability of the three different types and sizes of liposomes and suggested that they are stable for more than two months, especially the liposomes of 100 nm diameter.

Another experiment which was carried out and examined by DLS is the size measurement of liposomes after extrusion at high temperature. According to the fluid mosaic model of cell membranes, the presence of cholesterol plays a regulatory role in maintaining the fluidity of the membrane at normal levels in extreme conditions such as low and high temperatures. High temperatures can cause fluidization, while low temperatures can cause rigidification of the membrane (Los and Murata, 2004). In this study, measurements, by, DLS of liposomes extruded at 75°C were determined, and this confirmed, how high temperatures can affect the fluidity of the liposomal membrane. This may be due to a change in the steroid ring of cholesterol, which becomes more bulky and increases the density of the hydrophobic section of the membrane as temperature increases.

However, it is important to note that, DLS is a somewhat variable technique, giving different values each time using the same sample. For example for the 100 nm liposomes, the same sample can give two different values (119 nm and 109.2 nm). According to Morton and colleagues, who prepared liposomes of various compositions using more than two lipids in different combinations, Nanoparticle Tracking Analysis (NTA) gives more accurate results than DLS. A possible explanation is that NTA gives an indication of size due to rate of movement in solution (Brownian motion) rather than physical measurement of actual dimensions (Morton et al.,

2012). In other words, NTA is able to measure the size of each nanoliposome from direct observations of diffusion in a liquid medium, independent of particle refractive index or density. However, our laboratory does not have access to NTA, which could have been used as complementary technique alongside DLS.

### **6.2.3 TEM investigation**

TEM was employed as a complimentary method to DLS and provided more information about the nanoliposomes, based on their size, shape and ultrastructure. The three types of nanoliposomes were easily imaged by applying negative staining and many characteristics which were impossible to observe using DLS, were revealed using TEM.

One of the most important findings using TEM was the way that the liposomes are arranged in the space at high and low concentrations. At high concentrations, liposomes have a tendency to come together and form clumps of liposomes. This would help to explain why the measurement of samples at high concentrations using DLS can sometimes give erroneous measurements. So, by use of TEM, we have highlighted the disadvantage of use of concentrated samples in DLS measurements. In contrast, samples with lower concentration did not form clumps when examined by TEM and their shape and size could be accurately determined using both TEM and DLS.

In addition, another important finding that TEM revealed was the lamellarity of the liposomes. The preparation method for the liposomes, as well as affecting their size and shape, also has an influence on their lamellarity. According to Traïkia et al.

(2000) and Supaporn, (2011) the freeze thawing and sonication methods helps the creation of unilamellar vesicles from multilamellar vesicles. The majority of the micrographs of liposomes presented above, showed a multilamellar structure (e.g. figures 4.3, 4.6, 4.8), which is something that must be taken into consideration in the future for further refinement of the method for preparation of the liposomes. In contrast, the samples that had undergone freeze thawing and sonication showed a unilamellar structure, confirming that the use of these two techniques is needed to make unilamellar liposomes. For our purposes, due to the fact that the only the outer surface of each liposome is decorated with inhibitory peptide, monolamellar structures would be highly preferable.

Another complementary technique along with TEM and DLS which could reveal important information about liposome size (diameter and height), morphology, surface properties, and changes in these characteristics during storage, is atomic force microscopy (AFM), which allows the visualization of nanoliposomes without any change in their physiological form (Ruozi et al., 2011). Ruozi et al. (2011) when comparing AFM with other techniques such as environmental scanning electron microscopy (ESEM), transmission electron microscopy (TEM) and confocal laser scanning microscopy (CLSM) for examination of liposome structure, these authors concluded that each of these microscopic techniques reveals its own unique information for the characterization of liposomes. For example, AFM gives information on the shape, morphology, dimensions and surface properties of liposomes; - TEM reveals information regarding their shape, morphology and dimension; while ESEM and CLSM reveal information regarding the dimensions and internal structure of liposomes, respectively.

In summary, TEM investigation was able to determine the basic characteristics of liposomes (size, shape and ultrastructure), but was unable to distinguish between the three types of liposomes (simple, PEGylated liposomes and PINPs). However, TEM was a suitable technique to characterize our liposome physical structures.

#### **6.2.4 MTS and Th-T assays investigation**

In order to test whether the three types of liposomes were toxic to neuroblastoma (SH-SY5Y) cells, they were incubated with the cells at different concentrations, in complete medium (DMEM), for 24 h. According to our results, the three types of liposomes proved not to be toxic to cells and their presence at different concentrations did not affect the growth of SHSY-5Y cells, although some slight stimulation of growth was observed, and this might even be statistically significant in some cases. This could be due simply to the supply of lipids for incorporation into cell membranes of cells. Furthermore, using the MTS assay on SH-SY5Y cells grown in the presence of different concentrations of PINPs it was proved that they were able to protect against the damaging toxic effects of A $\beta$ , while simple and PEGylated liposomes were unable to do this. This confirms that the presence of RI-OR2-TAT peptide is required.

Additionally, from the Th-T assay, we did not manage to get expected results for PINPs but comparing them with PEGylated liposomes, PINPs did show some inhibition to the aggregation of A $\beta$ , especially when present at high concentrations. However, it is important to mention that the Th-T assay proved to be very variable, giving different values each time, nanoliposomes (PINPs) are not mixed well with A $\beta$

and sometimes the A $\beta$  failed to aggregate, resulting in erroneous and unreliable data.

### **6.2.5 Cell penetration investigation**

As referred to in the results section (cell penetration), the aggregation of A $\beta$  starts inside cells and then extends to the exterior (Takahashi et al., 2002). For that reason the candidate drug (PINPs), in addition to its ability to pass through the BBB, must be also able to penetrate into cells and inhibit A $\beta$  aggregation or prevent the release of it outside of the cell. In our cell penetration assay both PEGylated liposomes and PINPs were tested at various concentrations and it was revealed that they are both able to penetrate into neuroblastoma SHSY-5Y cells. However, PINPs showed a greater efficiency to penetrate into cells due to presence of the 'TAT' transit sequence. The trans-activating transcriptional activator (TAT) peptide is the most commonly used cell penetration peptide in biological systems. 'TAT' is derived from the transcriptional activator protein present in HIV type 1 (Torchilin, 2008; Jeang et al., 1999). In agreement with our data, a previous study (Torchilin et al., 2001) has revealed that large drug carriers (200 nm liposomes) incorporating the 'TAT' sequence are able to penetrate into cells.

An overview of the main characteristics of the three types of liposomes made here is shown in table below.

Characteristics	TYPES OF LIPOSOMES		
	Simple liposomes	PEGylated liposomes	PINPs
Toxic to SHSY-5Y cells	x	x	x
Able to rescue SHSY-5Y cells from A $\beta$ toxicity	x	x	✓
Ability to inhibit A $\beta$ oligomer formation	x	x	✓
Ability to penetrate into the SHSY-5Y cells	-	✓	✓

**Table 6.1:** This table shows the main characteristics of the three types of liposomes which revealed from the methods which were applied in the current study.

### 6.3 Study's limitations

As we know, each scientific study has many possible limitations which can affect the study. I will refer to the most important limitations which had the greatest potential impact on the quality of my results, as well as those limitations which had a potential impact on my ability to answer the main objectives of my project. The majority of the limitations in the current study relate to the experimental procedures that were used during the production of the liposomes.

The first limitation was the extrusion of liposomes which was carried out using the Avanti's mini extruder; the second limitation was the multiple transfers of the liposome suspensions into many different vials before the final stage, involving purification of PINPs by gel filtration column chromatography, could be carried out;

finally, Steward's method for determination of lipid content did not work well. All of the above limitations affected my results, both qualitatively and quantitatively. The Avanti's mini extruder for the preparation of liposomes permits a maximum volume that can be extruded of only 1 mL per batch. This is an important limitation because the bulk production of liposomes, for larger scale experiments or for preclinical research, is impractical. Also, multiple passages of the lipids through the membrane is time consuming, and increases the risk of contaminating the lipid suspensions with bacteria. In addition, the many transfers of the liposome suspension from vial to vial, as well as the column chromatography method for the separation of PINPS from the unbound peptide, resulted in a substantial proportion of the lipids being lost each time. This was confirmed by the use of the WAKO phospholipid assay. These limitations, apart from the quantitative consequences for the results presented here, would have a negative impact on the production of liposomes for commercial purposes, including the cost of their preparation as a potential drug. Consequently, in order to improve the quality and to limit the waste of lipids, the replacement of mini extruder with Liposofast LF-50 extruder is recommended.

With regard to Steward's method for lipid determination, which was required in order to determine the phospholipid recovery of liposomes after extrusion, this could not be used in the current study for technical reasons (lack of the suitable equipment-specific glass cuvettes). It was therefore necessary to use an alternative technique (WAKO assay). In Stewart's assay, phospholipids (sphingomyelin) form a complex with ammonium ferrothiocyanate. An important advantage of the Stewart's assay comparing with a similar assay (Barlett assay) is that any inorganic phosphate does not interfere and therefore PBS buffer can be used. On the other hand, the



WAKO assay is a practically easier and quicker technique. This assay is based on an enzymatic reaction using N-ethyl-N-(2-hydroxy-3-sulfopropyl)-3,5-dimethoxyaniline (DAOS) as a blue pigment. Both phospholipid assays have the similar level of sensitivity, and so the WAKO assay did prove to be a suitable alternative to Stewart's assay.

#### **6.4 Future prospective**

It is clear that there is a need for further investigation and optimization of this study in order to yield reproducible and reliable results, but also to reach to the desired goal, which is further research *in vivo*. The current project presented important results for the structure and size of liposomes, and also their ability to inhibit A $\beta$  toxicity and aggregation. It is important to mention again that the current study examined three types of liposomes of three distinct sizes. Some further experiments which could be carried out in future studies are presented below:

##### *Examination of the three different sizes of PINPs crossing the BBB*

Following on from the preparation the three different sizes of liposomes, further experiments are possible to investigate their differential properties. An interesting experiment would be to examine the ability of the three different sizes of nanoliposomes to pass through the BBB. This could be carried out most easily by using an artificial BBB model, such as the monolayer of hCMEC/D3 cells described by (Salvati et al. (2013). Here, PINPs and liposomes are applied to one the side of the cell monolayer, and then attempts are made to detect them on the other side, which reveals transcytosis of the nanoliposomes through the artificial BBB. This technique

was employed by Dr. Salvati and colleagues to show that PINPs of a standard size (100 nm) can effectively cross the BBB.

The optimal size of nanoparticles as drug delivery systems is something that has concerned many scientists. The appropriate size of nanoparticles and specifically nanoliposomes, should not be too large or too small. According to previous work, liposomes smaller than 100 nm have a longer half-life in the blood circulation and fewer interactions with plasma proteins. In contrast, larger nanoliposomes (~200-300 nm) have an increased drug holding capacity, but a shorter half-life in the blood circulation because they are rapidly removed by the RES (Bozzuto and Molinari 2015; Fanciullino and Ciccolini 2009). Based on this type of information, the appropriate size for nanocarriers is generally thought to be in the range 100-150 nm. However, it would be interesting to examine the relative merits of the three distinct sizes of our liposomes produced here as potential drugs.

#### Lactate dehydrogenase (LDH) assay

As regards the ability of liposomes to affect A $\beta$  aggregation and protect against cytotoxicity, neither the simple nor the PEGylated liposomes showed any positive results. In contrast, PINPs showed positive and promising results for the inhibition of A $\beta$  toxicity towards neuronal cells in this study, as assessed by the MTS assay. It would be useful to confirm this by use of alternative techniques, such as the Lactate dehydrogenase (LDH) assay. This assay measures cell proliferation rather than cell survival, giving a different perspective on the protective effect of PINPs towards cells.

#### Production of liposomes using tetradecanol-1 lipid as alternative to cholesterol

Other studies have used various different compositions of lipids for the development of liposomes (Franzen et al., 2011). According to a previous study (Ali

et al., 2010) fatty alcohols, and specifically tetradecanol-1, can be used as an alternative to cholesterol in lipid based drug delivery. Cholesterol and tetradecanol-1 have similar chemical and biological properties and so they behave in a similar way in the liposomal membranes. However, the formation of liposomes using fatty acid alcohols as an alternative to cholesterol has revealed some differential results when they are examined for parameters such as drug loading and drug release. Liposomes made with tetradecanol-1 were found to shown to be better for drug delivery, compared to those containing cholesterol (Ali et al., 2010). In addition, another reason why tetradecanol-1 may be a more suitable lipid than cholesterol is due to the fact that cholesterol has some issues with contamination, because of its source (usually from animals). Consequently, we should consider the use of tetradecanol-1 as an alternative to cholesterol in development of PINPs as a drug.

#### *Encapsulation of peptide inhibitor in the interior side of the liposome*

Based on previous information, the presence of tetradecanol-1 in the liposomes has a positive impact on drug loading and drug release, and this could lead to evolution of a more potent and safer version of our drug (Ali et al., 2010). Moreover, other approaches have involved encapsulation of the drug into the interior space of the liposomes, instead of incorporating it onto their surface (Hu et al., 2010). So, we might be able to produce a more effective drug by using a combination of drug delivery systems, involving incorporation of the RI-peptide onto the surface of the liposomes, as well as by inserting it into the liposome core. This new type of 'dual delivery' mechanism would then be tested in various *in vitro* and *in vivo* experimental systems. The encapsulation of the RI-peptide inhibitor into the core of the liposomes could also create a safer drug since the peptide inhibitor would

not be able to evoke any adverse immune reactions during its circulation throughout the body.

#### Storage of PINPs

A basic rule for the development of any drug is for it to be stable for a long time, either at room temperature or at 4°C. According to the results that we obtained for the three types of nanoliposomes, their stability in terms of size, as measured by DLS, was maintained for some months. However, desiccation (freeze-drying) of the drug prior to its reconstitution as a liquid, when required, could be advantageous for long-term storage. The general idea is to remove the moisture from the liquid suspension of liposomes. Based on a previous study by Misra et al (2009), the conversion of liquid liposomes to a liposomal dry powder formulation (LDPF) is an efficient and simple technique which can be used to enhance the stability of the drug. Here, the homogenized liposome solution is dispersed into a suitable carrier and then converted to powder form by using freeze drying, spray drying or spray freeze drying. In addition, the conversion of drug from liquid form to powder form can change the route for drug administration (e.g. from injected drug to inhaled drug therapy), making it easier for patients to administer.

#### Complementary technique of TEM (Transmission Electron using freeze fracturing)

A previous study (Gradauer et al., 2012) has involved the characterization of liposome samples using two powerful techniques: negative stain EM and freeze fracture EM. Both of them revealed important information about the liposomes, but the freeze fracture technique is recommended for characterization of liposomes by shape or surface modification. Consequently, in the current study it would have been advantageous to use freeze fracture EM as a complementary method of visualization

in order to reveal more accurate information about the morphology of various types of liposomes (Misra et al., 2009).

#### *Centrifugation using Vivaspin 6 an alternative of column purification*

As referred above, one of the most important limitations of the current study was that during the preparation of PINPs we lost a substantial quantity of the lipids from the many transfers between vials, and also from the separation of PINPs from unbound peptide using column chromatography. Consequently, a promising technique that may lead to fewer losses is to replace the column purification by centrifugation of the liposome suspension using Vivaspin 6 tubes. Vivaspin 6 tubes are specially designed tubes, with a membrane which would leave the more concentrate sample (PINPs) in the upper chamber, while the solvent and the less concentrated sample (filtered PBS and unbound peptide) should pass through the membrane.

### **6.5 Conclusion**

In conclusion, the main objective of the current study was the development of the methods required for the production and characterization of three different types of liposomes, in three distinct sizes (200, 100 and 50 nm), as a means of transferring the technology for production of nanoliposomes and PINPs to our laboratory in Lancaster. The original method for liposome preparation was developed at The University of Milano-Bicocca, by Professor Massimo Masserini and Dr. Maria Gregori. Based on the work presented here, we are now able to produce the liposomes by ourselves, giving us the ability in future to manufacture the drug

(PINPs), and any future derivatives or modifications, at Lancaster. The three different sizes and types of liposomes were characterized by size, shape-ultrastructure, and examined for their ability to inhibit the aggregation and the toxicity of A $\beta$ , and their ability to penetrate into SHSY-5Y neuroblastoma cells. According to the results, these different types of liposomes were prepared according to plan, and lead us to the conclusion that only PINPs, and not the other two types of liposomes, are able to inhibit the aggregation and toxicity of A $\beta$ . Additionally, TEM and DLS were the two powerful techniques used for this study, and helped us to understand how to prepare liposomes of suitable size and appearance (shape and ultrastructure).

To sum up, the current study constitutes an important step in the evolution and improvement of our drug (PINPs), hopefully to the point where it can fulfill its promise as a prospective treatment for AD. Moreover, the study of nanoliposomes has brought us into contact with the field of nanomedicine, which is an exciting and expanding area of drug discovery.

## References

- Adessi, C. and Soto, C.** (2002) Beta-sheet breaker strategy for the treatment of Alzheimer's disease. *Drug Dev. Res.* **56**: 184–193.
- Akbarzadeh, A., Rezaei-Sadabady, R., Davaran, S., Joo, S.W., Zarghami, N., Hanifehpour, Y., Samiel, M., Kouhi, M., Nejati-Koshki, K.** (2013) Liposome: classification, preparation, and applications. *Nanoscale Res. Lett.* **8**: 102.
- Albanese, A., Tang, P.S., and Chan, W.C.W.** (2012) The effect of nanoparticle size, shape, and surface chemistry on biological systems. *Annu. Rev. Biomed. Eng.* **14**: 1–16.
- Allen, T.M.** (1995) Long-circulating (Stealth) liposomes: therapeutic applications. In: Puisieux F, Couvreur P, Delattre J, Devissaguet JP, editors. *Liposomes: New systems and new trends in their applications.* **1995**: 125–155.
- Ali, M.H., Kirby, D.J., Mohammed, A.R. and Perrie, Y.** (2010) Solubilisation of drugs within liposomal bilayers: Alternatives to cholesterol as a membrane stabilising agent. *J. Pharm. Pharmacol.* **62**: 1646–1655.
- Allsop, D. and Mayes, J.** (2014) Alzheimer's disease. *Essays Biochem.* **56**: 99-110.
- Amarnath, S., Sharma, U.S.** (1997) Liposomes in drug delivery: progress and limitations. *Int. J. Pharm.* **154**: 123–140.
- Apostolova, L.G., Hwang, K.S., Andrawis, J.P., Green, AE., Babakchianian, S., Morra, J.H., Cummings, J.L., Toga, A.W., Trojanowski, J.Q., Shaw, L.M., Jack, C.R Jr., Petersen, R.C., Aisen, P.S., Jagust, W.J., Koeppe, R.A., Mathis, C.A., Weiner,**

- M.W., Thompson, P.M.** (2010) Alzheimer's disease neuroimaging initiative. 3D PIB and CSF biomarker associations with hippocampal atrophy in ADNI subjects. *Neurobiol. Aging*. **31**: 1284-303.
- Areosa, S.A., Sherriff, F., McShane, R.** (2005) Memantine for dementia. *Cochrane Database Syst. Rev.* **3**: CD003154.
- Atamna, H., Nguyen, A., Schultz, C., Boyle, K., Newberry, J., Kato, H., Ames, B.N.** (2008) Methylene blue delays cellular senescence and enhances key mitochondrial biochemical pathways. *FASEB J.* **22**: 703–712.
- Austen, B.M., Paleologou, K.E., Ali, S.A.E., Qureshi, M.M., Allsop, D. and El-Agnaf, O.M.A.** (2008) Designing peptide inhibitors for oligomerization and toxicity of Alzheimer's  $\beta$ -amyloid peptide. *Biochemistry*. **47**: 1984–1992.
- Bachman, D.L., Wolf, P.A., Linn, R.T., Knoefel, J.E., Cobb, J.L., Belanger, A.J., White, L.R., D'Agostino, R.B.** (1993) Incidence of dementia and probable Alzheimer's disease in a general population: the Framingham Study. *Neurology*. **43**: 515–519.
- Bangham, A.D., Standish, M.M., Watkins, J.C.** (1965) Diffusion of univalent ions across the lamellae of swollen phospholipids. *J. Mol. Biol.* **13**: 238–252.
- Barbet, J., Machy, P., Leserman, L.D.** (1981) Monoclonal antibody covalently coupled to liposomes: specific targeting to cells. *J. Supramol. Struct. Cell Biochem.* **16**: 243–258.



- Bayer, T.A., Cappai, R., Masters, CL., Beyreuther, K., Multhaup, G.** (1999) It all sticks together—the APP-related family of proteins and Alzheimer’s disease. *Mol. Psychiatry*. **4**: 524–28.
- Bedu-Addo, F.K., Tang, P., Xu, Y., Huang, L.** (1996) Effects of polyethyleneglycol chain length and phospholipid acyl chain composition on the interaction of polyethyleneglycol-phospholipid conjugates with phospholipid: implications in liposomal drug delivery. *Pharm. Res.* **13**: 710–717.
- Biessels, G.J., De Leeuw, F.E., Lindeboom, J., Barkhof, F., and Scheltens, P.** (2006) Increased cortical atrophy in patients with Alzheimer’s disease and type 2 diabetes mellitus. *J. Neurol. Neurosurg. Psychiatry*. **77**: 304–307.
- Bird, T.D.** (2008) Genetic aspects of Alzheimer’s disease. *Genet. Med.* **10**: 231–239.
- Blennow, K., De Leon, M.J. and Zetterberg, H.** (2006) Alzheimer’s disease. *Lancet*. **368**: 387–403.
- Bouchon, A., Dietrich, J., Colonna, M.** (2000) Cutting edge: inflammatory responses can be triggered by TREM-1, a novel receptor expressed on neutrophils and monocytes. *J. Immunol.* **164**: 4991-5.
- Bozzuto, G. and Molinari, A.** (2015) Liposomes as nanomedical devices. *Int. J. of Nanomedicine*. **10**: 975–999.
- Brody, H., Breteler, M.M., Dekosky, S.T., Dorenlot, P., Fratiglioni, L., Hock, C., Kenigsberg, P-A., Scheltens, P. and Strooper, B.D.** (2011) The world of dementia beyond 2020. *J. Am. Geriatr. Soc.* **59**: 923–927.

- Burda, C., Chen, X., Narayanan, R., El-Sayed, M.A.** (2005) The chemistry and properties of nanocrystals of different shapes. *Chem. Rev.* **105**: 1025–102.
- Chafekar, S.M., Malda, H., Merkx, M., Meijer, E.W., Viertl, D., Lashuel, H.A., Frank, Baas, F. and Scheper, W.** (2007) Branched KLVFF tetramers strongly potentiate inhibition of beta-amyloid aggregation. *Chem. Biochem.* **8**: 1857–1864.
- Cherny, R.A., Atwood, C.S., Xilinas, M.E., Gray, D.N., Jones, W.D., McLean, C.A., Barnham, K.J., Volitakis, I., Fraser, F.W., Kim, Y., Huang, X., Goldstein, L.E., Moir, R.D., Lim, J.T., Beyreuther, K., Zheng, H., Tanzi, R.E., Masters, C.L., Bush, A.I.** (2000) Treatment with a copper-zinc chelator markedly and rapidly inhibits beta-amyloid accumulation in Alzheimer's disease transgenic mice. *Neuron.* **30**: 665–76.
- Cherukuri, P., Gannon, C.J., Leeuw, T.K., Schmidt, H.K., Smalley, R.E., Curley, S.A., Weisman, R.B.** (2006) Mammalian pharmacokinetics of carbon nanotubes using intrinsic near-infrared fluorescence. *Proc. Natl. Acad. Sci.* **103**: 18882–86.
- Chetanachan, P., Akarachalanon, P., Worawirunwong, D., Dararutana, P., Bangtrakulnonth, A., Bunjop, M. and Kongmuang, S.** (2008) Ultrastructural characterization of liposomes using transmission electron microscope. *AMR.* **55-57**: 709-711.
- Chithrani, B.D., Ghazani, A.A., Chan, W.C.** (2006) Determining the size and shape dependence of gold nanoparticle uptake into mammalian cells. *Nano Lett.* **6**: 662–68.
- Cho, N-J., Hwang, L.Y., Solandt, J.J.R. and Frank, C.W.** (2013) Comparison of extruded and sonicated vesicles for planar bilayer self-assembly. *Materials.* **6**: 3294-3308.

- Chorev, M., and Goodman, M.** (1995) Recent developments in retro peptides and proteins: An ongoing topochemical exploration. *Trends Biotechnol.* **13**: 438–445.
- Conti, M., Tazzari, V., Baccini, C., Pertici, G., Serino, L.P., De Giorgi, U.** (2006) Anticancer drug delivery with nanoparticles. *In Vivo.* **20**: 697-701.
- Corder, E.H., Saunders, A.M., Strittmatter, W.J., Schmechel, D.E., Gaskell, P.C., Small, G.W., Roses, A.D., Haines, J.L., Pericak-Vance, M.A.** (1993) Gene dose of apolipoprotein E type 4 allele and the risk of Alzheimer's disease in late onset families. *Science.* **261**: 921–923.
- Davies, L., Wolska, B., Hilbich, C., Multhaup, G., Martins, R., Simms, G., Beyreuther, K. and Masters, C.L.** (1988) A4 amyloid protein deposition and the diagnosis of Alzheimer's disease: prevalence in aged brains determined by immunocytochemistry compared with conventional neuropathologic techniques. *Neurology.* **38**: 1688–1693.
- De Jong, W.H., Hagens, W.I., Krystek, P., Burger, M.C., Sips, AJAM., Geertsma, R.E.** (2008) Particle size dependent organ distribution of gold nanoparticles after intravenous administration. *Biomaterials.* **29**: 1912–19.
- Dobson, C.M.** Protein misfolding, evolution and disease. (1999) *Trends Biochem. Sci.* **24**: 329–332.
- Dong S., Duan Y., Hu Y., Zhao, Z.** (2012) Advances in the pathogenesis of Alzheimer's disease: a re-evaluation of amyloid cascade hypothesis. *Transl. Neurodegener.* **1**: 18.

- Drummond, D.C., Meyer, O., Hong, K., Kirpotin, D.B., Papahadjopoulos, D.** (1999) Optimizing liposomes for delivery of chemotherapeutic agents to solid tumors. *Pharmacol. Rev.* **51**: 691–743.
- Dua, J.S., Rana, A.C., Bhandari, A.K.** (2012) Liposome : Methods of preparation and applications. *Int. J. Pharm. Studies and Res.* **III**: 14-20.
- Etheridge, M.L., Campbell, S.A., Erdman, A.G., Haynes, C.L., Wolf, S.M., McCullough, J.** (2013) The big picture on nanomedicine: the state of investigational and approved nanomedicine products. *Nanomedicine.* **9**: 1–14.
- Euliss, L.E., DuPont, J.A., Gratton, S., DeSimone, J.** (2006) Imparting size, shape, and composition control of materials for nanomedicine. *Chem. Soc. Rev.* **35**: 1095–1104.
- Fanciullino, R., Ciccolini, J.** (2009) Liposome-encapsulated anticancer drugs: still waiting for the magic bullet? *Curr. Med. Chem.* **16**: 4361–4373.
- Ferri, C.P., Prince, M., Brayne, C., Brodaty, H., Fratiglioni, L., Ganguli, M., Hall, K., Hasegawa, K., Hendrie, H., Huang, Y., Jorm, A., Mathers, C., Menezes, P.R., Rimmer, E., Sczufca, M.** (2005) Global prevalence of dementia: a Delphi consensus study. *Lancet.* **366**: 2112–17.
- Forsberg, A., Engler, H., Almkvist, O., Blomquist, G., Hagman, G., Wall, A., Ringheim, A., Langstron, B. and Nordberg, A.** (2008) PET imaging of amyloid deposition in patients with mild cognitive impairment. *Neurobiol. Aging.* **29**: 145-1465.

- Franzen, U., Vermehren, C., Jensen, H. and Østergaard, J.** (2011) Physicochemical characterization of a PEGylated liposomal drug formulation using capillary electrophoresis. *Electrophoresis*. **32**: 738–748.
- Fu, H.J., Liu, B., Frost, J.L., Lemere, C.A.** (2010) Amyloid-beta immunotherapy for Alzheimer's disease. *CNS Neurol. Disord. Drug Targets*. **9**: 197–206.
- Gabathuler, R.** (2010) Approaches to transport therapeutic drugs across the blood–brain barrier to treat brain diseases. *Neurobiol. Dis.* **37**: 48-57.
- Gabizon, A., Goren, D., Cohen, R., Barenholz, Y.** (1998) Development of liposomal anthracyclines: from basics to clinical applications. *J. Control Release*. **53**: 275–279.
- Gandy, S.** (2005) The role of cerebral amyloid beta accumulation in common forms of Alzheimer disease. *J. Clin. Invest.* **115**: 1121–29.
- Geerts, H.** (2004) NC-531 (Neurochem). *Curr. Opin. Investig. Drugs*. **5**: 95–100.
- Ghanta, J., Shen, C.L., Kiessling, L.L. and Murphy, R.M.** (1996) A strategy for designing inhibitors of  $\beta$ -amyloid toxicity. *J. Biol. Chem.* **271**: 29525-29528.
- Ghiso, J. and Frangione, B.** (2002) Amyloidosis and Alzheimer's disease. *Adv. Drug Delivery Rev.* **54**: 1539–1551.
- Glenner, G.G. and Wong, C.W.** (1984) Alzheimer's disease: initial report of the purification and characterization of a novel cerebrovascular amyloid protein. *Biochem. Biophys. Res. Commun.* **120**: 885–890.

- Godin, B., Tasciotti, E., Liu, X., Serda, R.E., Ferrari, M.** (2011) Multistage nanovectors: from concept to novel imaging contrast agents and therapeutics. *Acc. Chem. Res.* **44**: 979-89.
- Gosal, W.S., Myers, S.L., Radford, S.E. and Thomson, N.H.** (2006) Amyloid under the atomic force microscope. *Protein Pept. Lett.* **13**: 261–270.
- Gradauer, K., Vonach, C., Leitinger, G., Kolb, D., Fröhlich, E., Roblegg, E., Bernkop-Schnürch, A., Prassl, R.** (2012) Chemical coupling of thiolated chitosan to preformed liposomes improves mucoadhesive properties. *Int. J. Nanomedicine.* **7**: 2523–2534.
- Gref, R., Luck, M., Quellec, P., Marchand, M., Dellacherie, E., Harnisch, S., Blunk, T., Müller, R.H.** (2000) Stealth' corona-core nanoparticles surface modified by polyethylene glycol (PEG): influences of the corona (PEG chain length and surface density) and of the core composition on phagocytic uptake and plasma protein adsorption. *Colloids Surf. B Biointerfaces.* **18**: 301–13.
- Gregori, M., Taylor, M., Salvati, E., Re, F., Minniti, S., Zambelli, V., Michael, M., Michail, C., Tinker-Mill, C., Kolsov, O., Sherer, M., Fullwood, N.J., Masserini, M., Allsop, D.** (2015) Retro-inverso peptide inhibitor nanoparticles as potent inhibitors of aggregation of the Alzheimer's A $\beta$  peptide. *Submitted to Nanomedicine: Nanotechnology, Biology and Medicine*).
- Guerreiro, R., Wojtas, A., Bras, J., Carrasquillo, M., Rogaeva, E., Majounie, E., Cruchaga, C., Sassi, C., Kauwe, J.S.K., Younkin, S., Hazrati, L., Collinge, J., Pocock, J., Lashley, T., Williams, J., Lambert, J.C., Amouyel, P., Goate, A., Rademakers, R., Morgan, K., Powell, J., George-Hyslop, P. St., Singleton, A.,**

- Hardy, J. and The Alzheimer Genetic Analysis Group** (2013) TREM2 variants in Alzheimer's disease. *N. Engl. J. Med.* **368**: 117 – 127.
- Haan, M.N.** (2006) Therapy insight: type 2 diabetes mellitus and the risk on late-onset Alzheimer's disease. *Nat. Clin. Pract. Neurol.* **2**: 159 – 166.
- Haass, C., Selkoe, D.J.** (2007) Soluble protein oligomers in neurodegeneration: lessons from the Alzheimer's amyloid [beta]-peptide. *Nature Rev. Mol. Cell Biol.* **8**: 101-12.
- Hardy, J. and Selkoe, D.J.** (2002) The amyloid hypothesis of Alzheimer's disease: progress and problems on the road to therapeutics. *Science.* **297**: 353–356.
- Howlett, D.** (2011) APP transgenic mice and their application to drug discovery. *Histol Histopathol.* **26**: 1611–1632.
- Hu, C.-M.J., Aryal, S. and Zhang, L.** (2010) Nanoparticle-assisted combination therapies for effective cancer treatment. *Ther. Deliv.* **1**: 323–334.
- Huang, Z., Li, X., Zhang, T., Song, Y., She, Z., Li, J. and Deng, Y.** (2014) Progress involving new techniques for liposome preparation. *Asian J. Pharm. Sci.* **9**: 176–182.
- Hudson, S.A., Ecroyd, H., Kee, T.W. and Carver, J.A.** (2009) The thioflavin T fluorescence assay for amyloid fibril detection can be biased by the presence of exogenous compounds. *FEBS J.* **276**: 5960–5972.

- Jeang, K.T., Xiao, H., Rich, H.E.A.** (1999) Multifaceted activities of the HIV-1 trans activator of transcription, *Tat*. *J. Biol. Chem.* **274**: 28837–28840.
- Jellinger, K.A.** (2004) Head injury and dementia. *Curr. Opin. Neurol.* **17**: 719–23.
- Karran, E., Mercken, M., De Strooper, B.** (2011) The amyloid cascade hypothesis for Alzheimer's disease: an appraisal for the development of therapeutics. *Nature Rev. Drug Discov.* **10**: 698–712.
- Kirchner, C., Liedl, T., Kudera, S., Pellegrino, T., Munoz Javier, A., Gaub, H.E., Stölzle, S., Fertig, N., Parak, W.J.** (2005) Cytotoxicity of colloidal CdSe and CdSe/ZnS nanoparticles. *Nano Lett.* **5**: 331-38.
- Kokkoni, N., Scott, K., Amijee, H., Mason, J.M., and Doig, A.J.** (2006) N-Methylated peptide inhibitors of  $\beta$ -amyloid aggregation and toxicity. Optimization of the inhibitor structure. *Biochemistry.* **45**: 9906 – 9918.
- Korgel, B.A., Van Zanten, J.H., Monbouquette, H.G.** (1998) Vesicle size distributions measured by flow field-flow fractionation coupled with multiangle light scattering. *Biophys. J.* **74**: 3264–3272.
- Laouini, A., Jaafar-Maalej, C., Limayem-Blouza, I., Sfar, S., Charcosset, C. and Fessi, H.** (2012) Preparation, characterization and applications of liposomes: State of the Art. *J. Colloid Sci. and Biotechnol.* **1**: 147–168.
- Lee, S.C., Lee, K.E., Kim, J.J. and Lim, S.H.** (2005) The Effect of cholesterol in the liposome bilayer on the stabilization of incorporated retinol. *J. Liposome Res.* **15**: 157-166.



- Los, D.A. and Murata, N.** (2004) Membrane fluidity and its roles in the perception of environmental signals. *BBA-Biomembranes*. **1666.1-2**: 142-157.
- Loureiro, J.A., Gomes, B., Coelho, M.A., Do Carmo Pereira, M., Rocha S.** (2014) Targeting nanoparticles across the Blood–Brain Barrier with monoclonal antibodies. *Nanomedicine* **9**: 709-722.
- Ma, Q.L., Yang, F., Rosario, E.R., Ubeda, O.J., Beech, W., Gant, D.J., Chen, P.P., Hudspeth, B., Chen, C., Zhao, Y., Vinters, H.V., Frautschy, S.A., Cole, G.M.** (2009)  $\beta$ -amyloid oligomers induce phosphorylation of tau and inactivation of insulin receptor substrate via c-Jun N-terminal kinase signaling: suppression by omega-3 fatty acids and curcumin. *J. Neurosci.* **29**: 9078-89.
- Mahley, R.W., Huang, Y., Weisgraber, K.H.** (2007) Detrimental effects of apolipoprotein E4: potential therapeutic targets in Alzheimer's disease. *Curr. Alzheimer Res.* **4**: 537–540.
- Mangialasche, F., Solomon, A., Winblad, B., Mecocci, P., Kivipelto, M.** (2010) Alzheimer's disease: clinical trials and drug development. *Lancet. Neurol.* **9**: 702–716.
- Martin, J.B.** (1999) Molecular basis of the neurodegenerative diseases. *N. Eng. J. Med.* **340**: 1970–1980.
- Maruyama, K., Yuda, T., Okamoto, A., Kojima, S., Suginaka, A., Iwatsuru, M.** (1992) Prolonged circulation time in vivo of large unilamellar liposomes composed of distearoyl phosphatidylcholine and cholesterol containing amphipathic poly(ethylene glycol). *Biochim. Biophys. Acta.* **1128**: 44-9.

- Masserini, M.** (2013) Nanoparticles for brain drug delivery. *ISRN Biochemistry*. **2013**: 18.
- Matsuzaki, K., Murase, O., Sugishita, K., Yoneyama, S., Akada, K., Ueha, M., Nakamura, A., Kobayashi, S.** (2000). Optical characterization of liposomes by right angle light scattering and turbidity measurement. *BBA – Biomembranes*. **1467**: 219–226.
- Mattson, P.M.** (2010) ER calcium and Alzheimer’s disease: In a state of flux. *Neuroscience*. **3**: 114-110.
- Mayeux, R.** (2003) Epidemiology of neurodegeneration. *Annu. Rev. Neurosci.* **26**: 81–104.
- Melchior, B., Garcia, A.E., Hsiung, B.K., Lo, K.M., Doose, J.M., Thrash, J.C., Stalder, A.K., Staufienbiel, M., Neumann, H., Carson, M.J.** (2010) Dual induction of TREM2 and tolerance- related transcript, Tmem176b, in amyloid transgenic mice: implications for vaccine-based therapies for Alzheimer’s disease. *ASN Neuro* **2**: (3).
- Meure, L.A., Foster, N.R., Dehghani, F.** (2008) Conventional and dense gas techniques for the production of liposomes: A Review. *AAPS Pharm. Sci. Tech.* **9**: 798-809.
- Misra, A., Jinturkar, K., Patel, D., Lalani, J., Chougule, M.** (2009) Recent advances in liposomal dry powder formulations: Preparation and evaluation. *Expert Opin. Drug Deliv.* **6**: 71-89.

- Moller, H.J. and Graeber, M.B.** (1998) The case described by Alois Alzheimer in 1911. Historical and conceptual perspectives based on the clinical record and neurohistological sections. *Eur. Arch. Psychiatry Clin. Neurosci.* **248**: 111–122.
- Morita, M., Hamada, T., Tendo, Y., Hata, T., Vestergaard Mun'delanji, C., Takagi, M.** (2012) Selective localization of Alzheimer's amyloid beta in membrane lateral compartments. *Soft Matter.* **8**: 2816.
- Mortimer, J.A., Borenstein, A.R., Gosche, K.M. and Snowden, D.A.** (2005) Very early detection of Alzheimer neuropathology and the role of brain reserve in modifying its clinical expression. *J. Geriatr. Psychiatry Neurol.* **18**: 218–223.
- Mortimer, J.A., Snowden, D.A., Markesbery, W.R.** (2003) Head circumference, education and risk of dementia. Findings from the Nun Study. *J. Clin. Exp. Neuropsychol.* **25**: 671–79.
- Morton, L.A., Saludes, J.P. and Yin, H.** (2012) Constant pressure-controlled extrusion method for the preparation of nano-sized lipid vesicles. *Journal of Visualized Experiments.* **64**: 1–6.
- Namba, Y., Tomonaga, M., Kawasaki, H., Otomo, E., Ikeda, K.** (1991) Apolipoprotein E immunoreactivity in cerebral amyloid deposits and neurofibrillary tangles in Alzheimer's disease and kuru plaque amyloid in Creutzfeldt-Jakob disease. *Brain Res.* **541**: 163–166.
- Nazem, A. and Mansoori, G.A.** (2008) Nanotechnology solutions for Alzheimer's disease: advances in research tools, diagnostic methods and therapeutic agents. *JAD.* **13**: 199–223.

- Needham, D., McIntosh, T.J., Lasic, D.D.** (1992) Repulsive interactions and mechanical stability of polymer-grafted lipid membranes. *Biochem. Biophys. Acta.* **1108**: 40-8.
- Neuwelt, E., Abbott, N.J., Abrey, L., Banks, W.A., Blakley, B., Davis, T., Engelhardt, B., Grammas, P., Nedergaard, M., Nutt, J., Pardridge, W., Rosenberg, G.A., Smith, Q., Drewes, L.R.** (2008) Strategies to advance translational research into brain barriers. *The Lancet Neurology.* **7**: 84–96.
- Nussbaum, R.L. and Ellis, C.E.** (2003) Alzheimer's disease and Parkinson's disease. *N. Engl. J. Med.* **348**: 1356 -1364.
- O'Brien, R.J. and Wong, P.C** (2011) Amyloid precursor protein processing and Alzheimer's disease. *Annu. Rev. Neurosci.* **34**: 185–204.
- Pan, K.M., Baldwin, M., Nguyen, J., Gasset, M., Serban, A., Groth, D., Mehlhorn, I., Huang, Z., Fletterick, R.J., Cohen, F.E.** (1993) Conversion of  $\alpha$ -helices into  $\beta$ -sheets features in the formation of the scrapie prion proteins. *Biochemistry.* **90**: 10962-10966.
- Pardridge, W.M.** (2007) Brain drug development and brain drug targeting. *Pharm. Res.* **24**: 1729 -32.
- Parthasarathy, V., McClean, PL., Hölscher, C., Taylor, M., Tinker, C., Jones, G., Kolosov, O., Salvati, E., Gregori, M., Masserini, M., Allsop, D.** (2013) A novel retro-inverso peptide inhibitor reduces amyloid deposition, oxidation and inflammation and stimulates neurogenesis in the APP<sup>swe</sup>/PS1 $\Delta$ E9 mouse model of Alzheimer's disease. *PLoS ONE*; **8**: e54769.

- Patil, Y.P. and Jadhav, S.** (2014) Novel methods for liposome preparation. *Chem. Phys. Lipids.* **177**: 8–18.
- Perrault, S.D., Walkey, C., Jennings, T., Fischer, H.C., Chan, W.C.W.** (2009) Nano Mediating tumor targeting efficiency of nanoparticles through design *Lett.* **9**: 1909–15.
- Petit, A., Bihel, F., Alves da Costa, C., Pourquie, O., Checler, F., Kraus, J.L.** (2001) New protease inhibitors prevent gamma-secretase mediated production of Abeta40/42 without affecting Notch cleavage. *Nature Cell Biol.* **3**: 507–11.
- Petersen, R.C.** (2004) Mild cognitive impairment as a diagnostic entity. *J. Intern. Med.* **256**: 183 – 194.
- Petkar, K.C., Chavhan, S.S., Agatonovik-Kustrin, S. and Sawant, K.K.** (2011) Nanostructured materials in drug and gene delivery: a review of the state of the art. *Crit. Rev. Ther. Drug Carrier Syst.* **28**: 101–164.
- Pfrieger, F.W.** (2003) Cholesterol homeostasis and function in neurons of the central nervous system. *Cell Mol. Life Sci.* **60**: 1158–1171.
- Ran, Y. and Yalkowsky, S.H.** (2003) Halothane, a novel solvent for the preparation of liposomes containing 2-4'-Amino-3'-Methylphenyl Benzothiazole (AMPB), an anticancer drug: A technical note. *AAPS Pharm. Sci. Tech.* **4**: 70-74.
- Ritchie, C.W., Bush, A.I., Mackinnon, A., Macfarlane, S., Mastwyk, M., MacGregor, L., Kiers, L., Cherny, R., Li, QX., Tammer, A., Carrington, D., Mavros, C., Volitakis, I., Xilinas, M., Ames, D., Davis, S., Beyreuther, K., Tanzi, R.E., Masters, C.L.** (2003) Metal-protein attenuation with iodochlorhydroxyquin

(cloquinol) targeting Abeta amyloid deposition and toxicity in Alzheimer disease: a pilot phase 2 clinical trial. *Arch. Neurol.* **60**: 1685–91.

**Ruozzi, B., Belletti, D., Tombesi, A., Tosi, G., Bondioli, L., Forni, F., and Vandelli, M.A.** (2011) AFM, ESEM, TEM, and CLSM in liposomal characterization: a comparative study. *Int. J. Nanomedicine.* **6**: 557–563.

**Salvati, E., Re, F., Sesana, S., Cambianica, I., Sancini, G., Masserini, M. and Gregori, M.** (2013) Liposomes functionalized to overcome the blood-brain barrier and to target amyloid- $\beta$  peptide: The chemical design affects the permeability across an in vitro model. *Int. J. Nanomedicine.* **8**: 1749–1758.

**Sandoval, K.E., Witt, K.A.** (2008) Blood-brain barrier tight junction permeability and ischemic stroke. *Neurobiol. Dis.* **32**: 200-19.

**Santos, A.O., Da Silva, L.C., Bimbo, L.M., De Lima, M.C., Simões, S., Moreira, J.N.** (2010) Design of peptide-targeted liposomes containing nucleic acids. *BBA – Biomembranes.* **1798**: 433-441.

**Saunders, A.M., Schmechel, K., Breitner, J.C., Benson, M.D., Brown, W.T., Goldfarb, L., Goldgaber, D., Manwaring, M.G., Szymanski, M.H., McCown, N., Roses, A.D.** (1993) Apolipoprotein E epsilon 4 allele distributions in late-onset Alzheimer's disease and in other amyloid-forming diseases. *Lancet.* **342**: 710–711.

**Schuber, F., Said Hassane, F., Frisch, B.** (2007) Coupling of peptides to the surface of liposomes – Application to liposome-based synthetic vaccines. In: Gregoriadis G (ed) *Liposome technology*, 3rd edn. *Informa Healthcare, New York, USA*, pp 111–130.

- Schüle, S., Schulz-Fademrecht, T., Garidel, P., Bechtold-Peters, K., Frieb, W.** (2008) Stabilization Of Igg1 In Spray-Dried Powders For Inhalation. *Eur. J. Pharm. Biopharm.* **69**: 793-807.
- Selkoe, D.J.** (2001) Alzheimer's disease: genes, proteins, and therapy. *Physiol. Rev.* **81**: 741-766.
- Sessa, G., Podini, P., Mariani, M., Meroni, A., Spreafico, R., Sinigaglia, F., Colonna, M., Panina, P., Meldolesi, J.** (2004) Distribution and signaling of TREM2/DAP12, the receptor system mutated in human polycystic lipomembraneous osteodysplasia with sclerosing leukoencephalopathy dementia. *Eur. J. Neurosci.* **20**: 2617-28.
- Shaheen, S.M., Shakil, A.F.R., Hossen, M.N., Ahmed, M., Amran, M.S., Ul-Islam, M.A.** (2006) Liposome as a carrier for advanced drug delivery. *Pak. J. Biol. Sci.* **9**: 1181–1191.
- Sherrington, R., Rogaev, E.I., Liang, Y., Rogaeva, E.A., Levesque, G., Ikeda, M., Chi, H., Lin, C., Li, G., Holman, K., Tsuda, T., Mar, L., Foncin, J.F., Bruni, A.C., Montesi, M.P., Sorbi, S., Rainero, I., Pinessi, L., Nee, L., Chumakov, I., Pollen, D., Brookes, A., Sanseau, P., Polinsky, R.J., Wasco, W., Da Silva, H.A., Haines, J.L., Pericak-Vance, M.A., Tanzi, R.E., Roses, A.D., Rommens, J.M. and St. George-Hyslop, P.H.** (1995) Cloning of a gene bearing missense mutations in early-onset familial Alzheimer's disease. *Nature.* **375**: 754 – 760.
- Spector, R., Johanson, C.E.** (1989) The mammalian choroid plexus. *Sci. Am.* **261**: 68–74.

- Spuch, C. and Navarro, C.** (2011) Liposomes for targeted delivery of active agents against neurodegenerative diseases (Alzheimer's disease and Parkinson's disease). *J. Drug Deliv.* p1.
- Soto, C.** (2003) Unfolding the role of protein misfolding in neurodegenerative diseases. *Nature Rev. Neurosci.* **4**: 49-60.
- Stewart, J.C.M.** (1980) Colorimetric determination of phospholipids with ammonium ferrothiocyanate. *Anal. Biochem.* **104**: 10-14.
- Sudimack, J., Lee, R.J.** (2000) Targeted drug delivery via the folate receptor. *Adv. Drug Deliv. Rev.* **41**: 147–162.
- Sriwongsitanont, S. and Ueno, M.** (2011) Effect of freeze-thawing process on the size and lamellarity of PEG-lipid liposomes. *The Open Colloid Science Journal.* **4**: 1-6.
- Tabner, B.J., El-Agnaf, O.M., Turnbull, S., German, M.J., Paleologou, K.E., Hayashi, Y., Cooper, L.J., Fullwood, N.J., Allsop, D.** (2005) Hydrogen peroxide is generated during the very early stages of aggregation of the amyloid peptides implicated in Alzheimer's disease and familial British dementia. *J. Biol. Chem.* **280**: 35789-35792.
- Takahashi, R.H., Milner, T.A., Li, F., Nam, E.E., Edgar, M.A., Yamaguchi, H., Beal, M.F., Xu, H., Greengard, P. and Gouras, G.K.** (2002) Intraneuronal Alzheimer abeta42 accumulates in multivesicular bodies and is associated with synaptic pathology. *Am. J. Pathol.* **161**: 1869–1879.
- Tassa, C., Duffner, J.L., Lewis, T.A., Weissleder, R., Schreiber, S.L., Koehler, A.N., Shaw, S.Y.** (2010) Binding affinity and kinetic analysis of targeted small molecule-modified nanoparticles. *Bioconjug. Chem.* **21**: 14-9.



- Taylor, M., Moore, S., Mayes, J., Parkin, E., Beeg, M., Canovi, M., Gobbi, M., Mann, D.M., Allsop, D.** (2010) Development of a proteolytically stable retro-inverso peptide inhibitor of  $\beta$ -amyloid oligomerization as a potential novel treatment for Alzheimer's disease. *Biochemistry*. **49**: 3261–72.
- Terry, A.V J.R., Buccafusco, J.J.** (2003) The cholinergic hypothesis of age and Alzheimer's disease-related cognitive deficits: recent challenges and their implications for novel drug development. *J. Pharmacol. Exp. Ther.* **306**: 821–27.
- Thornton, E., Vink, R., Blumbergs, P. C., Van Den Heuvel, C.** (2006) Soluble amyloid precursor protein  $\alpha$  reduces neuronal injury and improves functional outcome following diffuse traumatic brain injury in rats. *Brain Res.* **1094**: 38-46.
- Tjernberg, L.O., Callaway, D.J.E., Tjernberg, A., Hahne, S., Lilliehook, C., Terenius, L., Thyberg, J. and Nordstedt, C.** (1999) A molecular model of Alzheimer amyloid  $\beta$ -peptide fibril formation. *J. Biol. Chem.* **274**: 12619–12625.
- Tjernberg, L.O., Naslund, J., Lindqvist, F., Johansson, J., Karlstrom, A.R., Thyberg, J., Terenius, L. and Nordstedt, C.** (1996) Arrest of  $\beta$ -amyloid fibril formation by a pentapeptide ligand. *J. Biol. Chem.* **271**: 8545–8548.
- Van Der Zee, J., K. Slegers, C., Van, Broeckhoven.** (2008) Invited article: The Alzheimer disease frontotemporal lobar degeneration spectrum. *Neurology*. **71**: 1191-1197.
- Traikia, M., Warschawski, D.E., Recouvreur, M., Cartaud, J., and Devaux, P.F.** (2000) Formation of unilamellar vesicles by repetitive freeze-thaw cycles: Characterization by electron microscopy and  $^{31}\text{P}$ -nuclear magnetic resonance. *Eur. Biophys. J.* **29**: 184–195.

- Torchilin, V.P.** (2008) Tat peptide-mediated intracellular delivery of pharmaceutical nanocarriers. *Adv. Drug Deliv. Rev.* **60**: 548-558.
- Torchilin, V.P., Rammohan, R., Weissig, V. and Levchenko, T.S.** (2001) TAT peptide on the surface of liposomes affords their efficient intracellular delivery even at low temperature and in the presence of metabolic inhibitors. *P. Natio. Acad. Sci. USA.* **98**: 8786–8791.
- Verdile, G., Fuller, S., Atwood, C.S., Laws, S.M., Gandy, S.E., Martins, R.N.** (2004) The role of beta amyloid in Alzheimer's disease: still a cause of everything or the only one who got caught? *Pharmacol. Res.* **50**: 397-409.
- Vemuri, S., Rhodes, C.T.** (1995) Preparation and characterization of liposomes as therapeutic delivery systems: a review. *Pharmaceutica. Acta Helvetiae.* **70**: 95–111.
- Vuilleumard, J.C.** (1991) Recent advances in the large-scale production of lipid vesicles for use in food products: microfluidization. *J. Microencapsul.* **8**: 547–562.
- Wagner, A., Vorauer-Uhl, K.** (2011) Liposome technology for industrial purposes. *J. Drug Deliv.* **2011**: 9.
- Wang, R., Xiao, R., Zeng, Z., Xu, L. and Wang, J.** (2012) Application of poly (ethylene glycol)-distearoylphosphatidylethanolamine (PEG-DSPE) block copolymers and their derivatives as nanomaterials in drug delivery. *Int. J. Nanomedicine.* **7**: 4185–4198.

- Wernette-Hammond, M.E., Lauer, S.J., Corsini, A., Walker, D., Taylor, J.M., Rall, S.C JR.** (1989) Glycosylation of human apolipoprotein E. The carbohydrate attachment site is threonine 194. *J. Biol. Chem.* **264**: 9094–9101.
- Westermark, P.** (2005) Aspects on human amyloid forms and their polypeptides. *FEBS J.* **272**: 5942-5949.
- Wischik, C.M., Bentham, P., Wischik, D.J., Seng, K.M.** (2008) Tau aggregation inhibitor (TAI) therapy with rember™ arrests disease progression in mild and moderate Alzheimer's disease over 50 weeks. *Alzheimer's and Dementia* 4. p.
- Wisniewski, T., Frangione, B.** (1992) Apolipoprotein E: a pathological chaperone protein in patients with cerebral and systemic amyloid. *Neurosci. Lett.* **135**: 235–238.
- Wisniewski, T., Ghiso, J. and Frangione, B.** (1997) Biology of A $\beta$  amyloid in Alzheimer's disease. *Neurobiol. Dis.* **4**: 313 – 328.
- Wong, H.L, Wu, X.Y, Bendayan, R.** (2012) Nanotechnological advances for the delivery of CNS therapeutics. *Adv. Drug Deliv. Rev.* **64**: 686-700.
- Woodle, M.C., Matthay, K.K., Newman, M.S., Hidayat, J.E., Collins, L.R., Redemann, C., Martin, F.J., Papahadjopoulos, D.** (1992) Versatility in lipid compositions showing prolonged circulation with sterically stabilized liposomes. *Biochim. Biophys. Acta.* **1105**: 193–200.
- Xiao, M.-J., Han, Z., Shao, B. and Jin, K.** (2009) Notch signaling and neurogenesis in normal and stroke brain. *Int. J. Physiol. Pathophysiol. Pharmacol.* **1**: 192–202.

**Zalipsky, S., Mullah, N., Harding, J.A., Gittelman, J., Guo, L., DeFrees, S.A.** (1997) Poly (ethylene glycol)-grafted liposomes with oligopeptide or oligosaccharide ligands appended to the termini of the polymer chains. *Bioconj. Chem.* **8**: 111–118.

**Zaman, M., Ahmad, E., Qadeer, A., Rabbani, G. and Khan, R.H.** (2014) Nanoparticles in relation to peptide and protein aggregation. *Int. J. Nanomedicine.* **9**: 899–912.

**Zasadzinski, J.A.** (1986) Transmission electron microscopy observations of sonication-induced changes in liposome structure. *Biophys. J.* **49**: 1119-1130.

**Zhang, G., Yang, Z., LuW Zhang, R., Huang Q Tian, M., Li, L., Liang, D., Li, C.** (2009) Influence of anchoring ligands and particle size on the colloidal stability and *in vivo* biodistribution of polyethylene glycol-coated gold nanoparticles in tumor-xenografted mice. *Biomaterials.* **30**: 1928–36.

### **Websites**

1. Promega Corporation, <https://www.promega.co.uk/> (Accessed 2015 July 12).